Phase Detection Techniques for Surface Plasmon Resonance Sensors

WU, Shu Yuen

A Thesis Submitted in Partial Fulfillment
of the Requirements for the Degree of
Doctor of Philosophy
in
Electronic Engineering

The Chinese University of Hong Kong
May 2011

ProQuest LLC.
789 East Eisenhower Parkway
P.O. Box 1346
Ann Arbor, MI 48106 - 1346

概述

本項目主要是關於開發和優化光學傳感器，於相位測量的變化與表面等離子體共振(SPR)的影響。相位(SPR)感應技術提供了高靈敏度的測量能力。全賴於這個相位改變是以一個梯級式的跳躍進行，發生於一個共振下沉的環境內。此變化的結果導致感測媒體中的一個非常微小變化，就出現巨大相位偏移。在研究中發現一個範圍內運用不同的測量技術，能增強了系統的靈敏度。再者，我們運用數學模型對相位之改變特徵進行了研究，當中環繞 SPR 之下沉區間，以不同方法探索去達到高靈敏度和寬動態範圍的基礎上進行單點測量。因爲 SPR 被引發在一個電子荷密度振盪在金屬表面，其中波動量所需的等離子波激發是常常大於在自由空間中，所以倒棱鏡耦合方案(棱鏡-金屬-電介質)是經常被運用的。與此同時，本研究亦運用倒棱鏡耦合方案，特別是 SPR 生物傳感器的高靈敏度的基礎上的 Mach-Zehnder 干涉儀。

本研究之設計基礎有此優勢，這是建基於 SPR 只是影響了 P-偏振，同時不能影響 S-偏振。這意味著微分相位測量介乎於 P-與 S-偏振，此結果將導致 P-與 S-兩者均不受共同噪音影響。此實驗結果獲得甘油/水的混合物表明本方法之靈敏度極限爲 $5.48*10^{-8}$ 折射率單位每 0.01°相變。

據我們所知，這是一個有效的改進並超越前人的紀錄。此紀錄是以黃金作爲傳感器的感測面。雖然承認精確的光學定位是一個關鍵的要求馬赫曾德爾干涉儀，在實際環境中它往往不容易保持一致的高精確度。有見及此，我們已經開發出一種多功能和低成本的單束自參考相位敏感表面 SPR 的傳感系統。該系統具有根均方根相位起伏爲 ± 0.0028°·此量度時間超過 45 分鐘，所得之解像度就是± 5.2 x 10^{-9} 折射率單位。以下三個基本元素去達至性能的增強：（一）真正的單束光架構能完整的自我參照，這樣令相位的改變只基於是 SPR 能檢測到的；（二）微分測量技術能消除雜散信號並不相關的傳感器反應；（三）在液晶相位調製器納入溫度穩定之控制即能消除漂移情況。我們的設計應使檢測靈敏度的非生物傳感標籤更接近這一 SPR 達到傳統的熒光爲基礎的技術。

此外，該項目還計劃研究可能提高相變的 SPR 傳感器。“雙”和“多通”的辦法，通過它 SPR 可以被放大後，傳感器表面打一次以上，已被實驗研究，成功地展示。比較於單次通過方法，一個雙通過方法能即時給予兩陪相位的變化。據此，多通過方法給予多於兩陪的相位變化。這種改善相位檢測是非常重要的，此在於一個生物檢測之應用，涉及小分子，小的蛋白質，DNA 等。另一種方法的檢測性能改進是把多層次配置的生物傳感表面，爲了改善動態測量反應，我們建議採用多共振角度測量技術結合單束自參考相位敏感的 SPR 的配置。隨著使用多種入射角，系統提供的檢測能力，覆蓋了折光指數（RI）1.33

至超過 1.38。一個 128 元陣列探測器是用來測量的共振相位變化對應入射角範圍，以確保一個合理的連續相位曲線從系統中得到。

Abstract

This project is concerned with the development and optimization of optical sensors based on measuring the phase change of surface plasmon resonance (SPR) effect. The phase sensitive SPR technique provides very high sensitivity performance due to the fact that an abrupt phase jump occurs near the resonance dip, thus resulting in large phase shift with very small change in the sensing medium. A range of different measurement techniques for enhancing system sensitivity have been investigated. Moreover we also studied the phase change characteristics around the SPR dip region by means of simulation in order to explore various approaches for achieving further improvement in sensitivity and as well as wide dynamic range. Since SPR is caused by electron charge density oscillations in metal surface in which the wave momentum required for plasmon wave excitation is always larger than that for free space, an inverted prism-coupling scheme (prism-metal-dielectric) is commonly used and this configuration was also employed in our experimental setup, particularly for the SPR biosensor based on differential phase Mach-Zehnder interferometer configuration. This design primarily operates by taking advantage of the fact that SPR only affects the p-polarization while leaving the s-polarization unchanged. This means that differential phase measurement between the p- and s- polarizations will result in SPR signals that are completely free from any disturbances that are common to both channels. Experimental results obtained from glycerin/water mixtures indicate that the sensitivity limit of our scheme is 5.48×10^{-8} refractive index unit per 0.01^{o} phase change. To our knowledge, this is a significant improvement over previously obtained results when gold is used as the sensor surface. While acknowledging that accurate optical alignment is a crucial requirement for the Mach-Zehnder interferometer and it is often not easy to maintain high degree alignment accuracies in practical situations,

we have developed a versatile and low cost single-beam self-referenced phase-sensitive surface SPR sensing system. The system exhibits a root-mean-square phase fluctuation of ±0.0028° over a period of 45 minutes, i.e. a resolution of $\pm 5.2\times10^{-9}$ refractive index units. The enhanced performance has been achieved through the incorporation of three design elements: (i) a true single-beam configuration enabling complete self-referencing so that only the phase change associated with SPR gets detected; (ii) a differential measurement scheme to eliminate spurious signals not related to the sensor response; (iii) elimination of retardation drifts by incorporating temperature stabilization in the liquid crystal phase modulator. Our design should bring the detection sensitivity of non-labeling SPR biosensing closer to that achievable by conventional florescence-based techniques.

In addition, this project also investigated schemes that might enhance the phase change in the SPR sensor. The "double-pass" and "multi-pass" approaches through which the SPR phase can be amplified upon hitting the sensor surface more than once, have been experimentally studied and successfully demonstrated. A double-pass method can immediately offer two times of phase change as compared to the single-pass one. Accordingly the multi-pass scheme offers a higher then two times phase enhancement. Such improvement in phase detection is extremely important for biosensing applications involving small molecules, small proteins, DNA and etc. Another approach for detection performance improvement is to incorporate a multi-layer configuration for the biosensing surface. In order to improve the dynamic measurement response, we proposed to use a multiple resonant angle measurement approach in conjunction with the single-beam self-referenced phase-sensitive SPR configuration. With the use of many multiple incident angles, the system provided sensing capability that covers a refractive index (RI) 1.33 to over 1.38. A 128-element

array detector was employed to measure the resonance phase change over the range of the incident angles to ensure a reasonably continuous phase response curves achievable from the system.

Acknowledgements

I am very grateful to my supervisor, Professor Aaron H.P. Ho, for his advice and continued support throughout the course of this research work. I wish to express my gratitude to Prof. J.B. Xu and Prof. S.P. Wong for their fully technical support and useful discussion. Special thanks are due to Dr. Y.K. Suen for his helpful discussions and kind support. I would also like to thank Dr. Rolly Ng for his stimulating discussions.

I am also grateful to the technical and secretarial staff of the Department of Electronic Engineering for their assistance at all times. I particularly wish to give thanks to Mr. W.K. Chan, Dr. N. Ke and Dr. W.Y. Cheung for their kind help. Special thanks are due to my fellow research group members: K.C. Lo, W.C. Law, C.L. Wong, Y. Wu and W.W. Wong.

I would finally like to thank my family for their constant encouragement, patience and understanding.

Contents

List of Table and Figures

(a) List of Figures

(b) List of table

CHAPTER 1

Introduction

1.1 Background and motivation

The research on optical based surface plasmon resonance (SPR) sensors has experienced phenomenal expansion in the last two decades especially for chemical and biological interaction detection. The SPR phenomenon was first observed by Wood [1] in 1902 to describe the loss of light projected onto a grating. Fano explained that as an excitation of electromagnetic surface waves and successively calculated its approximated amplitudes in 1941 [2]. Some 50 years later, surface plasmons (SP) were theoretically explained by Ritchie [3]. In 1968 Otto presented the attenuated total reflection (ATR) method to optically excite SP through an air gap [4]. Then Kretschmann proposed a more practical approach, in which optical excitation of SPR through ATR is achieved with a prism coupler [5]. Till today, this method has been the most popular technique for generating surface plasmon waves. First practical SPR systems for detecting chemical and biological agents were demonstrated by Nylander and Liedberg in 1982 and 1983 [6-7]. Since then SPR sensing techniques had attracted lots of attention from the scientific and instrumentation communities, especially for applications highly related to biological applications such as measuring

molecular interactions like antibody-antigen, receptor-ligand, protein-DNA, etc. which are always on top of the medical health care list [8-10]. At the same time, SPR biosensing can naturally provide the two most attractive features, i.e. real-time and label-free measurement. Recently, research and development of SPR have been mainly directed towards biosensing applications which include drug screening, clinical studies, food safety, environmental monitoring, and cell membrane mimicry due to growing demand of such sensors in the healthcare related market. At present, several companies are offering commercial SPR biosensor systems targeting customers conducting basic research in the field of life sciences. In fact, SPR biosensors have already become an indispensable tool for characterizing and quantifying biomolecular interactions in many laboratories. Recently applications of the SPR sensing technique are also expanding into the fields of environmental pollution, chemistry, theoretical physics and experimental optics. Our literature search shows that the annual number of research papers on SPR increased by almost 108 folds, from 6 to 651, during the period between 1990 to 2002 [11-14] which clearly indicates the technological impact of SPR sensors.

SPR sensors offer the capability of measuring very low concentrations of chemical and biological species near on the sensing surface in real time by monitoring the value

of the refractive index in the vicinity of the same surface. Thus, any physical phenomenon at the surface that alters the refractive index will elicit a response. Moreover, since the sensor head is probed by an external optical beam, the front-end of the transducer can possibly operate in extreme environmental conditions such as high pressure and temperature. Until now, the SPR effect has already found applications in a number of optoelectronic devices including light modulators [15,16], optical tunable filter [17,18], gas sensors [19,20], liquid sensors [21,22], bio-sensors [23,24], thin film thickness monitors [25,26] and SPR image [27,28].

The typical SPR devices are using optical waves as the source to couple the photon energy to surface plasmon waves and the sensing configuration is generally referred to as the Kretschmann prism arrangement. We also employed this method in our proposed experiments and we will go through detail later. A thin metal film, normally using gold or silver [11], is coated on one of the surfaces of a prism or alternatively the metal film can be deposited onto a glass slide that is brought into contact with the prism using refractive index matching fluid or gal. This metal film forms the sensor surface on which the sample is placed. Light is launched into the prism, where it is both coupled into the plasmonic wave on the metal film as well as being partially reflected off the metal film to a photodetector. The changes in the amount of light

arriving at the detector represent the sensor output. Such output is affected by the refractive index changes of the sample medium on the metal film and consequently changes the amount of light that couples into the surface plasmon mode on the metal film. Traditional methods for observing SPR phenomenon are primarily concentrated at analyzing the intensity [6, 7] angular [29, 30] and wavelength [31, 32] around the resonance absorption dip. Recently, some researchers paid much attention to SPR phase sensing techniques because it should provide extremely high sensitivity due to the resonant behavior which exhibits a steep phase jump [33]. The first reported experimental setup for SPR phase measurement came from Nelson, Johnston and Yee who successfully demonstrated the measurement of SPR phase by using pure silver as the sensor surface [33] and the measurement sensitivity as good as 5×10^{-7} refractive index units (RIU) has been demonstrated. The drawback of the reported configuration is that it required too many high frequency electronic components as signal splitter and mixers which make the system very complicated. For simplifying phase detection for SPR, an interferometer was first introduced to SPR sensing system by Kabashin et. al. [34, 35]. After that some researchers try to use this scheme to extract the phase information from SPR phenomenon applied on real-time sensing applications [36, 37]. The main drawback of this scheme is that the system is very sensitive to mechanical movements in the optical components. Any mechanical vibrations in the mirrors or

variations of temperature will inevitably cause the optical beam to move and thus leading to phase measurement errors [38]. When gold is used as the sensing surface, because of the smaller free electrons concentration in gold, the best reported sensitivity limit is 3×10^{-7} RIU [11]. However, silver is not a preferred choice in practical sensor applications due to gradual oxidation as a result of chemical reaction with the analyte.

1.2 Objectives and Goals of this Research

In this project, we aim to develop feasible solutions to fulfil the stringent requirements for practical configurations of SPR sensing systems from engineering aspects. It is very important to enable SPR sensors as common and useful tools for both research and industrial applications. In order to achieve this goal, we propose a new scheme to minimize most of the measurement fluctuations that come from the optical system. The main feature of the new scheme is to perform parallel interferometry formed by p-polarization and s-polarization simultaneously. Since the SPR phenomenon only affects the p-polarization, it acts as the probe beam while the unaffected s-polarization serves as the reference. As both the probe beam and reference beam traverse the identical optical path, common-mode noises due to small mechanical vibrations and movements can be eliminated. In addition, a digital signal analysis program has been

developed to eliminate the noise and extract the phase information in real-time.

Apart from conventional interferometry, we can also measure the phase quantities in SPR via polarization approach. In the second part of the thesis, we present another system in which a liquid crystal phase modulator is used to produce a periodic phase retardation change between p- and s- polarized light so that we can extract the phase quantity by measuring the amplitude of interference signal between the two polarized light. A simple single-beam self-referencing SPR phase sensing system has been developed and the differential measurement technique is also employed to enhance the signal to noise.

In the third part of the thesis, we propose an alternative approach to improve the overall system performance, i.e. both sensitivity and dynamic range by simulation and experimental work. First of all, a simple optical scheme is proposed for enhancing the phase response from SPR phase sensing system. One can imagine that the SPR sensing head as an optical phase retarder, when the light beam launches into it with a suitable resonance condition and passes though a round trip, the phase change of the light beam doubles the original. Therefore, a simple phase amplification scheme for SPR phase measurement from both double-pass and multi-pass configurations has

been demonstrated. In addition, we have also studied another scheme to enhance the phase response of SPR sensing system and demonstrate its performance via numerical simulations using Fresnel equations. In order to find other possible ways to enhance the phase response, a simulation model of multi-layer sensing surface is employed to investigate the phase characteristics of SPR. We also propose an optoelectronic technique based on the use of multi-layer configurations to achieve tunable phase SPR sensing with wide dynamic range. Finally, a more practical scheme for dynamic measurement has been demonstrated using a multi-resonance angle measurement technique in conjunction with the single-beam self-referenced phase-sensitive SPR configuration. With many incident angles happening simultaneously, the system provides measurement range that covers refractive indices from (RI) 1.33 to over 1.38. A 128-elements array detector is employed to measure the resonance phase change over a range of the incident angles to provide a reasonably continuous phase response curves.

CHAPTER 2

Literature Review

2.1 SPR phenomenon

The phenomenon of SPR is an excited charge density oscillation propagating along the boundary between a metal and a dielectric. The charge density oscillation can be induced by an optical wave, electro-magnetic wave, or electron beam etc. In this section, we shall discuss the coupling of SPR from an optical light beam and the conditions governing such coupling. The Attenuated Total Reflection (ATR) scheme is a good example to illustrate the principle behind energy coupling from optical wave to SPR. The waveguide and grating coupling schemes will also be discussed.

2.2 Total internal reflection

It can be starting from the phenomenon of total internal reflection of light at the interface of two dielectric media. In this case, the phenomenon is described by Snell's law as shown in Fig. 2.1. Basically, Snell's law stated the relationship between the angles of incidence and refraction according to the following equations:

$$n_1 \sin\theta_i = n_2 \sin\theta_t \quad , \quad \text{if } \theta_t = 90^\circ \text{, so } \quad \theta_c = \sin^{-1}\left(\frac{n_2}{n_1}\right) \qquad (1)$$

where θ_i and θ_t are the incident and transmitted angles, respectively. θ_c is the critical angle. There are three cases to be concerned with and are as follows:

(1) When the angle of incidence is less than the critical angle, the incoming light ray is split into two parts, the reflected ray and the refracted ray (Fig.2.1).

(2) When the angle of incidence is equal to the critical angle, the reflected light beam will propagate along the boundary between the two media.

(3) When the angle of incidence is larger than the critical angle, all of the incident light is reflected back into the high refractive index medium. And so it is called total internal reflection (TIR) (Fig. 2.1).

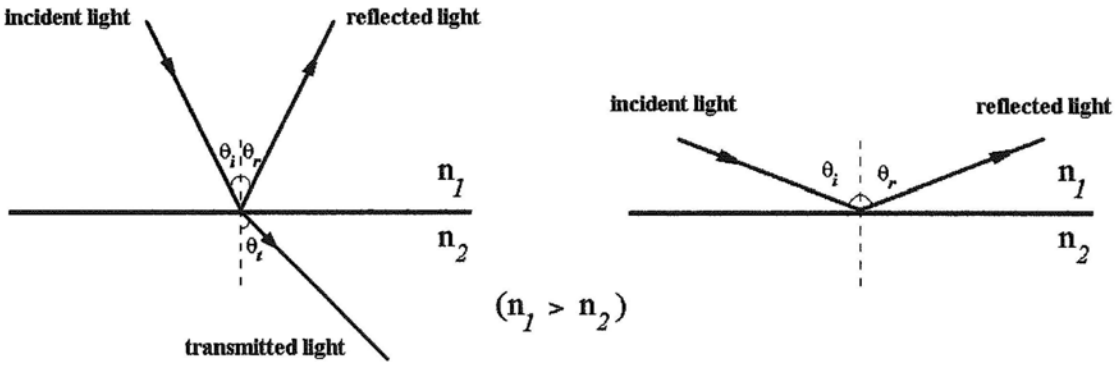

Fig. 2.1. *Light ray incident at an interface between two media, (left) reflection and refraction ($\theta_i < \theta_c$) and (right) total internal reflection ($\theta_i > \theta_c$)*

During TIR, an interesting physical quantity called evanescent wave is also induced at the same time. The net energy of the light beam does not suffer any loss across the boundary of the two media when TIR occurs. But part of the electrical field intensity will continue to propagate into the lower refractive index medium. This evanescent wave has the same frequency as the incident light but its amplitude decreases

exponentially with the distance from the boundary. Also interesting is the phenomenon that the evanescent wave can interact with a layer of conducting material deposited on the boundary interface if the layer is thin enough. In fact the evanescent wave can penetrate into the metal layer and excite electromagnetic waves that propagate along the interface between the dielectric sample medium and the metallic layer. Such wave is due to oscillations of the free electrons in surface of the metal film. These electron oscillation waves are called surface plasmon waves (SPW), and their propagation characteristics are very similar to those of light waves.

2.3 Conditions for Surface Plasmon Resonance

In order to efficiently couple the energy from photons to SPW, the orientation of the incident light of electric field vector must be equal to the orientation of free electrons oscillation on the metal film. This means that SPWs can only be excited by p-polarized light if the metal film. Fig. 2.2 helps us understand the situation better. The optical wave with an electric field normal to the boundary and propagation along the x-axis is called transverse magnetic (TM) polarization. Others refer it as p-polarization. The s-polarized, transverse electric (TE) polarization, cannot couple into the plasmon mode since its electric field vector is oriented parallel to the metal film. For a non-magnetic metal like gold and silver, the surface plasmon mode will

also be p-polarized, and it will create an enhanced evanescent wave field. The energy becomes heat and then it disappears. In Fig. 2.2, we show the excitation of evanescent wave, which has its intensity enhanced because of the presence of surface plasmons and penetrates into the dielectric medium.

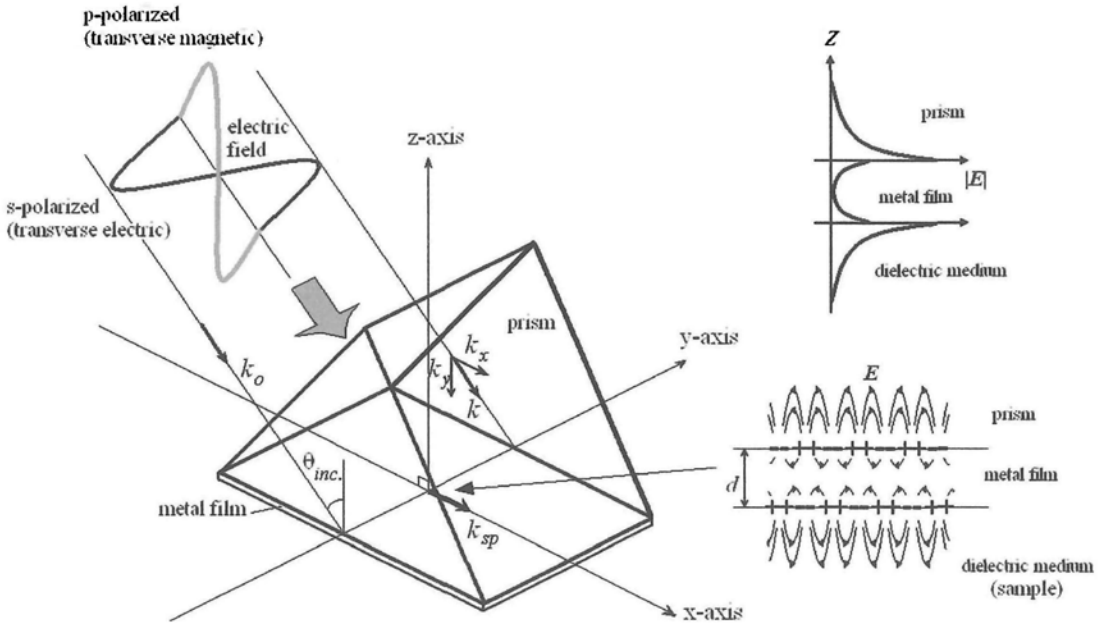

Fig. 2.2. *Definition of p- and s-polarization and the enhanced evanescent wave generated by SPR penetrates of the order of one wavelength into the medium on the opposite side, decaying exponentially with distance from the surface.*

To better understand the conditions of optical excitation of SPR, the momentum of the incident light and the propagation constant of SPW must be considered. In mathematical concept, the momentum of the incident light can be illustrated in the form of a vector. This vector can be resolved conceptually into two components: one is parallel while the other is perpendicular to the metal-dielectric boundary see (Fig.

2.3). The magnitudes of these two components can be modified by varying the incident angle (θ_i). As for the SPW, its propagation is confined to the boundary. The momentum of this wave can be affected by factors such as thickness of the metal layer and dielectric constant of the metal film and its surrounding media. The mathematical treatment will be further described in Section.2.4. SPW can be induced in the conducting materials (e.g. gold and silver) only when the momentum of the incident light vector parallel to the boundary is matched to the momentum of the SPWs. Under such conditions, the energy of the incident light is transferred to SPWs. Therefore the intensity of the light reflected from the surface is reduced. For this reason, the amplitude of the wave vector in the plane of the metallic film depends on the angle (θ_{spr}) at which it strikes the interface. An evanescent (decaying) electrical field associated with the plasmon wave extends for a short distance into the medium from the metallic film. Because of this, the resonant frequency of the SPW (and thus θ_{spr}) depends on the refractive index of the medium. Therefore it can be applied on sensing applications with extremely high sensitivity.

There are two simple ways to modify the momentum vector of the incident light parallel to the boundary matched to the momentum of the surface plasmons. One is to vary the incident angle, which modifies the relative magnitudes of the vector between

the parallel and perpendicular components to the boundary; the other is to change the wavelength, which changes the incident photon energy and thus the momentum. As shown in Fig. 2.3, these two approached are commonly known as angular interrogation and wavelength interrogation. In SPR sensors based on angular interrogation, the light used has a fixed wavelength (monochromatic light). The reflected light beam experience a dip as the incident angle of light is scanned. In here the angle of the SPR absorption dip shift corresponds to the variation of dielectric constant of the sample medium near the metal surface. In wavelength interrogation, the spectral absorption response exhibits an absorption dip and the location of the dip are closely related to the refractive index of the sample medium (see Fig. 2.3). Any refractive index variation in the sample medium will lead to a shift in the absorption dip.

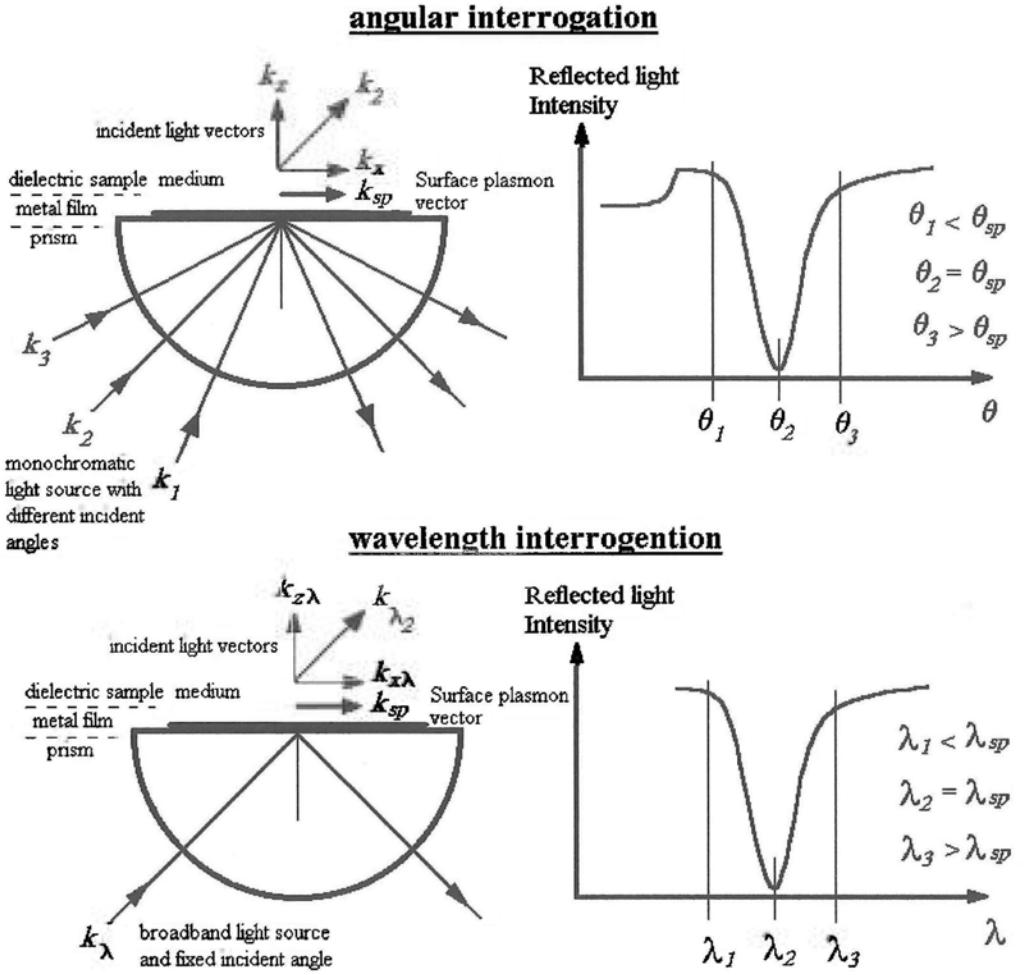

Fig. 2.3. *Angular and wavelength interrogation schemes are commonly used in practical SPR sensing instruments.*

2.4 Wave vectors

To illustrate the SPR phenomenon, resonance conditions are explained with the use of wave vectors. Wave vectors are mathematical expressions that describe the propagation of light and other electromagnetic phenomena. Under SPR, a high concentration of the electromagnetic field associated with the SPW exists in the both media as described in Fig. 2.2. Therefore, the condition for resonant interaction between an optical wave and the SPW is very sensitive to the change of optical

properties in the sample medium. The relationship between the wave vector of the incident light and that parallel to the interface (k_x) is given by the following equation:

$$k_x = k_o n_{glass} \sin(\theta_{inc}) \qquad (2)$$

where k_o is the free space wave vector of the optical wave, n_{glass} the refractive index of the prism, and θ_{inc} the angle of incidence. An approximation of the SPW wave vector (k_{sp}) is given by

$$k_{sp} = k_o \sqrt{\frac{\varepsilon_{metal}\varepsilon_{sample}}{\varepsilon_{metal} + \varepsilon_{sample}}} \qquad (3)$$

where ε_{metal} and ε_{sample} are respectively the dielectric constants of metal and the sample medium. When SPW excitation occurs, we have k_x equal to k_{sp}. Disregarding the imaginary portion of ε, k_{sp} can be rewritten as follows:

$$k_{sp} = \frac{2\pi}{\lambda} \sqrt{\frac{n_{metal}^2 \cdot n_{sample}^2}{n_{metal}^2 + n_{sample}^2}} \qquad (4)$$

where $n_{metal} = (\varepsilon_{metal})^{1/2}$ is the refractive index of the metal and $n_{sample} = (\varepsilon_{sample})^{1/2}$ is the

refractive index of the sample.

Since the dielectric constant of glass prism, metal film and sample are function of wavelength, λ, of light, the conditions (dispersion relation) for surface plasmon excitation at the interface between metal and dielectric are given by

$$n_{glass} \cdot \sin\theta = \sqrt{\frac{\varepsilon_{metal} \cdot \varepsilon_{sample}}{\varepsilon_{metal} + \varepsilon_{sample}}} \qquad (5)$$

The imaginary component of the complex refractive index term is represented by absorbance of light, the unit of measurement commonly encountered in Beer's law for transmission-based absorbance spectrophotometers. The sensing technique that is carried out in the majority of SPR applications detects the real refractive index change due to chemical or biochemical interactions. Therefore, the equations used here will neglect the imaginary component. The other properties of SPW are surface plasmon propagation and the decay length of the field into the metal film and a dielectric layer [39]. The propagation length of surface plasmon is related to the imaginary part of the surface plasmon wavevector, $k_{sp} = k_{sp}^{real} + ik_{sp}^{imag}$, using the following equation:

$$\delta_{sp} = \frac{1}{2k_{sp}^{imag}} = \frac{c}{\omega}\left(\frac{\varepsilon_{metal}^{real} + \varepsilon_{sample}}{\varepsilon_{metal}^{real}\varepsilon_{sample}}\right)^{3/2} \frac{\left(\varepsilon_{metal}^{real}\right)^2}{\varepsilon_{metal}^{imag}} \qquad (6)$$

where dielectric function of metal film can be expressed as $\varepsilon_{metal} = \varepsilon_{metal}^{real} + i\varepsilon_{metal}^{imag}$.

The decay length of the field penetrated into the dielectric medium is of the order of half the wavelength of light involved and the decay length into the metal film is determined by the skin depth.

2.5 Surface plasmon resonance described by Fresnel's theory

In SPR sensors, a simple prism-coupling scheme, Kretschmann configuration, can be used to enhance wave vector momentum to permit coupling to the SPW. To study the reflected light in the Kretschmann configuration, one can start from analyzing the multiple reflections inside a simple three layers system (prism-metal-sample) as illustrated in Fig. 2.4.

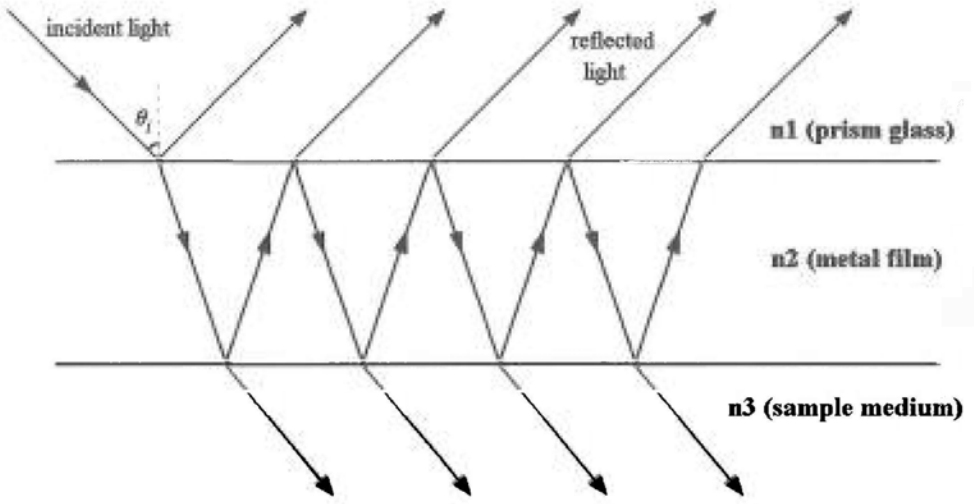

Fig. 2.4. *Ray tracing of multiple reflection of a three-layer system.*

For understanding the SPR reflection curve, a theoretical treatment based on Fresnel`s theory of light reflection in a multilayered system is desirable [40]. For the present

case, the reflection coefficient, r_{123}, of the optical light is given by

$$r_{123} = \frac{r_{12} + r_{23}\exp(2ik_{z1}d)}{1 + r_{12}r_{23}\exp(2ik_{z1}d)} \qquad (7)$$

where d is the thickness of the metal film and r_{ij} is the Fresnel coefficient of s- and p-polarized light between the i-layer and j-layer in the prism-metal-dielectric configuration given by

$$r_{ij} = \frac{Z_i - Z_j}{Z_i + Z_j}, \qquad (8)$$

$Z_i = \varepsilon_i / k_{zi}$ (for p-polarized light)

$Z_i = k_{zi}$ (for s-polarized light)

where k_{zi} is the component of the wave vector in i-layer in the z direction given by

$$k_{zi} = k_o(\varepsilon_i - \varepsilon_o \sin^2\theta)^{1/2} \qquad (9)$$

The reflectivity of prism-metal interface, R, can be expressed by

$$R = |r_{123}|^2 . \qquad (10)$$

and the phase relationship, ϕ, can be written as

$$r_{123} = |r_{123}|e^{i\phi_{123}} \qquad (11)$$

With the aid of above equations, in which the complex values of dielectric constants, ε_I, of all the media concerned may be found from the relevant data books, one can accurately calculate the SPW characteristics and the conditions for SPR. Such

information is extremely useful for performing simulation on experimental data.

2.6 SPR signal detection schemes

The reason why SPR is so useful for sensing applications is two-fold. First, the resonance condition is extremely sensitive to any changes in refractive index. Second, the metal surface can be conveniently made to be in contact with a liquid medium so that any material bound to the surface may lead to a strong signal, thereby making the device very appropriate for detection affinity reactions between any target biomolecular species. The shift of resonance usually accompanies with a change in the coupling efficiency from photon energy to SPW. The theoretical aspects of this effect have been dealt with in previous sections. In this section, we shall present the various techniques for extracting the SPR information, namely the angular [29,30], wavelength [31,32] or phase [33,34] interrogation schemes. Practical systems which are commercially available will also be reviewed.

2.6.1 Angular interrogation

The angular interrogation scheme involves measuring the reflectivity variation with respect to incident angle under monochromatic light illumination. In Fig. 2.5a, we show some numerical simulation result obtained from solving the Fresnel's equations

for a SPR system when we vary the incident angle. The sample medium is water with refractive index 1.3333. The absorption dip where the reflected light intensity is at its minimum is often called the SPR coupling angle (θ_{spr}) and θ_{spr} is shown to change in accordance to a change in the dielectric constant value of the sample medium from 1.3333 RIU(refractive index unit) to 1.3403 RIU (Fig. 2.5b). In this simulation we also need to input other parameters including (i) the light source being a He-Ne laser operating at 632.8nm, the gold film being 50 nm thick and the prism being made from BK7 glass.

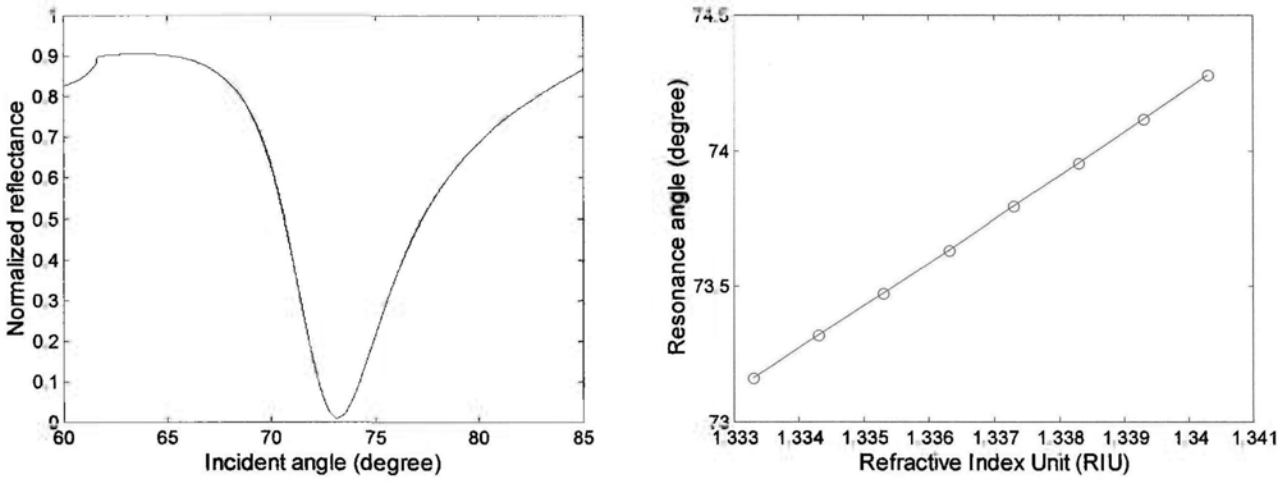

(a) **(b)**

Fig. 2.5. *Typical angular SPR response curve and results: (a) angular SPR absorption dip observed in p-polarized reflected light; (b) shift of the resonant angle caused by variation of refractive index of sample medium.*

2.6.1.1 Commercial systems based on angular interrogation

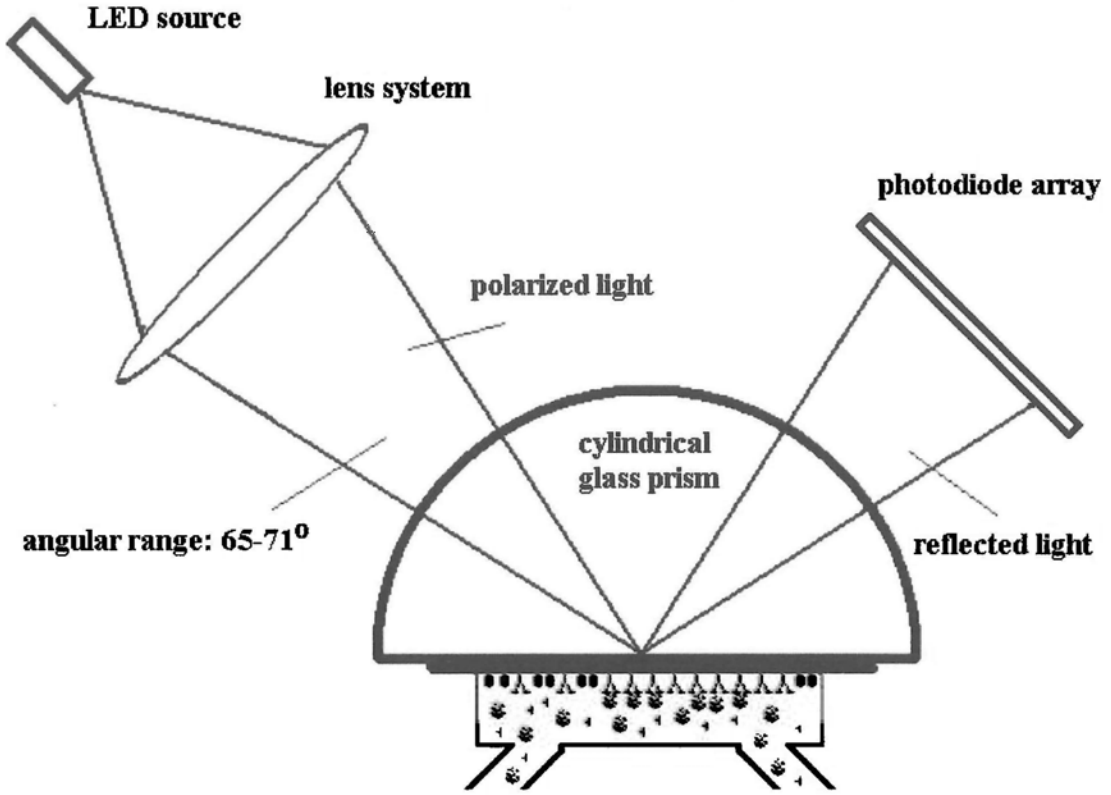

Fig. 2.6. *Diagrammatic illustration of biomolecule detection using a commercial SPR instrument (Pharmacia BIAcore).*

Pharmacia Biosensor AB is the pioneer of commercialization of SPR based biosensing devices. The first product based on angular interrogation scheme was launched in 1990 [41]. Several generations of BIAcore instruments including BIAcore (series 1000, 2000 and 3000) as well as the BIAlite™ (1994), BIAcore X (1996), BIAQuadrantTM, BIAcore S51 and BIAcore J (2001) are in existence in the market. They offer varying degrees of automation and parameter specifications. The optical design of BIAcore AB [42] is shown in Fig. 2.6. When a monochromatic light source is focused onto the metal film, a high-resolution photodetector array detects the variation of reflectivity with respect to angle. This can eliminate the use of high

precise mechanical rotational stage. Most BIAcore systems are designed to work in a refractive index range from 1.33 to 1.36 RIU, making them well suited for sensing of biomolecular interaction in aqueous media.

An alternative SPR biosensor design based on the angular interrogation scheme has been reported by Texas Instruments Sensor Group [43]. Also named as SPREETA, this integrated design employs a novel miniaturization and fabrication methods that allow the entire device to be packed inside one molded transducer module. As shown in Fig. 2.7, a narrow-bandwidth infrared AlGaAs LED is used as a light source [31]. The range of incident angles is controlled by an internal aperture and p-polarized light is selected by using a polarizer. The light beam does not focus at any point on the sensing layer. Instead it is divergent beam covering the entire length of the sensor surface. A photodetector array is required to collect the SPR information. A temperature sensor is integrated into the assembly to provide the feedback for temperature compensation.

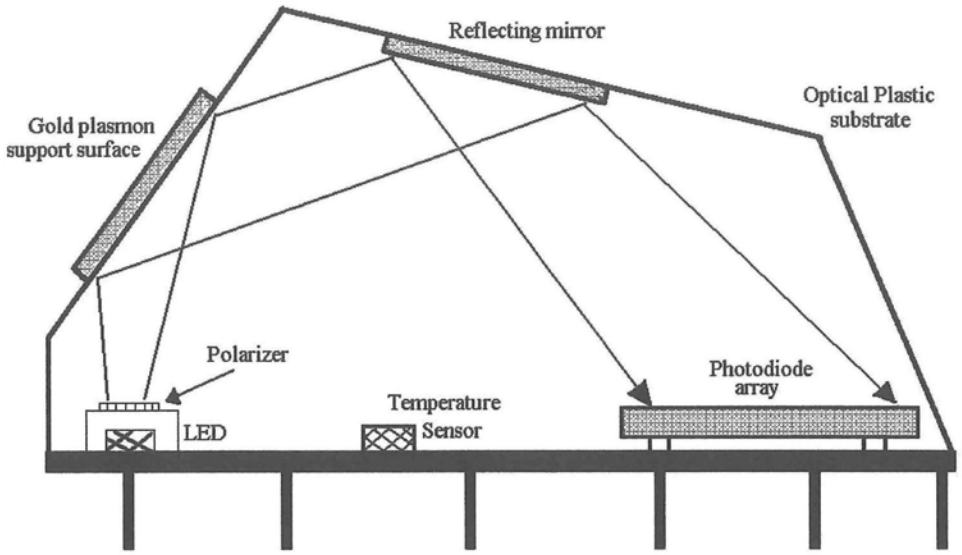

Fig. 2.7. *The miniaturized, integrated surface plasmon resonance transducer (SPREETA, TI-SPR-1) made by Texas Instruments Sensor Group [43].*

Several successful SPR biosensing instruments are already in existence in the market. Table 2.1 provides a brief comparison between the SPR instruments supplied by different manufacturers. The performance of a SPR biosensing system is concerned with its minimum resolvable refractive index change of sample medium. This value is mainly governed by the signal to noise (S/N) ratio and drift of components. Another figure of merit is concerned with minimum sample volume consumed by each measurement. Often bio-related materials do come with very small quantity. In order to ensure minimal sample wastage, microfluidic system may be incorporated. Since the SPR effect itself is a temperature sensitive phenomenon, it is also necessary to active control the ambient temperature. Furthermore, by reducing the size of the entire system, unwanted drift may also be reduced. This can be seen from SPREETA, in

which everything has been packed to a small volume. Some companies, like BIAcore, also supply pre-treated biosensor chips with well-defined surface chemistry to fit different applications.

Table 2.1 Comparison between several commercially available SPR biosensors [42]

Model	*BIAcore 3000* (prism-based SPR)	*IBIS* (vibrating mirror SPR)	*Plasmoon* (broad-range SPR)	*SPREETA* (prism-based SPR)	*IASys* (resonant mirror)
Flow-injection analysis (FIA) system	√	√	×	√	√
Temperature control	√	√	√	×[1]	√
Autosampler	√	×	√	×	√
Microfluidics	√	×	×	×	×
Disposable sensing element	√	√	√	optional	√
Refractive index range	1.33–1.40	1.33–1.43	1.33–1.48	1.33–1.40	--
Minimum sensitivity (RIU)	$3x10^{-7}$	$2x10^{-6}$	$6x10^{-6}$	$3x10^{-7}$	$>1x10^{-6}$

[1]Does not offer temperature control but offers temperature compensations by correcting the signal for temperature fluctuations.

2.6.2 Wavelength interrogation

The wavelength interrogation technique operates through the combined effect due to spectral dispersion (i.e. variation of dielectric permittivity in relation to wavelength) of the prism, metal film and sample medium. In this case, one can use a fixed illumination angle and simply observe the variation of reflectivity at different wavelengths using a spectrometer. A spectral absorption dip signifies the presence of SPR. The spectral location of the dip is defined as the resonant wavelength, λ_{spr}. To

perform the simulation of spectral SPR response curve, one can solve the Fresnel's equations using dispersion characteristics of each of the materials involved. A set of simulated SPR response curves is shown in Fig. 2.8a. The SPR system is the same as the one used in the previous case as shown in Fig. 2.5 and the angle of incidence is 70.0°. If we plot resonant wavelength, λ_{spr}, versus refractive index of the sample medium, as shown in Fig. 2.8b, we can see that the spectral dip shifts towards a longer wavelength as the refractive index of the sample medium gradually increases.

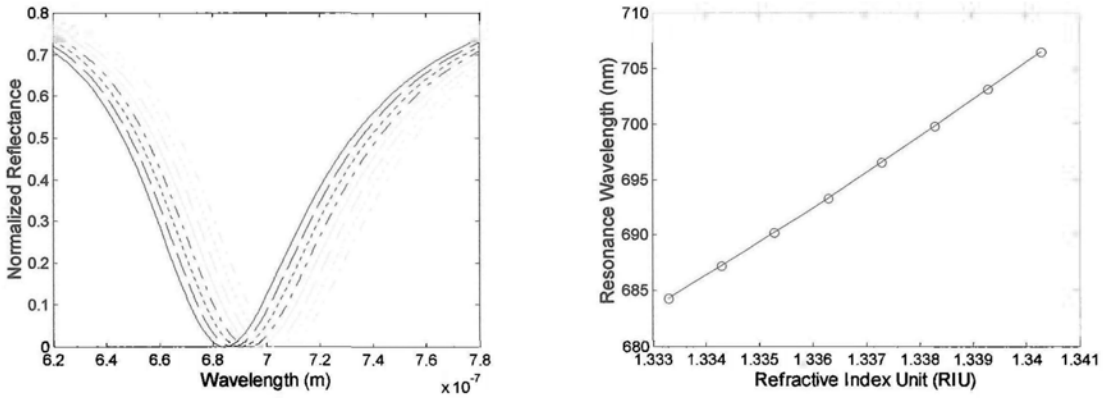

Fig. 2.8. *Simulation results of SPR wavelength interrogation: (a) typical spectral SPR response curves; (b) plot between resonant wavelength of absorption dips as obtained from simulation curves shown in (a) and refractive index of sample medium.*

2.6.2.1 Practical systems based on wavelength interrogation

For the hardware configuration of wavelength interrogation, both ATR prism coupler and waveguide coupler schemes may be used. However, most of the reported systems are based on ATR prism coupler scheme. The difference is that the light source used a

broadband light source and the incident angle of light is fixed. This makes the optical instrumentation less complicated since there will be no need for any rotational stage for angular scanning. As for the broadband light source, a halogen lamp may be a good choice as long as proper calibration of the spectral characteristics has been conducted during the set up stage of the instrument. Typically an optical fiber is used for carrying the light source to the entrance of the sensor head [21,25]. Apart from flexibility, optical fiber offers inherent beam profile shaping and isolation of heat from the lamp. One important point must be mentioned is that the beam entering the prism has to be collimated in order to ensure a sharp spectral dip which provides minimum measurement error. The exit beam from sensor head is then analyzed using common spectrometer. The resolution of the spectrometer also defines the sensitivity limit of the instrument. As an effort to further simplify the optical design of wavelength interrogation scheme, we previously reported that a white light emitting diode may be taken as a direct replacement of the halogen lamp and fiber coupler system [44]. The approach has significantly reduced the size and cost of the instrument and hence improved the marketability of wavelength interrogation SPR systems. As for the spectrometer, high resolution ones are the obvious choice, but cost is an unfavorable factor. It has been suggested that low resolution spectrometers (16-channel) may be used instead of high resolution ones (1024-channel) without much compromise in

performance. The rationale is that SPR response curves are fairly well-defined absorption curves that can be fitted with a set of invariant curve-fitting parameters. It has been shown that the switch to 16-channel spectrometers can still provide a measurement resolution of the resonant dip of 0.02nm [44]. With 0.02 nm as the wavelength measurement resolution, simulation results indicate that the sensitivity limit of wavelength interrogation scheme is 2×10^{-5} RIU when the spectral window is around 630nm [11]. Longer operation wavelength can provide a better sensitivity [45]. An improved sensitivity resolution of 1×10^{-6}RIU can be achieved by operating the system in a spectral region around 850nm.

In fact wavelength interrogation has an advantage over waveguide SPR sensing devices since this scheme can be operated on fixed incident angle of light. Based on the linewidth of broadband light source wide enough, the wavelength interrogation method can provide a wide sensing range on waveguided coupler scheme. It is an important parameter for general applications use of SPR sensing devices. Fiber SPR sensing devices can provide the highest degree of miniaturization as small as ~2μm to be demonstrated [46]. The small physical size of SPR sensing device can provide highly potential on widely real application. The waveguided devices, optical fibers and optical waveguided, are commonly designed as SPR sensors by coating a thin

metal film on around the exposed core. The sensitivity of these sensors based on wavelength interrogation typically can achieve the level as 10^{-5} RIU to 10^{-6} RIU with a wide sensing range [21,47,48]. One of the reasons limited the system sensitivity is that the inherent modal noise in multimode fibers causes the strength of the interaction between the fiber-guided light wave and SPW to fluctuate. In order to break through the limitation, a single-mode polarization-maintaining optical fiber was proposed as the substrate. This fiber optic SPR sensor is successful demonstrated to resolve the change of refractive index as low as 4×10^{-6} RIU under moderate fiber deformations [48]. The waveguided coupler scheme does not only applied on fiber optics but it also have been applied on multi-channel planar light pipe sensing substrate [49], channel waveguide [46] and miniaturization of side active retro-reflector [21].

2.6.3 Phase interrogation

The fact that SPR is a resonant effect also means that as the system goes in and out of resonance, the phase of the incident optical wave experiences a massive jump. The steepness and extent of the phase jump depends on the materials chosen and the thickness of the metal film. It is interesting to note that since SPR occurs only in p-polarization and not s-polarization, any phase change caused by SPR actually

appears as retardation variation on the beam. i.e. The optical beam goes from linearly polarized to elliptically polarized. Nonetheless, it has been reported that, because of the very steep phase change across resonance [50,51], the measurement of SPR phase leads to the best sensitivity factor in comparison to angular and spectral techniques. Fig. 2.9 shows a set of simulated response curves for different thickness of gold film thickness. The ATR prism substrate is BK7. The conditions of the simulation are λ = 633 nm and $\theta = 73.5°$, with the sensor structure same as the previous examples.

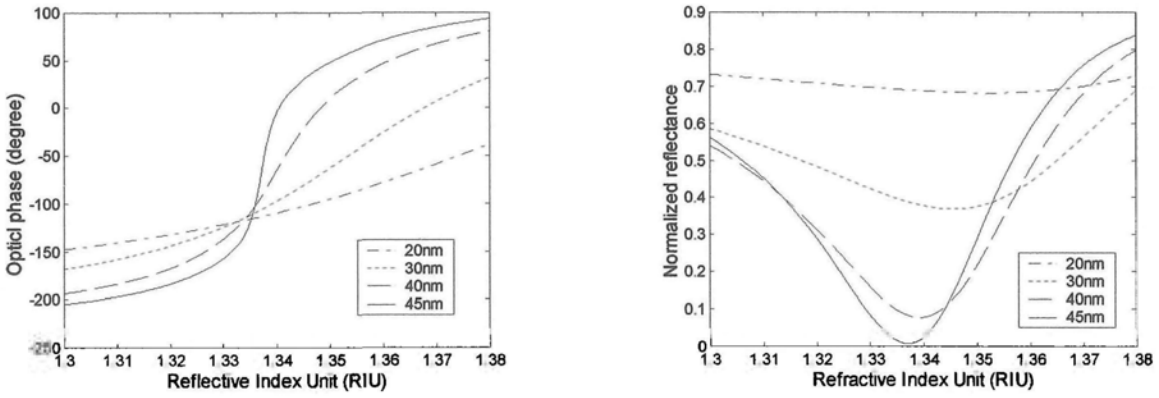

(a) (b)

Fig. 2.9. *SPR Phase and reflectivity responses versus refractive index with various thicknesses of gold layer from 20nm to 45nm, (a) phase; (b) amplitude.*

For achieving optimal phase response of the SPR sensor, we need to consider two important parameters, which are the incident angle of the light bean and the gold film thickness. For example, if the sample medium is water (1.333RIU), the incident angle will be required $\theta = 73.0°$ and the gold film thickness 47nm. If the sample medium is 1.37RIU, the incident angle will be required $\theta = 79.3°$ and the gold film thickness

44nm.

2.7 Practical systems based on phase interrogation

The first practical SPR phase sensing system reported by Nelson et al in 1996 was based on a heterodyne phase detection scheme [33]. An acousto-optic modulator (AOM) frequency modulates a 45° polarized HeNe laser at a frequency close to 100 MHz. In this setup, the AOM modulated input beam is split into two parts, one as the reference while the other as the signal beam, which goes through the ATR prism sensor head. The phase difference between the signals detected from the reference and signal beams provides the phase change induced by the SPR effect. The phase change can then be related to the refractive index of sample medium. The refractive index resolution of this system has been reported to be as high as 5×10^{-7} RIU. An alternative design based on the use of a Zeeman laser, in which the laser itself provides a built-in signal modulation, has simplified the system considerably [52]. The SPR phase detection technique has also been applied to fiber SPR biosensor with encouraging success [35]. This system offers a sensitivity factor of 2×10^{-6} RIU. Other configurations based on the Mach-Zehnder interferometer have also been reported [35,53-56]. In particular, we recently demonstrated a differential phase system in which a sensitivity factor as high as 5.5×10^{-8} RIU is possible [54]. Fig. 2.10 shows the optical setup of our design. The main contribution of this design is that both the

reference and the signal beams go through identical optical paths except for the short region between the output Wollaston prism and the two photodetectors. This ensures that much of the noise present in the system will be common to reference as well as signal channels. The phase difference between the two channels will eliminate such common-mode fluctuations. An experimental stability of ~0.01° phase fluctuation over a period of one hour has been demonstrated [55]. Apart from much increased sensitivity factor, another very important benefit is the ease to perform imaging, which means that a large number of sensor sites may be monitored simultaneously. Finally the use of Mach-Zehnder interferometer in a channel waveguide SPR sensor structure also highlights the promising possibility of building very compact biosensors on a planar waveguide device [56].

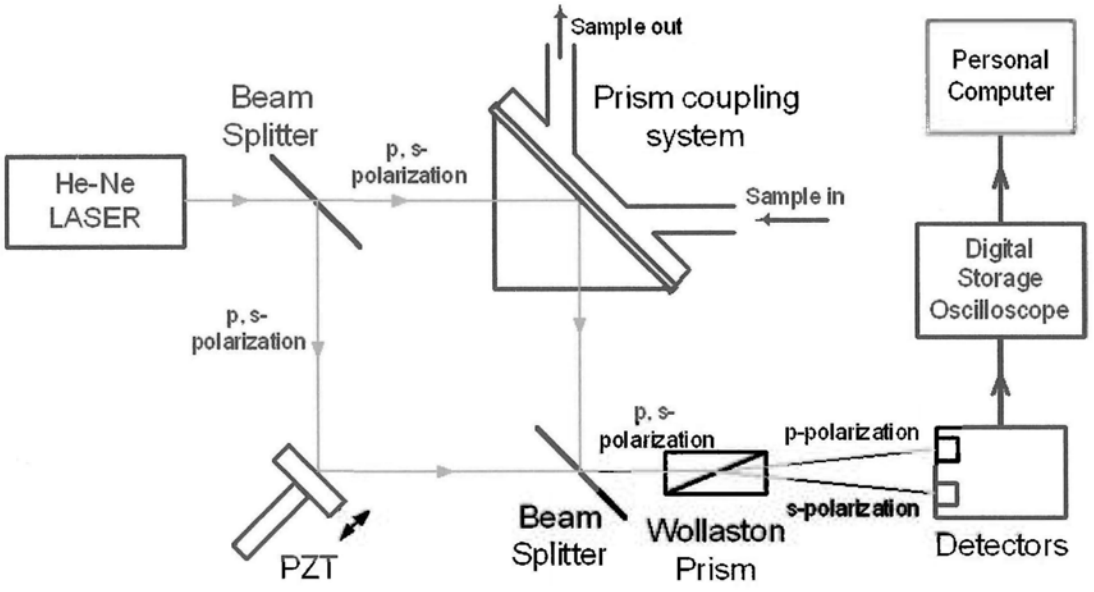

Fig. 2.10. *Differential phase SPR sensor based on the Mach-Zehnder interferometer configuration* [55].

2.7 Biomoleucle sensing applications

Application of SPR based sensors to biomolecular interaction monitoring was first demonstrated in 1983 [7]. The first bio-specific interaction real-time analysis method appeared [57] in 1994. Since then, extensive experiments have been performed on all kinds of bio-related species to establish better understanding of binding reactions. Literally most of the common bio-molecules related life science and possess some form of specific binding would have been tried one way or another. The main reason behind the expansion is that SPR biosensing is a real-time and label-free technique, thus making it well suited for studying reaction kinetics and affinity constants. Affinity-based biosensor systems commonly make use of an immobilized molecule with specific recognition properties to monitor binding events near on the sensing surface. A simple illustration is shown in Fig. 2.11. Biological binding reactions such as antibody/antigen, ligand/receptor and protein/DNA interactions are amount the commonest experiments. While the general effort on studying interaction processes between various biomolecular species is ongoing, there is also the trend to push for the detection of low molecular weight materials such DNA. Recently researchers also use SPR sensing technology for drug screening and clinical studies [58-61], food and environmental monitoring [42,63-66], and cell membrane mimicry [67-71].

SPR sensors have in fact become standard biophysical tools in both academic and

industrial research laboratories. Some manufacturers nowadays provide different levels of optical SPR biosensor solutions, from complete to simple miniaturized modules, to suit customers' needs. Table 2.2 provides a list of SPR sensor manufacturers and their web sites.

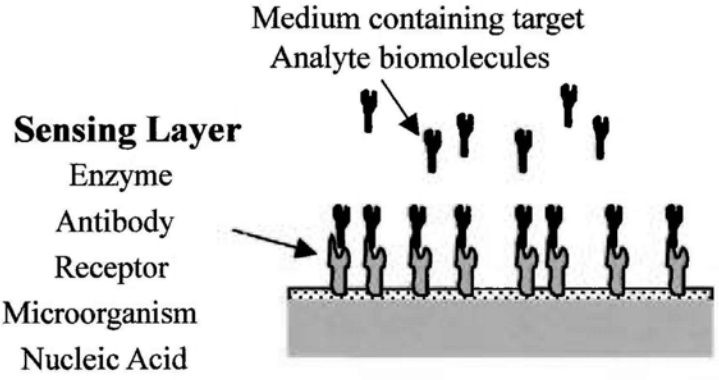

Fig. 2.11. *Typical biosensor surface containing a binding sensing layer which has specific affinity towards target analyte bio-molecules.*

Table 2.2. *Information of commercial SPR sensing instruments and their websites* [72]

Manufacturer	Instrument	Website
Biacore AB	BIACORE 1000, 2000, 3000, T100,...	www.biacore.com
IBIS Technologies	IBIS I, IBIS II	www.ibis-spr.nl/homeframe.htm
Texas Instruments	Spreeta	www.ti.com/snc/products/sensors/spreeta.htm
Analytical μ-Systems	BIO-SUPLAR 2	www.micro-systems.de
Artifical Sensing Instruments	OWLS	www.microvacuum.com/products/biosensor
Farfield Sensors Ltd	*Ano*Light Bio250	www.farfield-sensors.co.uk
Luna Innovations	Fiber optic prototype	www.lunainnovations.com
ThreeFold Sensors	Label-free prototype	http://ic.net/~tfs
HTS Biosystems	SPR array	www.htsbiosystems.com
SRU biosystem	BIND	www.srubiosystems.com

Complete commercial solutions of SPR biosensors consist of three parts: hardware, data analysis program and sensing chip coated with specific surface chemistry. As far as hardware is concerned, the instrument is required to have high sample

measurement speed, fully automation and high sensitivity factor. For the data analysis software, a curve fitting process is often used to study the biomolecular interaction model such as (A+B=AB) etc and then calculate the reaction rate constants and the binding coefficients. Software simulations may help user obtain a best reaction model to fit the experimental results. In order to improve measurement consistency, some manufacturers supply surface treated sensing chips for most common applications. Table 2.3 provides a list of the surfaces available from BIACORE and affinity sensors together with their general applications.

Table 2.3. *Available SPR sensing surfaces* [73]

Chemistry	General Application
(BIACORE)	
CM5 – carboxymethyl dextran	Routine analysis
SA – streptavidin	Biotin conjugation
NTA – nickel chelation	His-tagged conjugation
HPA – hytdrophobic monolayer	Create hybrid lipid bilayers
C1- flat carboxymethylated	No dextran
J1 – gold surface	User-defined surface
L1- lipophilic dextran	Capture liposomes
(Affinity sensors surfaces)	
CM- carboxymethyl dextran	Routine analysis
Hydrophobic planar	Create lipid monolayers
Amino planar	Alternative coupling chemistry
Carboxylate planar	No dextran
Biotinylated planar	Streptavidin conjugation

From a literature review conducted for commercial optical biosensors in Year 2000

[74], the majority of reported articles (over 500 articles) were performed by using BIAcore systems and the investigation included proteins, antibodies, cell surface receptors, peptides, small molecules, oligonucleotides, lipids and self-assembled monolayers, extracellular matrix, carbohydrates, particles and viruses, crude analytes, and other configurations. Some 50 articles reported results obtained using SPR biosensing instruments from other manufacturers such as the IAsys (based on based on evanescent waves similar to SPR), IBIS, Spreeta etc.

As for reported cases of biomolecular sensing using SPR, the majority of the experiments have been performed are on biological binding reactions such as antibody/antigen, ligand/receptor and protein/DNA interactions are amount the. While this general effort on studying interactions is ongoing, there is a growing trend to push for the detection of low molecular weight materials for which SPR has been thought to be not a suitable choice due to weak responses. As detection instrument improves and better choice of bio-molecules has been adopted, real-time label-free detection of low molecular weight species is now becoming possible. Recently researchers also expand SPR sensing technology to drug screening [75,76], clinical diagnostics [58-61], food and environmental monitoring [42,63-66], and cell membrane mimicry [67-71], which are more related to healthcare related applications.

Chapter 3

Optical Excitation Schemes of Surface Plasmon Resonance

3.1 Optical excitation schemes of Surface Plasmon (SP)

We know that if the energy of a photon is to be transformed into surface plasmon (SP), its angular frequency and momentum must match with those of the plasmon. For optical excitation of SPs, three simple coupling schemes, ATR prism coupler, grating coupler and waveguides coupler, are commonly used to transfer energy from photons to SPR.

3.2 Coupling scheme using attenuated total reflection (ATR) optical prism coupler

This ATR optical prism scheme has been widely used for sensing applications. The incident light is required to pass through a dielectric medium, typically plastic or glass (usually in the form of a prism), which refractive index n is greater than the surrounding medium. In order to modify the wave vector of the light, a higher refractive index medium is employed to decrease the phase velocity (increasing the momentum) of the photons. Since the refractive index of prism, n_p, is related to the propagation speed of light, v, through $n_p = c/v$, it can be predicted that the phase velocity in high refractive index medium is smaller than the light speed in air, c [77]. The momentum of photons can therefore be increased simply by using a higher

refractive index of the glass. If a metal film is coated on the prism surface and its thickness is thin enough, it is possible to excite a SP when the momentum of photon is equal to the propagation vector of SPW ($k_x = k_{sp}$). This requirement is depicted in Figure 3.2.

For the conditions of resonance, excitation of SPs can only occur under total internal reflection so that the angle of incident must be greater than the critical angle, θ_c. So the SP is excited evanescently and this is called ATR coupler scheme. The evanescent field can penetrate through the metal film thus leading to the formation of SP at the metal-dielectric interface.

Two schemes using the ATR effect for coupling energy from photons to surface plasmons have been reported. Fig. 3.1a shows the one proposed by Otto in 1968 [4], while Fig. 3.1b shows a second more practical scheme reported by Kretschmann [5]. As shown in Fig. 3.1a, a small gap, typically one wavelength wide, is maintained between the metal and the prism surface. When total internal reflection occurs at the interface, the evanescent field created at the interface between the prism and metal decays exponentially in the dielectric medium (sample) and excites the surface plasmon wave at the interface between dielectric (sample) and metal surface. Since the condition of surface plasmon resonance is very dependent on the width of the gap,

this configuration is suitable more for studying SPR in solid phase media and physical phenomenon. For biosensing applications, this method is relatively less suitable due to the fact that it is very difficult to control the thickness of a thin liquid layer in nanometer scale. If the distance between the prism surface and the metal becomes to larger, it reduces the efficiency of coupling between the SPs and the incoming light beam. Because of these factors, the Otto configuration is not frequently used in real sensing system [5,77].

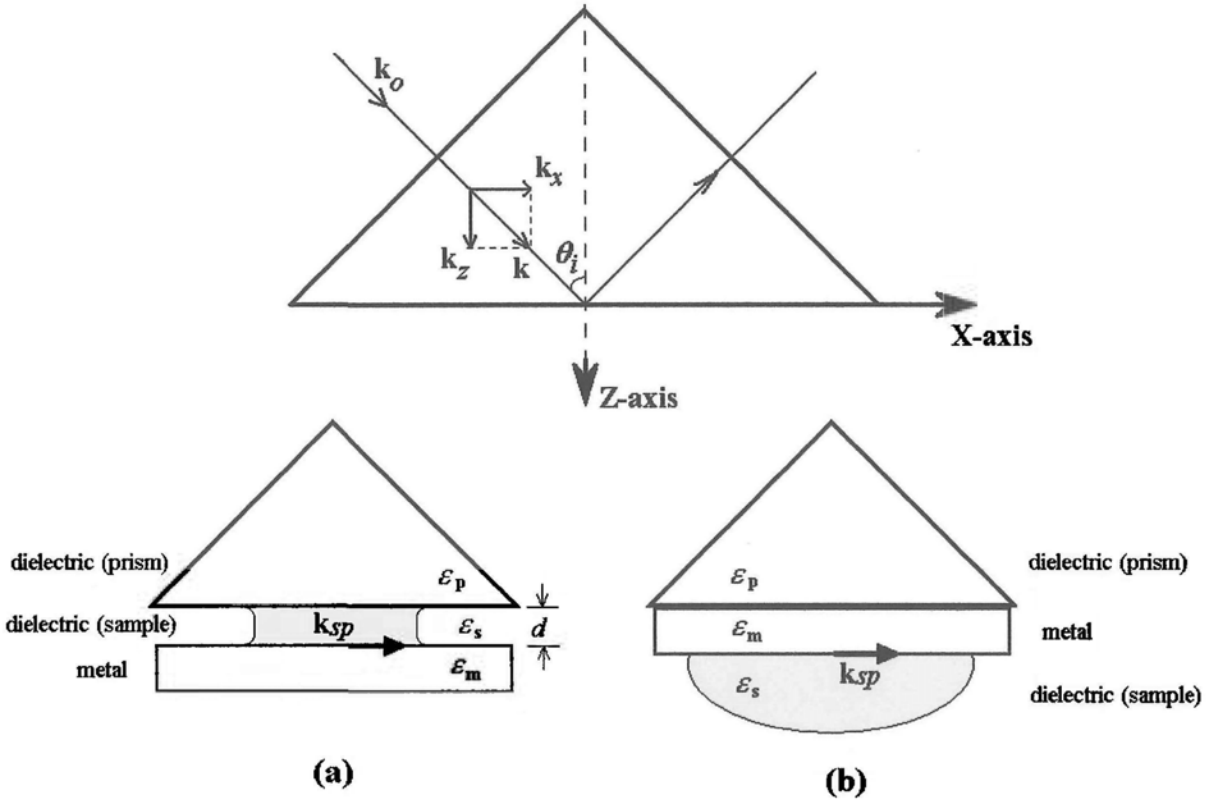

Fig. 3.1. *Optical configurations for SPR (ATR method). In the Otto arrangement (a) the dielectric sample lies between the prism and the metal surface. (b) Metal coating deposited on the prism and SPs is coupled by evanescent field, so called Kretschmann configuration.*

An alternative configuration was introduced by Erwin Kretschmann in 1971 and since

then this has become a very common approach for optical excitation of surface plasmons (Fig. 3.1b). The evanescent wave penetrates into both sides of the thin metal layer and directly excites SPs. The evanescent field created at the interface between the prism and the dielectric medium decays exponentially into the metal film and the surface plasmons were excited at the boundary between the metal and the dielectric medium as shown in Fig. 2.2. The reasons for the Kretschmann configuration being so widely used in real applications over the Otto configuration are due to its higher efficiency in SP coupling and the generated SP is in direct contact with the analyte medium. To achieve specific configuration of a thin metal film deposited on the prism base is much easier than to make a precise gap in nanometer scale as required by the Otto configuration. It is important to mention that unit now the Kretschmann configuration plays an important role in the development of practical SPR measurement systems for chemical and biological sensing applications.

3.3 Coupling scheme using grating couplers

The operation of grating couplers may be explained by first showing the dispersion relations of a SPW propagating in a planar metal-dielectric interface as shown in Fig. 3.2. The wave vector of light is always less than the wave vector of the SPW for all frequencies. As previously explained, SPW can only be excited when the wave vector of the incident light is enhanced. Apart from using a high refractive index prism,

which has been explained in previous sections, one can increase the value of wave vector using a scattering effect. When the optical beam is allowed to impinge on a periodically distorted surface, as shown in Fig. 3.3, optical diffraction will occur. This will generate a series of diffracted beams, which exit the surface at angles very different from the angle of reflection, thus indicating that the wave vector has been modified by the grating structure.

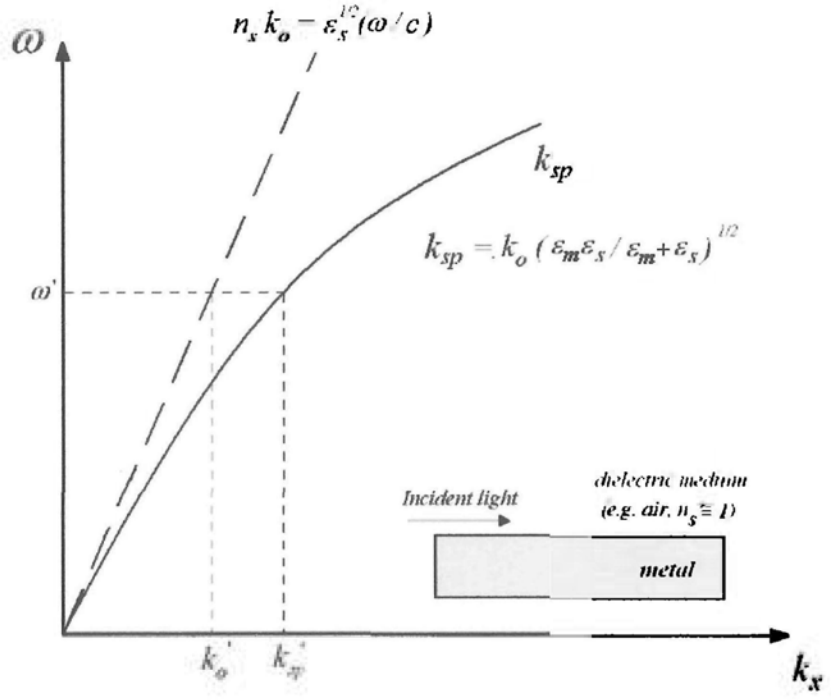

Fig. 3.2. *The dispersion curves are describing a mismatch problem of the momentum between incident light and SPW propagating in a planar metal-dielectric interface, Ksp, where the permitivities of the dielectric and metallic media are* $\varepsilon_S = n_S^2$ *and* ε_m, *respectively, the wave vector of the surface plasmon wave is* k_{sp}, *the wave vector of the incident light is* $k_o = (\varpi/c)$. *The dashed line shows the maximum possible value of wave vector of an incoming photon propagating paralle to the interface. The momentum of SPW* ($\hbar k_{sp}'$) *is always larger than that of free space photon* ($\hbar ko'$) *of the same frequency* (ω').

In here a portion of the wave vectors may propagate along the x-axis in which the grooves of a diffraction grating are oriented perpendicular to the plane of incidence [78]. The component of diffracted light along the interface (x-axis) is altered as follows:

$$k_{xm} = \frac{2\pi}{\lambda} n_S \sin\theta_i + mG = k_{sp} \qquad (12)$$

where n_s is the refractive index of dielectric medium (sample), θ_i is the angle of incidence of the optical light. m is an integer, G is the grating wave vector ($G = 2\pi/\lambda_G$), λ_G is grating constant (the pitch of the grating) and k_{xm} is the wave vector of the diffracted optical wave. It is assumed that the dispersion properties of the SPW are not disturbed by the grating. The momentum conservation for an optical wave exciting an SPW via a diffraction grating may be rewritten as [79]:

$$n_S \sin\theta_i + m\frac{\lambda}{\lambda_G} = \pm\sqrt{\frac{\varepsilon_m \varepsilon_S}{\varepsilon_m + \varepsilon_S}} \qquad (13)$$

where the sign on right side of the equation '+' corresponds to the diffraction order m>0 or '–' corresponds to diffraction order m<0. Similar to prism coupler scheme, the energy of incoming photon is coupled to the surface plasmon in grating-based optical structures can be observed by monitoring the variation of the minimum reflectivity at a certain incident angle with a fixed wavelength [80] or the wavelength at a fixed angle of incidence [79-84] or the reflected light intensity variation at SPR [85].

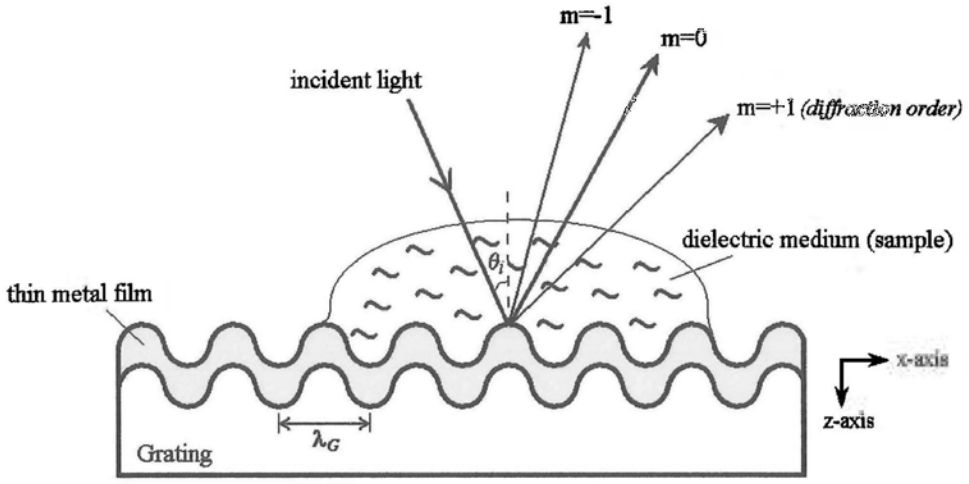

Fig. 3.3. *Typical grating coupler-based SPR configuration*

3.4 Coupling scheme using optical waveguides

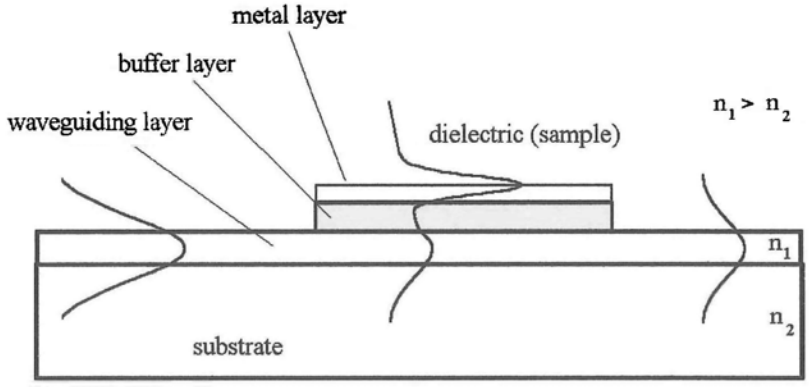

Fig. 3.4. *The concept of optical waveguides is based on the total internal reflection phenomenon. An optical wave propagates through the planar waveguide and couple some of its energy into a guided surface plasmon coupled mode and back [86].*

In optical waveguides, photons can propagate for a long distance with minimal loss. The use of optical waveguides in practical SPR sensing system offers several advantages: small size, ruggedness and the ease to control the optical path within the sensor system. In principle, SPW excitation in an optical waveguide structure is similar to that in the ATR coupler scheme. When a thin metal film is deposited on a

waveguide as shown in Fig. 3.4, the evanescent wave generated by TIR may be able to penetrate through the metal layer and interact with the dielectric medium above. This means that it is possible to excite a SPW at the outer surface of the thin metal film if the SPW and the guided optical mode are phase-matched. Theoretically, the best achievable sensitivity factor of waveguide-based SPR devices can be the same as that of corresponding ATR configurations when they put under similar operation conditions.

For practical systems, step index optical fibers may be used. A simple modification of the fiber is required for generating the required SPW. A short length of fiber cladding is polished away in order to expose the core. An evanescent wave may leak out from the core. When a thin metal layer is deposited on the polished surface, the evanescent wave will generate SPW on the outer surface, leading to a simple miniaturized fiber-based SPR sensor device.

Despite its simplicity, the waveguide SPR sensor scheme does have its limitations. Since the incident angle at the metal-dielectric interface cannot be changed, the measurement range (i.e. dynamic range) of such sensors may be limited. For minimizing this problem, performance parameters including metal film thickness,

choice of material for the metallic layer (e.g. gold versus silver), and wavelength of the light source should be carefully selected. For this reason, the wavelength interrogation technique is commonly used in waveguide SPR sensing devices. A broadband light source illuminates the fiber end and the SPR response can be obtained by analyzing the spectral attenuation characteristics of the exit beam [87]. It should be mentioned that when one uses a multimode instead of a single mode optical fiber, the output signal tends to fluctuate because mechanical vibration can disturb the modal distribution of light in the fiber and this effect is particular strong in the sensor surface [88,89]. Once the procedures are right, optical fibers can be easily adapted to SPR sensors. The first practical fiber-coupled SPR system was demonstrated by Jorgenson and Yee [32] in 1993.

CHAPTER 4

Experiment

4.1 General Interferometric SPR Phase Detecting System

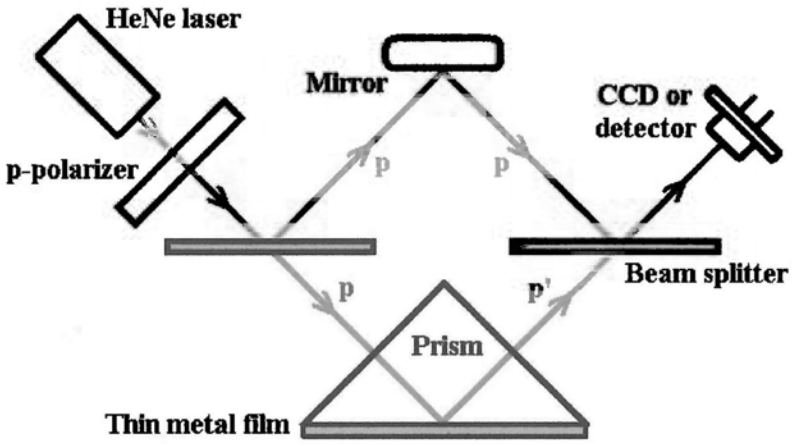

Fig.4.1. *SPR phase measurement system reported in [34,35].*

A Mach-Zehnder interferometer is a well-known method used to determine the relative optical phase shift of the reunited beam coming from the two splitted optical light paths known as the probe and reference arm. The p-polarized light beam from the coherent light source is collimated and divided into the probe and reference arm by the first beam splitter. The beams recombine to interfere with each another by the second beam splitter. The phase information between the probe and reference arm can be observed from a resultant interference fringe or pattern. The SPR phase measurement system shown in Fig. 4.1 is reported by Kabashin et al [35]. A Mach-Zehnder interferometer is employed to extract the phase information. Basically, a Mach-Zehnder interferometer is constructed by using two beam splitters and two mirrors. The prism, SPR sensor in the Kretschmann arrangement, is the mirror in the probe arm of the interferometer. In real practice, the condition of SPR sensing is not set to the optimum point for coupling of optical wave to surface plasmon waves (SPW)

because there is theoretically no light reflected so no signal can be detected. Therefore the SPR configuration is usually adjusted with an offset from the optimum coupling condition. When any small change of refractive index in the sample medium occurs, the resonant condition will be also modified. It includes the phase of the reflected light beam coming from the sensing head. If an interference pattern is obtained by recombining the reflected probe beam and reference beam at the second beam splitter, any refractive index change on the sensing surface will be translated into localized fringe movements. It may give a very high sensitivity on the SPR phase measurement, estimated as $\Delta n = 4\times10^{-8}$RIU. The main drawback of this design is that all the optical components for the probe and reference arm have to be very stable. Any small vibration of the optical components can cause a short-term phase fluctuation. If any temperature difference between the optical components or small mechanical draft of the optical mounts exists, a long-term phase draft error will occur. In this thesis, a new differential phase detection technique for the removal of parasitic drifts and noises is proposed and implemented.

4.2 Experimental Setup of Scheme I

Experimental Scheme I: Differential phase-sensitive surface plasmon resonance (SPR) biosensor based on Mach-Zehnder configuration

4.2.1 Materials

A) Optical components

1) He-Ne laser (632.8nm) with 10mW optical power output
2) Two beam splitters (50:50)
3) Sample flow chamber
4) 60° equilateral BK7 glass prism
5) Piezoelectric transducer (PZT)
6) Mirror
7) Wollaston prism
8) Two photodetectors

B) Electronic components

Programmable functional generator (HAMEG, Model# HM8130)

PZT controller (THORLABS, Model# MDT694)

Digital oscilloscope (LeCroy DSO, Model# LT264)

Personal computer

Other components including photo-detectors and chamber flow cell are homemade because of our special requirements. Moreover, the gold transducing layer of the SPR module is prepared in-house and the thickness of the film is nominally ~40-55nm. We use a sputtering deposition technique. It should be noted that the sensitivity of the system is greatly affected by the quality of the components as also pointed out by Yee [33].

4.2.2 In-House device fabrication

(a) Chamber flow cell

The flow cell chamber was made from a chemically inert material called polytetrafluroethylene (PTFE). In order to smooth flow of fluid in and out of the flow cell with as little sample consumption as possible, the depth of the chamber was designed to be 250μm. The design of the chamber is that the inlet of fluid flow is in the lower region, while the outlet is in the upper region. This design aims to avoid air bubble formation inside the chamber. Moreover, we have to ensure that the chamber does not have any leakage when sample fluid is being injected into the flow cell. The contact region between the flow cell and the prism must be well polished to ensure a good seal. The metal coated prism must be firmly secured onto the chamber by screws. In order to prevent the unwanted deformation of the PTFE, an aluminum supporting structure is implemented as shown in Fig. 4.2.

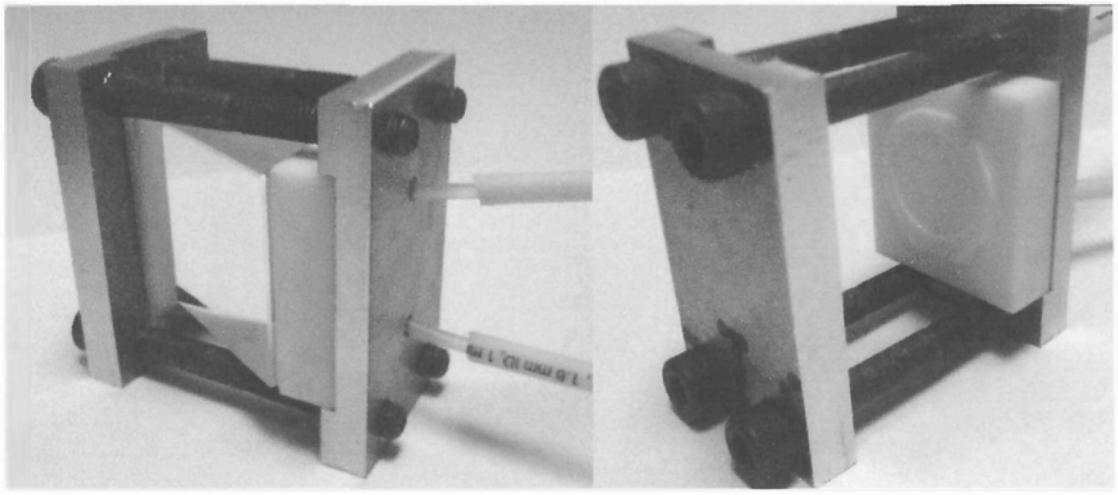

Fig.4.2. *Flow cell of sensor system*

(b) Photodetectors

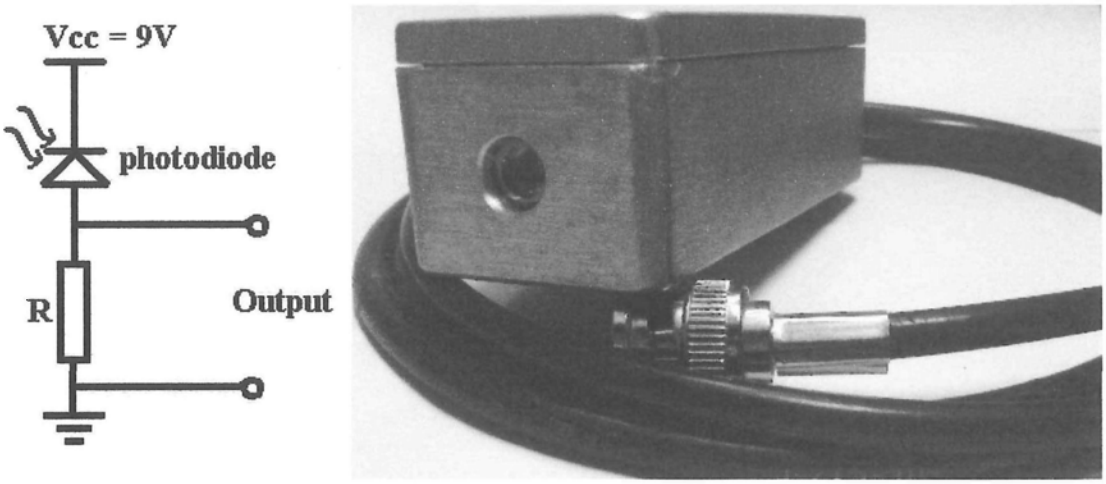

Fig.4.3. *Photodetector module and its circuit*

The photographs of the photodetector is shown in Fig.4.3. The unit consists of a 9V battery, photodiode (model: OSD15-5T), load resistor (R=10kΩ±5.0%), coaxial cable (length of cable (RG58): ≤ 1.1m), BNC male connector and aluminum case. The silicon photodiodes is designed to be active for the spectral range of 430 to 900nm. Here we use the photovoltaic mode with a reverse bias in the photodiode for achieving lower capacitance. The entire unit is sealed in an aluminum case in order to minimize the noise picked up from the surrounding environment.

4.2.3 Optical setup with Optical Phase Stepping

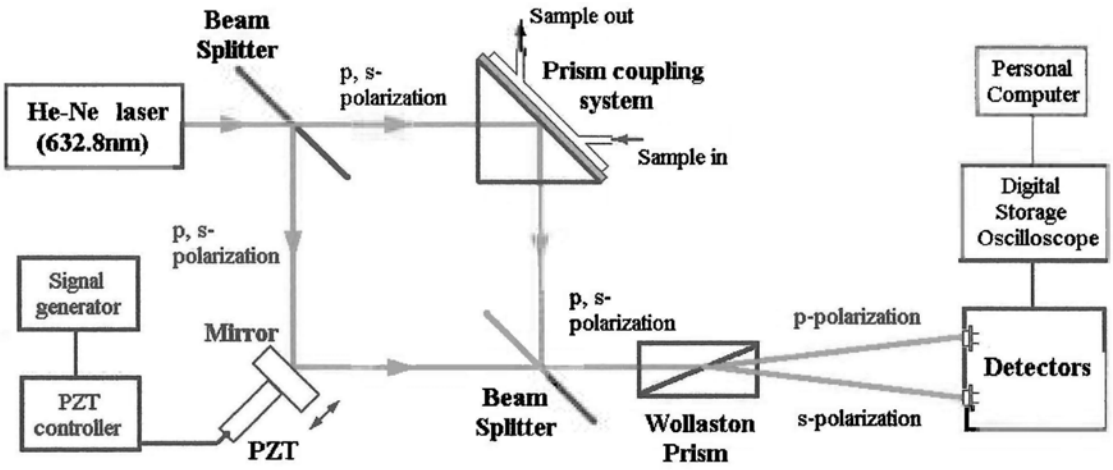

Fig. 4.4. *Experimental setup for measurement of differential SPR phase shift indicating s and p polarizations on the figure*

Figure 4.4 shows the schematic diagram of the differential SPR phase measurement system. A Mach-Zehnder interferometer is fed by a linearly polarized 10mW He-Ne laser source operating at the wavelength of 632.8nm. The laser is oriented in such a way that its polarization direction is at 45° from both p- and s-polarization. A 50:50 beam splitter is employed to separate the beam into two halves. One beam is for the probe arm and the other beam is for the reference arm. For the sensor head, we use a gold-coated 60° equilateral prism coupler made from BK7 glass. The sensor surface is a nominally 47nm gold coating. During experiment, sample fluid was injected through into the flow cell using a syringe. A rotational stage permits adjustment of the incident angle to around 73.0°. In the reference arm, a saw-tooth wave oscillating at 83 Hz is used for driving a piezoelectric transducer (PZT) on which a mirror is mounted. The PZT introduces periodic linear phase shift to the optical beam traversing in the reference arm. The distance traveled by the mirror is sufficient to produce more than 10 interference fringes. Finally the probe and reference beams are recombined at a second beam splitter to produce the required interference signals. A

Wollaston prism is used for separating the exit beam into p- and s-polarized light. The optical system may be considered as two independent interferometers operating in parallel. Two silicon detectors and a digital storage oscilloscope are used for signal detection and waveform capture. A detection program is constructed for real-time phase exaction and monitoring. In the first experiment, a set of glycerin/water mixtures in various weight ratios was used as the samples. In the second experiment, the binding reaction between BSA and BSA antibodies were used to demonstrate the ability of our system for monitoring binding reaction between biomolecules.

4.3 Experimental Setup of Scheme II

Experimental Scheme II: Single-beam self-referenced phase-sensitive surface plasmon resonance sensor

4.3.1 Materials

A) Optical components

2) He-Ne laser (632.8nm) with 12mW optical power output

3) Two mirrors

4) Liquid crystal modulator (LCM) (Newport LCR-VIS-05)

5) Beam splitter

6) BK7 glass dove prism

7) Sensor chip with sample flow chamber

8) Two polarizers

9) Two photodetectors

10) Temperature controlled box fit for LCM

B) Electronic components

Programmable functional generator (HAMEG, Model# HM8130)

LCM controller (Newport 932-CX)

Digital oscilloscope (LeCroy DSO, Model# LT264)

Temperature control circuit

Personal computer

As previously mentioned in Section 4.2.2(b), some of the modules including the photo-detector, sample flow chamber and temperature control box are built in-house to suit our special requirements. We also prepare the SPR sensor film in-house by a sputtering process.

4.3.2 Special items

(a) 4.3.2.1.1 Sensor chip with sample flow chamber

Here we report a new sensor chip with the sensing surface and sample flow chamber integrated in one unit, which contains an inlet and an outlet so that it becomes much more convenient for real applications. The concept of this design is a simple and low cost approach for fabricating SPR biosensor chips. We also incorporate a sample flow chamber for single point measurement, multi-channel detection and imaging sensing applications. A detail discussion of our biosensor chip will appear in the section on results and discussions

4.3.2.1.2 Fabrication steps of biosensor chip

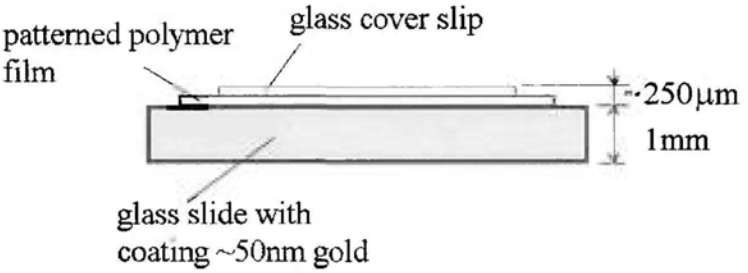

Fig. 4.5. *The structure of our biosensor chip, which is essentially constructed from one slide of glass and one glass cover slip sandwiching a patterned polymer film.*

A basic structure of our biosensor chip design is very simple as shown in Figure 4.5. A 1mm thickness of glass slide (model: Fisher Scientific, *Fisherfinest,Premium, Cat. No. 12-544-1*) is used as the substrate. The original size of microscope glass slide is 3"×1", so we need to cut it into the required size, 1"×1" first. The glass slide is pre-cleaned but it may be contaminated during re-sizing. A second cleaning process is required to remove unwanted substances such as oil and dust. The cleaning procedures are shown below:

(1) Blow-off glass surface to removes dust.

(2) Clean sample in ultrasonic bath of acetone for 5-8 minutes.

(3) Clean sample in ultrasonic bath of ethanol for 5-8 minutes.

(4) Clean sample in ultrasonic bath of deionized water for 5-10 minutes.

(5) Blow-off glass surface until dry.

(6) Plasma clean for 8-15 minutes (optional)

After process step (5), the glass surface becomes free of oil but there might still be the possibly of a few unwanted chemicals left on the surface. In order to ensure the surface is absolutely clean, a plasma cleaning process is employed to help us remove

all unwanted substances. Before the fabrication of the sensor chip, a thin layer of metal is deposited on the glass slide surface as the transducing layer. Thin film deposition is carried out in a high vacuum chamber with magnetron D.C. sputtering. The system is a dual sputtering head coater. In the experiment, the cleaned glasses were carefully placed on the rotating sample mount. A base pressure of about 6×10^{-4} Pa was typically used before the sputtering step. Then argon gas was introduced as the sputtering gas and the pressure increased to around 9.5×10^{-1} Pa. The sample mount started to rotate and the calibrated thickness monitor was set to a ready position. A dc voltage of 520V at a current of 25mA was supplied to the sputtering head. Sputtering process then began in a typical manner, a potential is setup between the sputtering target and the surrounding mount. The sputtering gas between the electrodes is ionized to form plasma. Ions in the plasma are accelerated by the electric field towards to the electrode-cathode (gold target) and collision cascade causes atoms from target to be sputtered away by the impinging ions. Some of the sputtered atoms will deposit onto the glass surface. The thickness of the deposited film can be monitored by using a thickness monitoring system.

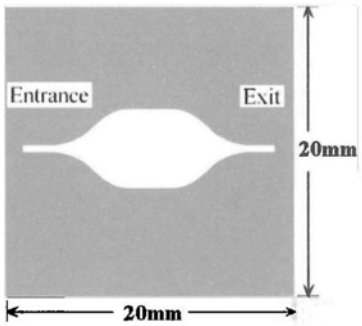

Fig. 4.6. Flow channel pattern with entrance and exit ports

For the sensor chip design, one first needs to identify an appropriate shape for the flow chamber. In our case, a single chamber is employed as shown in Fig. 4.6. The

streamline profile is adopted to avoid air traps inside the chamber and minimize dead regions during liquid flow inside the chamber. The second step in the fabrication process is to print the designed pattern on a polymer film. Initially this was manually done using a cutter. Despite being straight forward, the approach cannot ensure reproducible size and shape in the final product. The pattern was prepared on a personal computer, and a transparent was printed out as a template for the final cutting step. The polymer film used was typically "Para film" used for laboratory wrapping and the size around 20mm×20mm, although polyethylene or polystyrene films would do the job quite well, as shown in Fig. 4.6. In-flow and out-flow channels were incorporated to the design. After patterning, the polymer film was placed on the gold-coated surface of the SPR sensor slide. A glass cover slip, 18mm×18mm, was placed on the entire structure as shown in Fig. 4.5. The whole item was then put inside an oven or on hot plate for curing the seal at a temperature around 100°C for a duration of 20 second.

After curing the patterned polymer film in a sandwiched structure, the basic functionality of the biosensor chip was obtained. Next was to add the inlet and outlet connectors to the chip. The connectors, made from Teflon, were put on the top of entrance region and exit hole. A pad, made of parafilm, was used as a seal between the connector and the chip. A second curing step was then performed. The whole structure was placed inside an oven at 85°C for 5 to 8 minutes. Afterwards the structure was finally ready for use.

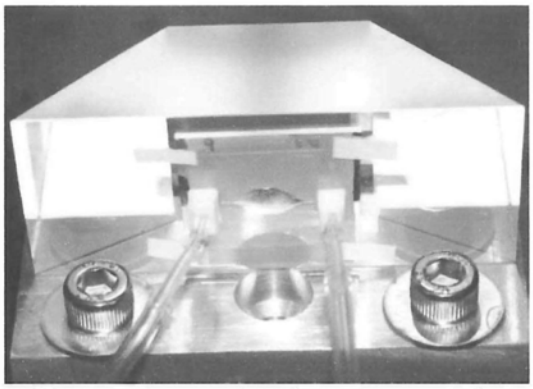

Fig. 4.7. *A single flow-cell is constructed with entrance and exit channels. This chip is attached to a dove prism by using refractive index matching oil (Lightspan, LS-5252).*

We have successfully used these flow-cells in our phase-sensitive SPR sensors reported in reference [90] without any compromise on the performance. We found that they are convenient to use and offer the flexibility of customizing flow-cell design for virtually any applications.

(b) 4.3.2.2 Temperature control box for liquid crystal modulator

A simple and inexpensive temperature controller has been built in-house for keeping the liquid crystal modulator (LCM) under constant phase retardation performance. It has been reported that the temperature fluctuation in a close environment can be minimized to microkelvin regime by using a multistage thermostat scheme [91]. We use a simple design based on proportional-integral-derivative (PID) control the thermally isolated heater box is shown in Fig. 4.8.

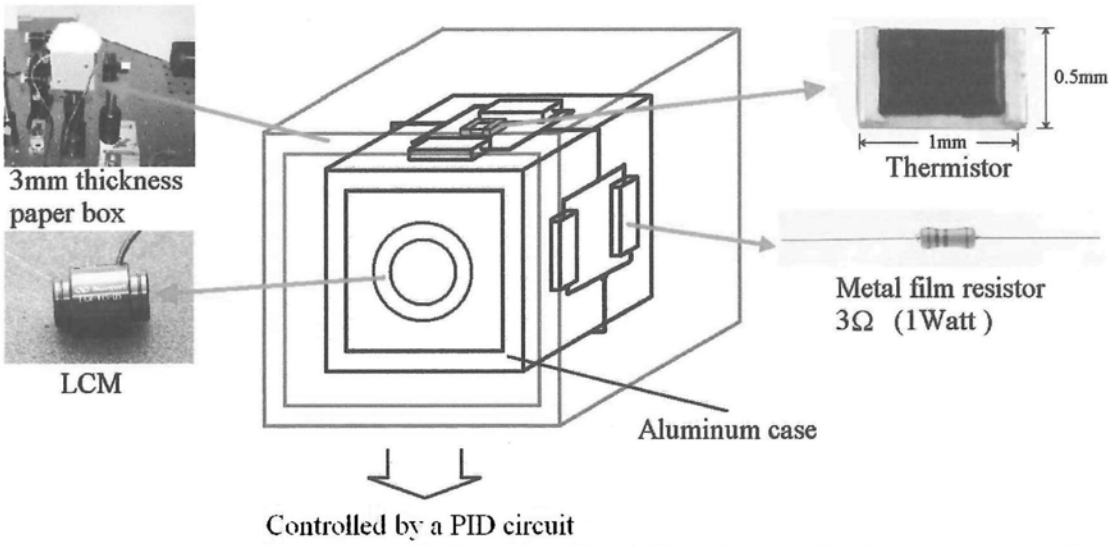

Fig. 4.8. *The design of temperature controlled box for liquid crystal modulator*

The inner part of the temperature-controlled box is constructed from aluminum and there are two 3mm × 12mm windows on its front and back surfaces in order to allow the passage the laser beam through the LCM. We use eight 3Ω resistors mounted on four different surfaces of the metal box as the heating element. Each surface is covered with two heating elements. This arrangement aims to have the LCM heated up evenly. A thermistor (Murata, NCP15WF104J03RC) is attached on the surface of the metallic box for monitoring its temperature. The outer cover is an important item to acheive good thermal stability for the temperature-controlled box. This thermal isolation box is constructed using a 3mm thick paper sheet. Between the metallic box and the thermal isolation box, the space is filled up with wool (ThermalCeramics, Superwool blanket 607) because of their low thermal conductivity. A control circuit is required to drive this box and the temperature of this box is set at a fixed value somewhere around 34°C. The thermistor is included in a Wheatstone bridge for the temperature sensing circuit. Any unbalance bridge signal is pre-amplified by an inverting operation amplifier with low-pass filtering, and fed to a PID controller. Finally, the output is changed to a level appropriate for driving the heater elements.

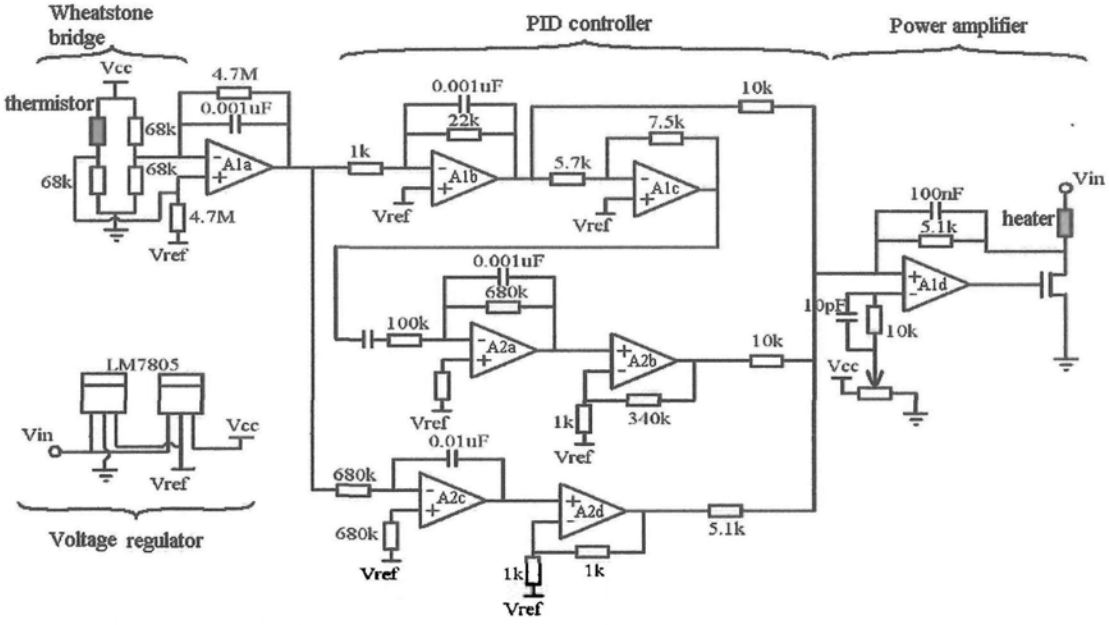

Fig. 4.9. *Circuit schematic of PID temperature controller*

The circuit diagram of the controller is shown in Fig. 4.9. One arm of a Wheatstone bridge is formed by a thermistor and metal film resistor with low thermal coefficient (KAMAYA OHM, RN1/4C6802F). The other is constructed by two fixed value metal film resistors. The error signal across the bridge is amplified by an operational amplifier A1a. The output of the preamplifier provides the input signal to a PID control amplifier. The proportional circuit, A1b, is used to amplify the error signal of the bridge directly. Higher gain in the proportional circuit can provide better compensation control but if the gain is too high, one might have unstable performance. The differentiator circuit, A2a and A2b, is to compensate oscillation and damping. The integrating function increases the loop gain at low frequencies, which allows the controller to prevent any long-term shift error at the designed temperature. It is because this circuit can accumulate any small error signal come from the bridge circuit until there is no error signal from the bridge. The PID signals are the inputs to the power amplifier, which is formed by A1d and a metal–oxide–semiconductor field-effect power transistor. The voltage supply is 12V and the supply voltage to the

operational amplifier (Vcc) is equal to 10V and Vref is equal to 5V by two voltage regulators (LM 7805).

4.3.3 Optical Setup of Scheme II incorporating liquid crystal modulator

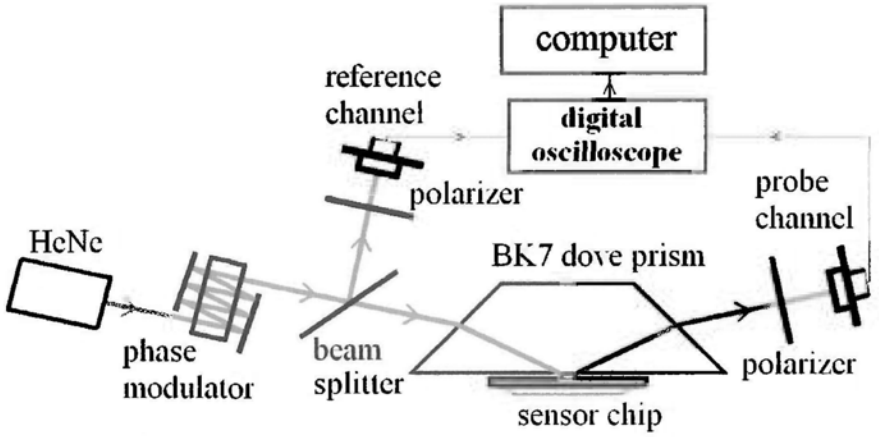

Fig. 4.10. *Experimental setup of LCM-based SPR sensing system.*

Our experimental setup is depicted in Fig. 4.10. This simple configuration is essentially a single-beam self-referenced differential phase-sensitive SPR sensor system capable of achieving high resolution. Large retardation modulation is obtained by placing the LCM element between two mirrors so that the optical beam travels through the modulator multiple times before leaving the cavity. The fast axis of the LCM is aligned to the p-polarization of the laser beam in order to obtain maximum retardation modulation depth. The LCM (Newport LCR-VIS-05) is driven by a controller (Newport 932-CX) which accepts an external drive signal for producing the required retardation modulation. In our case, we used a programmable function generator (HAMEG HM8130) to generate a 10-Hz saw-tooth waveform oscillating between 0−13 V for achieving maximum retardation modulation depth. The light source is a 12-mW linearly polarized He-Ne laser at the wavelength of 632.8 nm. The optical polarization axis of the laser beam is set at 45° from both p- and s-polarization orientation so that the optical power is initially divided into two equal halves along

the p- and s-polarization axes. However, the power distribution may be adjusted as necessary for signal-to-noise ratio (SNR) optimization. A 9:1 beam splitter is placed after the LCM for producing a reference signal. While all subsequently captured signals are compared against this reference, any fluctuation in the characteristics of the LCM will be eliminated through a differential measurement approach. We have implemented the aforementioned temperature controlled chamber to stabilize the temperature of the LCM to within ±0.01°C. We found that this is very important for achieving the expected performance in the sensor system. The LCM is placed between two mirrors so that the beam gets folded a number of times and attains a larger retardation modulation depth. In the present case, the total retardation depth is 14π (i.e. going through the LCM 7 times). The reference beam passes through a linear polarizer at 45° off the p-polarization axis so that interference between p- and s-polarized lights can provide the necessary intensity variation as we modulate the retardation using the LCM. We take the p-polarized light as the probe beam, while s-polarized light as the self-reference beam, then the system will naturally eliminate common-mode noises which are not due to the phase difference between the two polarizations (i.e. retardation). The SPR sensing head consists of two elements: a prism coupler and a sensor chip covered by a flow-cell. The dove prism coupler is made from BK7 glass and the sensor chip is a microscope glass slide (25mm × 25mm × 1mm) coated with a nominally 46-nm-thick gold film. Further details of the sensor chip and the flow-cell may be found from our previous paper [90]. The sensor chip is optically coupled to the backside of the dove prism through a layer of refractive index matching oil. During the experiment, sample fluid was injected into the flow-cell using a syringe. A rotational stage permits adjustment of the incident angle to around 73° so that the experiment may start at the minimum of the SPR absorption dip. At the

exit of the sensor head, a photodetector collects the interference signal from the reflected beam through another polarizer positioned at 45° from the p-polarization axis. A digital storage oscilloscope (DSO, LeCroy LT264) is used for recording the signal waveforms of the probe and reference channels and the raw data will be processed with a computer. A software program has been constructed for real-time phase extraction and monitoring. The signal processing procedures include data averaging, signal trace conversion and normalization to truncated sine wave, band-pass filtering and point-wise differential phase extraction. Further details of our phase extraction algorithm can be found in Section 5.1.3. In order to verify the performance of this system, we performed a set of refractive index measurement experiments on glycerin-water mixtures in various weight ratios. In addition, real-time monitoring DNA-DNA interaction experiments were also performed.

4.4 Experimental Setup of Scheme III

Experimental Scheme III: Wide dynamic range phase-sensitive surface plasmon resonance sensor

4.4.1 Materials

A) Optical components

1) Infrared laser diode (785nm) with 70mW optical power output (CW) (Sanyo, DL-7140-201S)
2) Temperature controlled laser diode mount
3) Three polarizers with rotational mounts
4) Liquid crystal modulator
5) Temperature controlled box fit for LCM

6) Beam splitter

7) Mirror

8) Beam expander

9) Cylindrical lens

10) BK7 glass prism

11) Sensor chip with sample flow chamber

12) Photodetector

13) 128-element photo-diode array (Hamamatsu, S8865-128)

14) Heat sink (MALICO, MBA45001-28W/2.6)

B) Electronic components

Laser diode diver circuit (Wavelength Electronics, WLD3343)

Temperature control module for laser diode

Multifunction data acquisition devices (National Instruments, PCI-6289)

Temperature control module for LCM

Personal computer

The module that are built in-house include photo-detector, photo-diode array driver, cooler unit for laser diode, LCM with temperature control, sensor chip with sample flow chamber.

4.4.2 Special items

(a) 4.4.2.1 Laser diode light source

The light source is a high operating temperature infrared laser diode (Sanyo, DL-7140-201S). The maximum operating temperature is 60°C at 70mW (CW). Temperature issues are critical for operation stability and lifetime of the device. A

custom-designed mount and cooler has been constructed for keeping the operating temperature at 20°C. If the temperature is set too low, there may be the chance of water condensation on the emission window. This may affect the laser beam profile. The home built laser mount includes a peltier cooler, heat sink, laser diode mount, collimation lens and its mount and a thermistor as shown in Fig. 4.11.

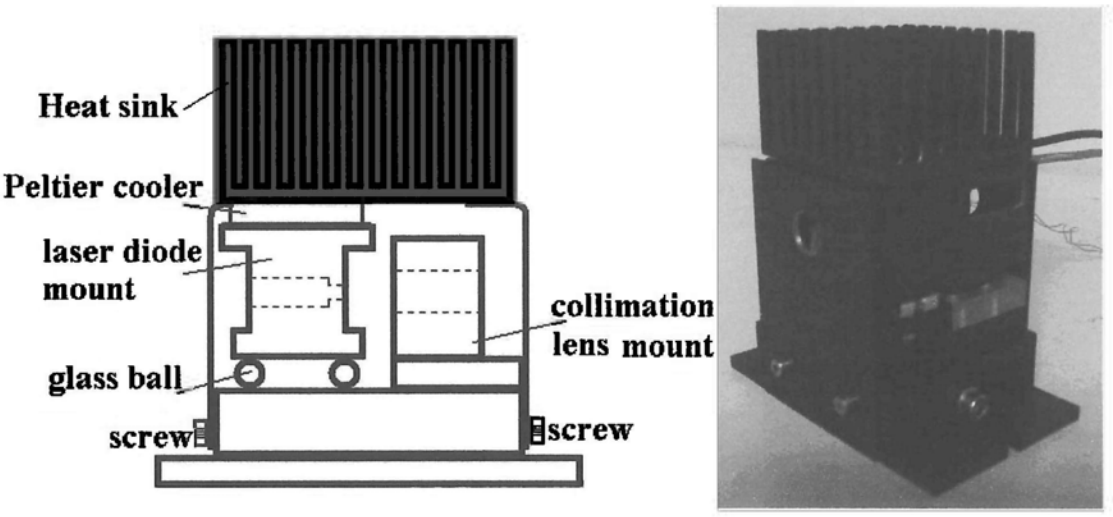

Fig. 4.11. *Laser diode light source*

A laser diode is mounted onto a copper heat spreader due to its high thermal conductivity. On the top of the laser diode mount, a peltier cooler is incorporated as a thermal pump to ensure rapid heat removal from the laser diode mount. Here, we use four glass balls to support this structure an act as a thermal isolator because of the lower thermal conductivity of glass and the small contact area. The polarization of the output light beam is rotated 45° degree relative to the p-polarization axis. The output light beam is collected and collimated by 8mm focal length glass lens. The numerical aperture is 0.3. The laser diode output power is controlled by a laser diode driver. A constant power mode circuit provided by its manufacturer is used to obtain a stable laser power output at around 10mW. As a means to minimize any possibility of laser power fluctuations, a temperature controlled environment is implemented. A PID

control circuit is designed with its circuit similar to the one described in Section 4.3.2.2. Here the resistor values in the bridge circuit are modified according to the present application and a NTC thermistor (10K ohm) is directly attached to the laser diode surface in order to ensure that the temperature signal is registered by the control circuit. Of course, the gain of the PID control circuit is also required to rearrange for this application. The operation method of the power amplifier is changed to pulse width modulation (PWM). It is an advantage for using PWM control because of its better energy efficiency, which results in less unwanted heat generated both in device and the circuit.

(b) 4.4.2.2 Photo-diode array

A 128-elements photo-diode array and its proprietary driver module (C9118) are purchased from Hamamatsu.. This particular photo-diode array offers high dynamic range and lower noise than typical charge couple devices (CCD). It also provides fast line-scanning rate of up to 3900 lines per second. The signal obtained from the photo-diode array is critical for achieving the expected phase demodulation data. In order to ensure good noise isolation, the photo-diode array and its drive module are kept inside a metal box as shown in Fig. 4.12

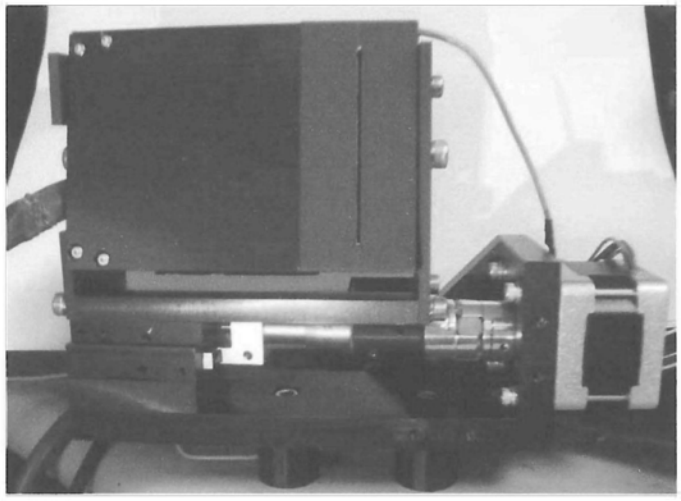

Fig. 4.12. *128-elements photo-diode array and its drive circuit*

The signal output from the photo-diode array module is captured by a multifunction data acquisition board installed in a personal computer.

(c) 4.4.2.3 Liquid Crystal Modulator

A twisted nematic (TN) liquid crystal cell is employed in our system. This TN type liquid crystal cell is custom-made by a manufacturer in Mainland China. Since the supplier did not provide details on the performance of this liquid crystal cells, we had to conduct our own characterization on the device. The LC cell changes its retardation between the fast and slow axes in proportion to an applied voltage. In our case, the maximum supply voltage is 13V and the active region is about 2.5V to 6V. In order to obtain a large degree of phase retardation, six LC cells are being combined together to form a complete LCM module. The interfaces between individual LC cells are filled by index matching gel. The electrical terminals of the six LC cells are connected in parallel. In order to achieve stable performance, the LCM is packaged in a temperature controlled box as shown in Fig.4.13.

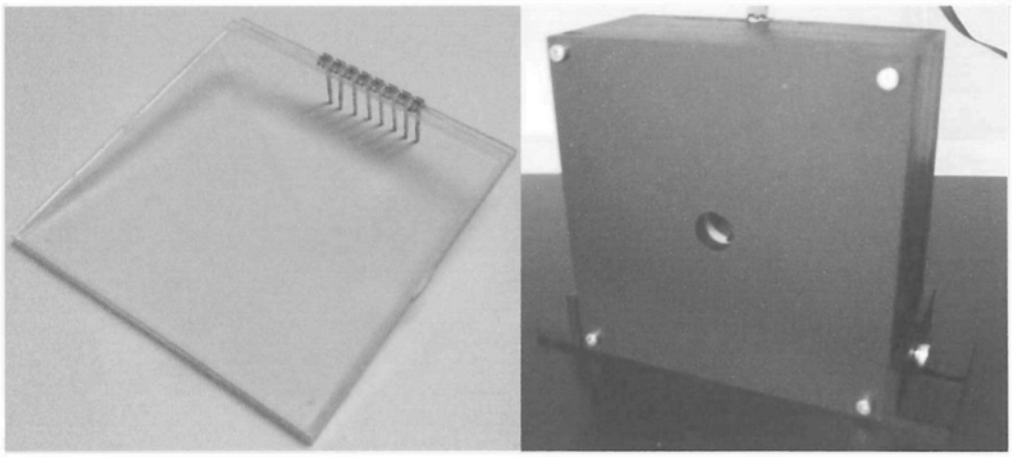

Fig. 4.13. *A single liquid crystal (TN) cell [left] and a liquid crystal modulator with thermal controlled box [right].*

In this box, there are 32 resistive heating elements inside to ensure that all the LC cells are being heated up evenly. The entire module, including the LCM and heating elements, are kept inside a plastic box with all the excess volume filled by silicone rubber (RTV-2). A NTC thermistor, 100k ohm, is directly attached on the surface of the LCM cells to provide temperature signal for the control circuit. Optical access to the LCM module is provided by the front and back windows which have an aperture of 8mm. A simple PID control circuit is employed. The design is very similar to the one described previously in Sections 4.3.2.2 and 4.4.2.1. The operation temperature is set at around 34°C.

(d) 4.4.2.4 Sensor head

The sensor head can be separated into two parts: upper part and lower part. The upper part is a sample flow system and the lower part is for interrogation optics. The structure of the sensor head is shown in Fig. 4.14.

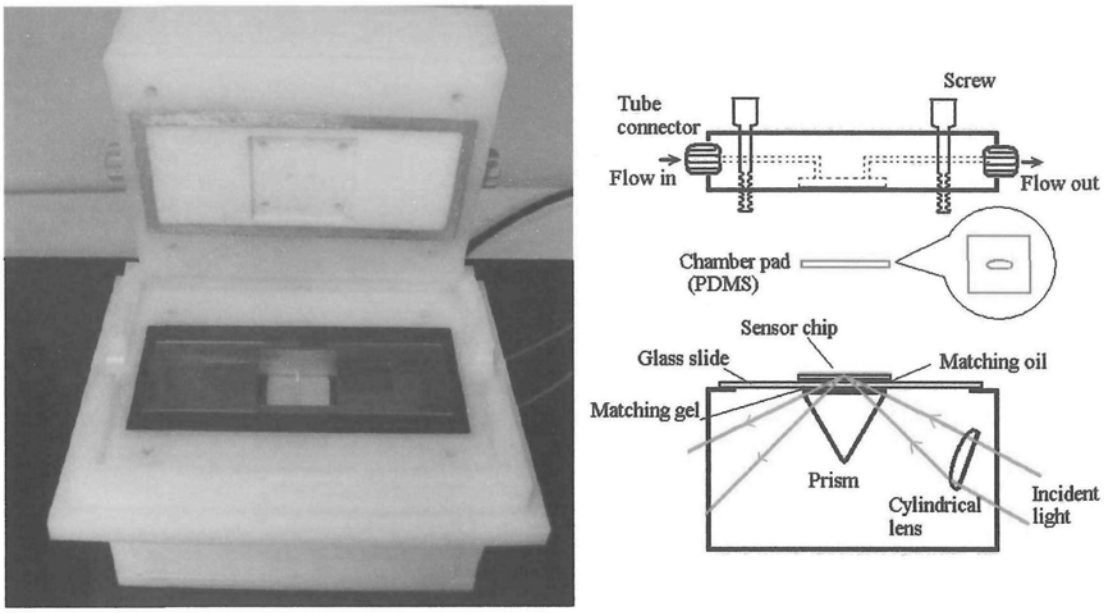

Fig. 4.14. *Sensor head of wide dynamic range phase sensing system*

The optical setup of the sensor head includes a prism, a cylindrical lens, the sensor chip and a glass slide. A glass slide is mounted on a prism by using refractive index matching gel, which also acts as a glue to hold the two parts together. The function of this glass slide is for providing mechanical protection for the prism surface. Before placing a sensor chip on the glass slide, it is required first to clean the surface of the glass slide. This is followed by dispensing a droplet of refractive index matching oil for providing optical linkage between the two components. A cylindrical lens is used for focusing the parallel laser beam onto the sensor surface in order to excite surface plasmon craves. In the upper part, a flow system made from Teflon permits fluid flow in two channels, with one for sample in-flow and the other for out-flow. Two fast-fit connectors installed at the end of the in-flow and out-flow. The connectors are for Teflon tubing side of 1.5mm outer diameter. For the chamber design, a pad made from polydimethylsiloxane (PDMS) is employed. PDMS is a silicon-based organic polymer with good chemical resistant properties. For most applications PDMS can be considered inert, non-toxic and non-flammable. Other physical merits are its softness

and high optical transparency. Moreover, it is quite easy to fabricate simple devices via conventional molding techniques. PDMS device fabrication involves first making a mold with which the designed pattern of the chamber is fabricated. Two small holes are also created in the mask for injecting the PDMS into the mold and allowing air to escape during injection. Using this method, one can easily fabricate a sample chamber in any shapes and sizes. The sample chamber is placed on the upper part of sensor head and the designed pattern of chamber fits exactly to the inlet and outlet of the flow channel so that sample fluid may flow through the chamber smoothly. In order to prevent the possibility of leakage of in the flow cell, four screw pins are used to hold the lid and sensor head in one piece.

4.4.3 Optical Setup of Scheme III for wide dynamic range phase-sensitive SPR sensing system

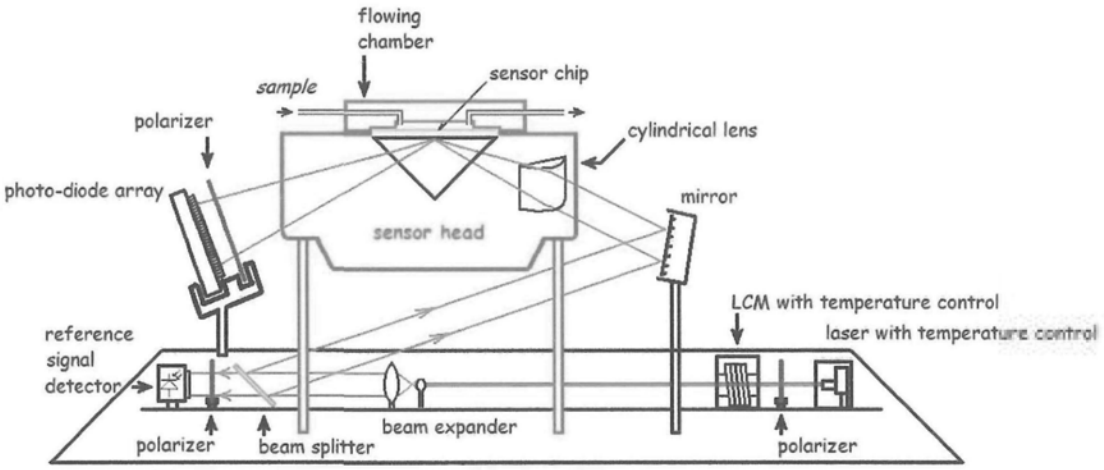

Fig. 4.15. *Experimental setup of wide dynamic range LCM-based phase SPR sensing system*

This basic configuration of our experiment is based on previous setup of a single-beam self-referenced differential phase-sensitive SPR sensing scheme. It improves the measurement dynamic range with good sensitivity by cooperating with angular interrogation scheme. It is described in Fig. 4.15. A laser diode is used as a light

source. Its maximum continuous wave optical output power is 70mW and the typical emission wavelength is 785nm at 25°C operation temperature. In here the actual optical output power is set at around 10mW and the output light beam is collected and collimated to a parallel beam with linear polarization. The optical polarization axis of the laser beam is set at around 45° from both p- and s-polarization orientation by rotating the laser diode. To control the polarization of output light beam, a polarizer with a rotational mount is placed in front of the laser diode. It is set at 45° from both p- and s-polarization orientation. The optical power is initially divided into two equal halves along the p- and s-polarization axes. A large optical phase retardation modulation is obtained by using the scheme of stacking six LC cells together with a parallel electrical connection. The fast axis of the LCM is aligned to the p-polarization of the laser beam to obtain the maximum depth of retardation. The LCM is directly driven by the analog output port of a multifunction data acquisition device with various signals to drive the LCM (developed by Mr. Wong Wing Wai). In the present case, the total retardation depth is at least 8π. The significance of this technique is the need to capture as many cycles of phase modulation as possible in every signal trace to increase the phase extraction accuracy as the subsequent data processing algorithm relies on comparing the phase locations of truncated sine waves. A 3Hz saw-tooth waveform oscillating with 2kHz square carrier wave between 0−10 V for achieving maximum retardation modulation depth is applied. After the light beam passes through the LCM, a beam expander using two microscopy objective lenses of the magnification on 10X and 40X is used to expand the beam to larger than 1cm. A 50:50 beam splitter is placed after the beam expander for producing a reference signal. While all subsequently captured signals are compared against this reference, any fluctuation in the characteristics of the LCM will be eliminated through a differential

measurement approach. We implement a temperature-controlled box for stabilizing the temperature of the LCM to within ±0.01°C. We find that this is an important event for achieving the expected performance in the sensor system. The reference beam passes through a linear polarizer and its angle is set the same as the previous one at 45° off the p-polarization axis so that interference between p- and s-polarized light can provide the necessary intensity variation as we modulate the retardation using the LCM. If we take p-polarized light as the probe beam, with s-polarized light as the self-reference beam, the system will naturally eliminate common-mode noises not due to the phase difference between the two polarizations (i.e. retardation). The SPR sensing head consists of two elements: an optical system and a sample flow-cell. The equilateral prism coupler is made from BK7 glass and the sensor chip is a microscope glass slide (25mm × 25mm × 1mm) coated with a nominally 46-nm-thick gold film. Further details of the sensor chip and the flow-cell can be found in the previous sections. The paralleled light beam is focused onto the sensor chip by using a 35mm focal length cylindrical lens to produce a various incident angle greater than 15°. The range of incident angle is around 63.5° to 78.5°. Of course, the final observable angle depends on the setting of the detector array. Finally, a polarizer is placed in front of the detector array and set at 45° from both p- and s-polarization orientation to induce the interference of p- and s-polarized light. For the setting of this experiment, a sample of DI water is used as a standard specimen to us to find out the suitable location for placing the detector array. The absorption dip of DI water is located on the initial fifth elements of the detector array. When the refractive index (RI) of sample is increasing, the resonance angle will shift to a larger incident angle. The maximum measurement dynamic range is designed to 1.38RI unit. During the experiment, sample fluid is injected into the flow-cell by using a peristaltic pump

(Instech, model# P625) and the flow rate can be controlled at the range of 1.6 to 34μL/min. A multifunction data acquisition device (National Instruments, PCI-6289) is used for recording the signal waveforms from the detector array and reference channel. The raw data is processed with a computer. A software program is developed for controlling the system. Real-time analyzing phase information and monitoring is done by Mr. Wong Wing Wai. The signal handling procedures include data acquisition, data reconstruction, data averaging, signal trace conversion and normalization to truncated sine wave, band-pass filtering and point-wise differential phase extraction. To verify the performance of this system, we perform a set of refractive index measurement experiments on glycerin-water mixtures in various weight ratios.

4.5 Sample Preparation

To verify the performance of each designed system, some practical measurements have been conducted by using glycerin-water mixtures with different concentrations. For scheme I, The solutions of glycerin and water mixtures concentrations (by weight %) were 0%, 0.1%, 0.25%, 0.5%, 1%, 2%, 4%, and 8%. For scheme II, the solutions concentrations (by weight %) were 0%, 0.05%, 0.1%, 0.25%, 0.5%, 1%, 2%, 4%, 8% and 16%. For scheme III they were 0%, 0.002%, 0.006%, 0.01%, 0.02%, 0.06%, 0.1%, 0.2%, 0.3%, 0.5% and 1%. To demonstrate the concept of wide dynamic range phase detecting SPR scheme, we prepare the sample from 0% to 8% (glycerin and water mixture in weight percentage) with 1% wt. in one increment. We also prepared the sample from 0% (water) to 46% with 2% weight per increment for investigating the dynamic range of the scheme III system. It means the RIU changes from 1.3330 to

1.3887. The relationship between the concentrations and the refractive indexes of glycerin and water mixtures are listed in Appendix A.

The dilution procedures are stated in below:

1) The containers, beakers, are cleared by using ultrasonic both with DI-water for 10 minutes before sample preparation.
2) Unit the beakers dried, the beaker is weighed by an electronic balance (A&D, ER-182A) with the resolution in 0.1mg and then set zero.
3) Filling certain amount of 3D (Double Deionized Distilled) water into the beaker and record the weight of the water.
4) Drop carefully a specific amount of glycerin into the water with a syringe and make the glycerin and water mixture of the required concentration in each beaker according to the following equation,

$$\text{Required concentration} = \frac{W_{glycerin}}{W_{water} + W_{glycerin}} * 100\%$$

$W_{glycerin}$ = weight of glycerin

W_{water} = weight of water

5) Make sure that the glycerin is well mixed by shaking it very slowly.
6) Cover the top of the beaker with polyethylene film (parafilm), which provides a good isolation to prevent the escape of the molecules out from the beaker or evaporation. Lower the possibility of variation in concentration of mixtures, corresponding to the refractive index change.
7) Repeat the procedures 2)-6) for each concentrations.

All samples are kept in room temperature and all experiments are conducted in room temperature. Notice that the refractive index is the function of temperature, so small

variation of temperature alters the refractive index. Since there is lack of data for the refractive indexes of the samples (glucose-water mixtures at different concentrations) at a wavelength of 632.8nm (HeNe laser) and 785nm (laser diode laser), they are measured at a temperature of 20°C and at a wavelength of 589.26nm [92] (sodium D line). Therefore, we suppose that all of our experiments are conducted at a sample temperature of 20°C and at a wavelength of 589.26nm laser source. This assumption does not affect the results but gives a relative measurement.

4.6 Simulation Studies

In most cases, research is concentrated on looking for improvements in the system sensitivity by reducing noise. We propose some novel ideas to improve the performance of the SPR sensing system via modification of the sensor head configuration and optical design in order to enhance the signal strength and dynamic range of phase SPR measurement. A standard approach to model the multiplayer system is matrices. This is a simple and useful technique in which a wave propagation analysis may be used to describe the amplitudes of electric and magnetic fields in any isotropic multi-layered media [40]. The 2×2 matrix notation is a systematic approach to deal with the problems of the reflection and transmission of electromagnetic radiation through the thin film system as shown in Fig.4.16.

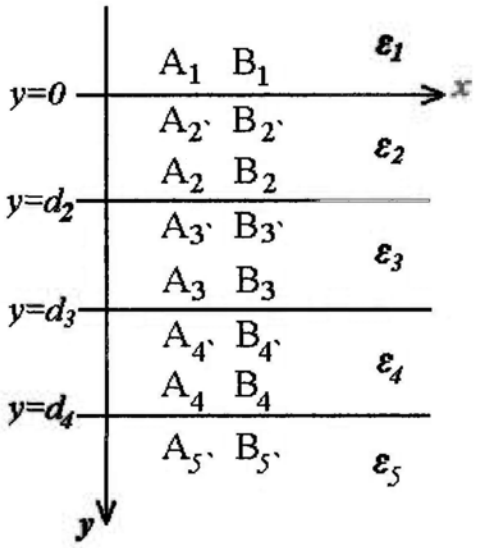

Fig.4.16. *Schematic diagram of a thin multi-layered film of dielectric medium*

An electromagnetic wave is thought to be propagating along the positive y-direction. ε_1, ε_2, ε_3, ε_4 and ε_5 are dielectric constants and d is the thickness of the film. The electric field can be written as

$$E(y) = De^{-ik_y y} + Ue^{ik_y y} = A(y) + B(y), \tag{4.1}$$

where $\pm k_y$ are the wave vector of the y components and D and U are constants. *A(y)* is the amplitude of the downward-traveling wave while *B(y)* is that of the upward-traveling one. The relationship between the amplitudes at the interface between layer *i* and layer *j* is given by

$$\begin{bmatrix} A_i \\ B_i \end{bmatrix} = M_{ij} \begin{bmatrix} A_j \\ B_j \end{bmatrix}, \tag{4.2}$$

with M_{ij} is given by

$$M_{ij} = \frac{1}{t_{ij}} \begin{pmatrix} 1 & r_{ij} \\ r_{ij} & 1 \end{pmatrix}, \tag{4.3}$$

where t_{ij} and r_{ij} are the Fresnel transmission and reflection coefficients for the p- and s- polarized wave respectively and are given by

$$r_{ij} = \frac{k_{yi}/\varepsilon_i - k_{yj}/\varepsilon_j}{k_{yi}/\varepsilon_i + k_{yj}/\varepsilon_j} \qquad r_{ij} = \frac{k_{yi} - k_{yj}}{k_{yi} + k_{yj}} \tag{4.4}$$

(p-polarized) , (s-polarized)

$$t_{ij} = \frac{2\varepsilon_i k_{yj}}{\varepsilon_i k_{yj} + \varepsilon_j k_{yi}} \qquad t_{ij} = \frac{2k_{yi}}{k_{yi} + k_{yj}} \tag{4.5}$$

The relationship between (A_j`, $B_j$`) and (A_j, B_j) in a particular layer is given by the propagation matrix P_j:

$$P_j = \begin{pmatrix} e^{ik_{yj}d_j} & 0 \\ 0 & e^{ik_{yj}d_j} \end{pmatrix}. \tag{4.6}$$

For the overall system, we have

$$\begin{pmatrix} A_1 \\ B_1 \end{pmatrix} = M_{12}P_2M_{23}P_3M_{34}P_4M_{45}\begin{pmatrix} A_5` \\ B_5` \end{pmatrix}. \tag{4.7}$$

In the real configuration as shown in Fig.4.18, layer 5 is the sample so the field of the downward-traveling wave is completely attenuated as a result of its semi-infinite thickness. This means that the amplitude of the upward propagating wave B5` is zero. The reflection coefficient from the glass substrate interface then becomes

$$r_{12345} = \frac{B_1}{A_1} = |r_{12345}|\exp(i\phi) \tag{4.8}$$

where ϕ is the phase of the reflected beam. By these equations, the r of p- and s-polarized light after reflection off the sensor head can be expressed as $r_p = |r_p|\exp(i\phi_p)$ and $r_s = |r_s|\exp(i\phi_s)$. Therefore, SPR phase shift between p- and s-polarized light can be denoted as $\Delta\phi = |\phi_p - \phi_s|$. And the reflectivity is

$$R = |r_{12345}|^2. \tag{4.9}$$

4.6.1 Simulation Experiment I: Phase response enhancement by using double-pass and multi-pass schemes

In most cases, research concentrates on looking for improving system performance on minimizing the noise level [53-56]. Here, we propose a novel idea to improve the performance of the phase detecting SPR sensing system via enhancement of phase response. The concept of this enhancement schemes assures the phase change quantity is governed by SPR phenomenon. If all things are fulfilled to the resonance conditions, an absorption and phase change of light occurred resulting from SPR effect. If the phase change quantity of SPR is 'n', we should obtain 'n+n' phase change by passing through twice to SPR sensing head. Therefore, we have an idea to enhance the phase response by using a double and multi pass schemes as shown in the Fig. 4.17.

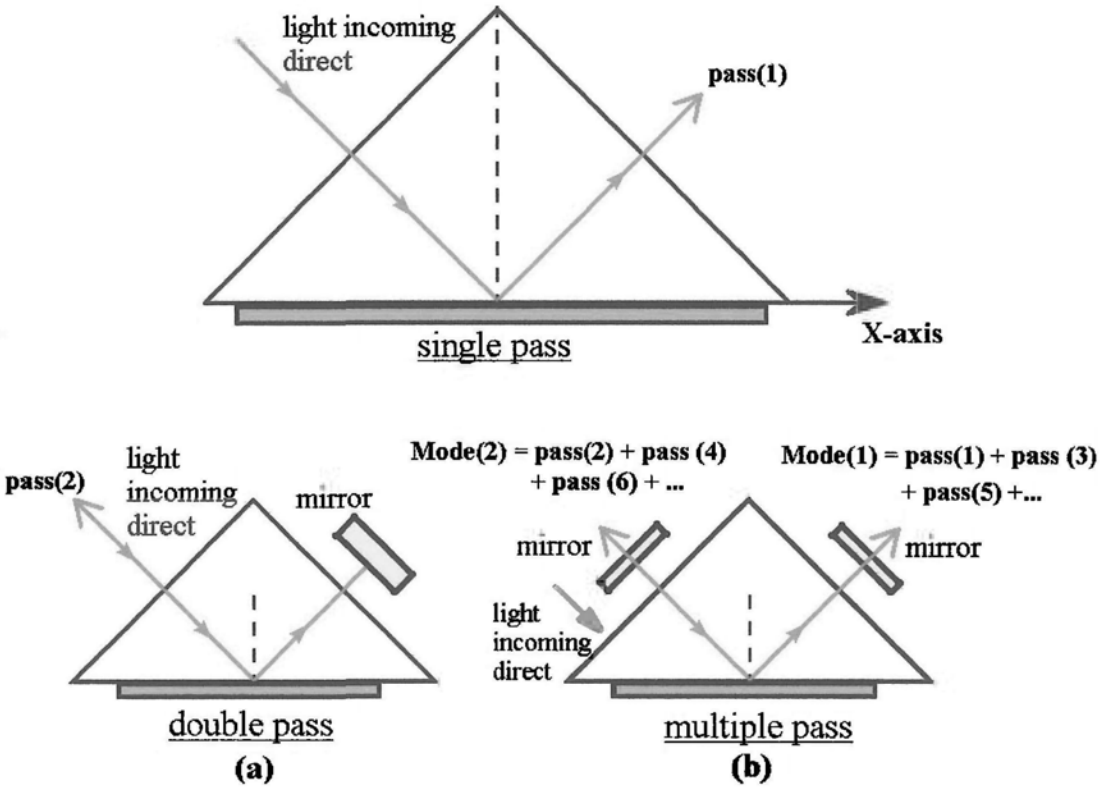

Fig. 4.17. *It shows a classical method (single pass) and phase enhancement methods (a) double pass, (b) multiple passs*

4.6.2 Simulation Experiment II: Multi-layer structure for improving system sensitivity

In most cases, research concentrates on looking for improvements in the optical design. Here, we propose a novel idea to improve the performance of the phase SPR sensing system via modification of the sensor head configuration. The basic design is shown in Fig. 4.18. The characteristic of this SPR sensor which uses composite metal-dielectric-metal as the transducing layer has been studied by using Fresnel formulas.

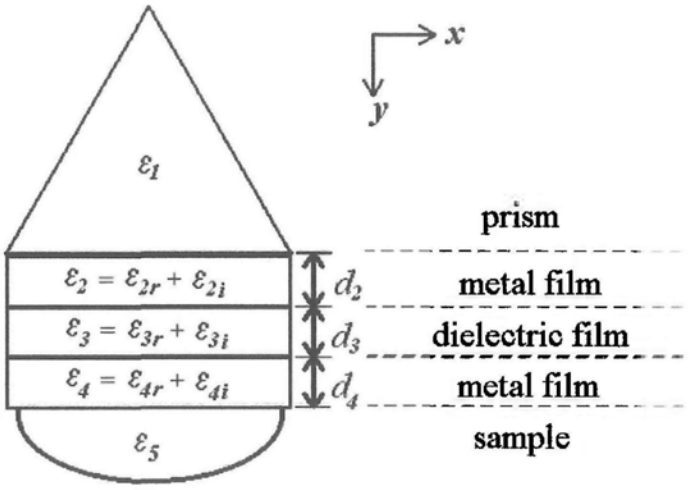

Fig. 4.18. *Schematic of our designed phase SPR sensor*

4.6.3 Simulation Experiment III: Eletro-optical tunable resonance for achieving wide dynamic sensing

In the previous section, we propose a method for improving the phase response of SPR sensing system by modifying configuration of SPR sensor head as shown in Fig. 4.18. We propose a novel idea to improve the performance not only on the phase response but also the solution of the problem of narrow dynamic range on phase SPR sensing system. The basic design is shown in the Fig. 4.19. An Electro-optical (EO) film is used as the dielectric film layer between the two metal layers as sandwich structure and the two layers of metal become electrodes of the EO film. If suitable voltage is applied to the EO film, the refractive index of the EO material can be modified. It means the resonance condition can be modified by tuning the applied voltage.

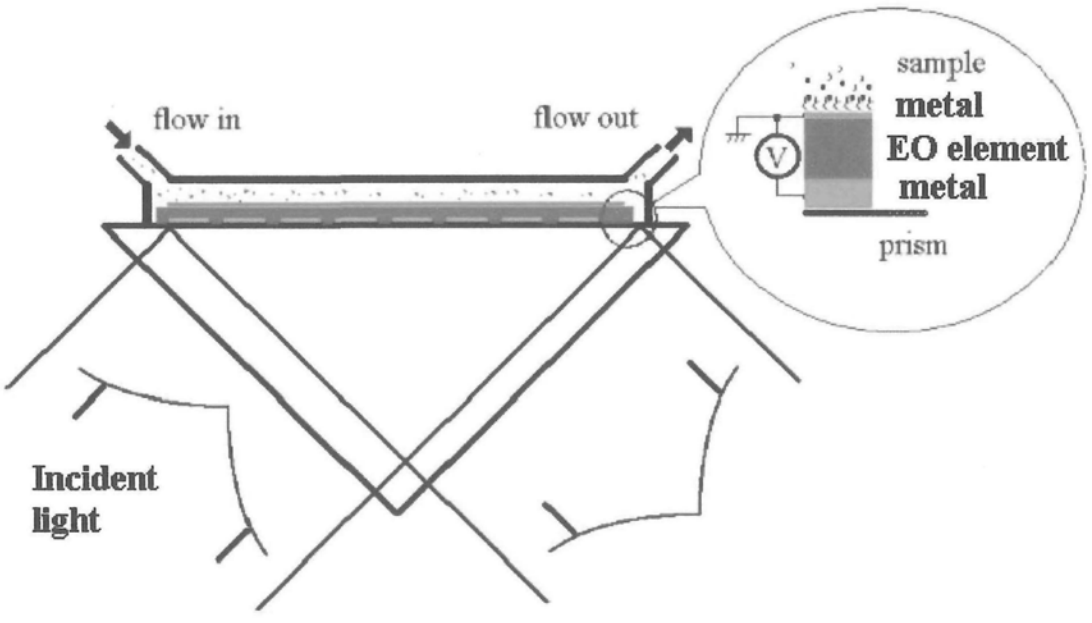

Fig. 4.19. *Schematic of the proposed EO tunable SPR sensor.*

CHAPTER 5

Results and Discussion

In this chapter, we shall present the results of experiments I to III and verify the system performance of each design. Numerical results from the modeling of the proposed ideas of simulation experiments I to III will also be discussed.

5.1 **Experiment I:** Differential phase-sensitive surface plasmon resonance (SPR) biosensor based on Mach-Zehnder configuration

In this experiment, we show that a high sensitivity surface plasmon resonance (SPR) biosensor based on the Mach-Zehnder interferometer is presented. The novel feature of the new design is the use of a Wollaston prism through which the phase quantities of the p- and s-polarizations are interrogated simultaneously. Since SPR only affects the p-polarization, the signal due to the s-polarization can be used as the reference. Consequently, the differential phase between the two polarizations will enable elimination of all common-path phase noise while monitoring the phase change caused by the SPR effect. The constructed experiment is shown in Fig. 4.4 and it was used for measuring the concentrations of constituent components in a liquid mixture. As a practical demonstration of the proposed approach, refractive index measurements were performed on glycerin-water mixture. Furthermore, demonstrations of real-time monitoring biological interaction for BSA (Bovine Serum Albumin) binding reaction with BSA antibodies were also performed.

5.1.1 Mach-Zehnder interferometer

In our experiment, the design of our optical setup was based on a Mach-Zehnder interferometer configuration. For using an interference to make a measurement, it

usually needs an optical arrangement in which the light beam split into two separate traveling paths and then they recombine to interfer. A typical Mach-Zehnder interferometry is shown in Fig. 5.1.

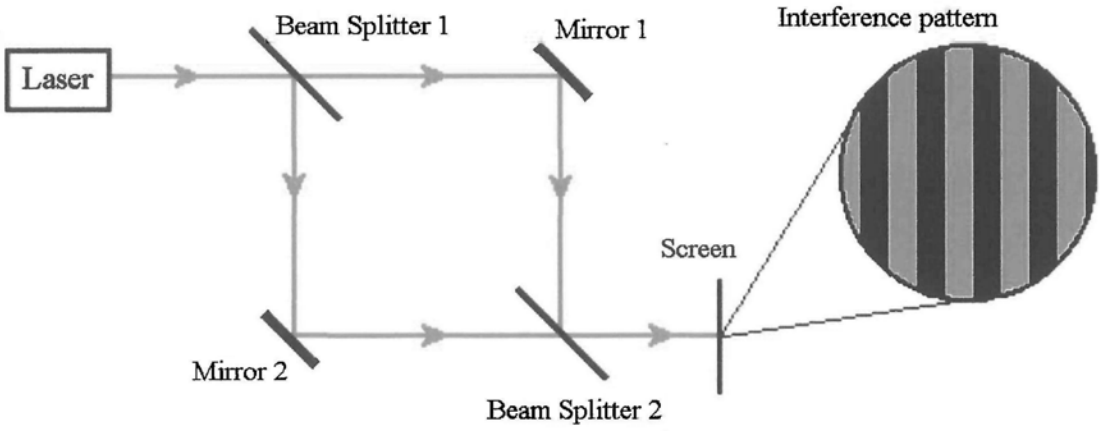

Fig. 5.1 *Mach-Zehnder interferometry.*

In our case, if a 1nm path changes between the two arms, the change of phase information in interference pattern will be around half degree variation. Therefore, the assumption is the reference arm to be a stationary. The difficulty is in ensuring no change in the reference. If 1nm variation occurs on the path of reference arm, it will take into account on the error of phase measurement around half a degree value. In next section, we will discuss our proposed method how to overcome this difficulty in practical SPR sensing application of interferometer. For the interference pattern, a dark or bright frame can be obtained when the two combined beams are aligned together perfectly. Otherwise, it will become an interference fringe pattern. The fringe spacing can be controlled by varying the angle between the beams emerging from the interferometer.

5.1.2 Phase-sensitive SPR sensing

A Mach-Zehinder interferometer used to extract the SPR phase information is first proposed by Kabashin et al [34,35]. Its structure contains one prism, two beam splitters and one mirror as shown in Fig. 4.1. The prism, SPR sensing in the Kretschmann prism arrangement, is embedded as a mirror on the probe arm of the interferometer. Similar experiment was also conducted in our laboratory for comparative assessment by our research team [38]. The sensor head was a two-channel flow cell constructed from a BK7 glass prism. The incident angle was set at 73.78±0.21°, which was near but not exactly at the resonance dip so that we could receive a sufficiently high level of reflected optical power. The thickness of the gold film was about 45.0±5.0nm. In order to investigate the stability of the system, the two-channel flow cell was filled with water and the variation of phase measurement was continuously monitored for a period of 60 minutes. Fig.5.2 shows the results obtained from this experiment. After the first trial, the experiment was repeated again with a new gold sensor film on the prism and the interferometer also re-aligned. Since the optical paths had been re-adjusted, the interferometer produced a different phase-shift baseline as compared to the first trial. Results obtained from the repeated experiment are also shown in Fig. 5.2. The experimental phase measurement drift has a maximum value of 7.41°

The phase drift of traditional sensing technique is difficult to minimize. It is due to the fact that the probe and reference arm going through different paths. This design is very sensitive to any mechanical movements in the optical components. Small mechanical vibrations in the mirrors or variations of temperature inevitably cause the

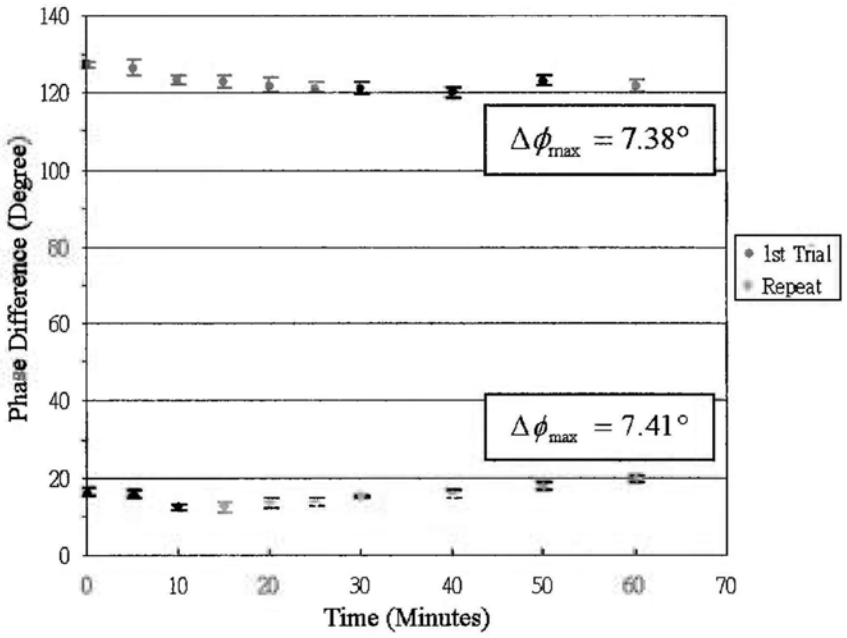

Fig.5.2. *Phase drift versus Time for "traditional" system. [38]*

optical beam to move and thus leading to phase measurement errors. In this thesis, we propose a new scheme to eliminate common-mode measurement fluctuations. We rely on the fact that the SPR phenomenon only affects p-polarized light, and not s-polarized light. The SPR phase can be extracted by comparing the phase difference between the interference signals of p-polarization (probe arm) and s-polarization (reference arm). Using a standard Mach-Zehnder interferometer together with a Wollaston prism placed in the output path, the two polarizations may be arranged to produce two independent interference signals from each polarization as shown in Fig 5.3.

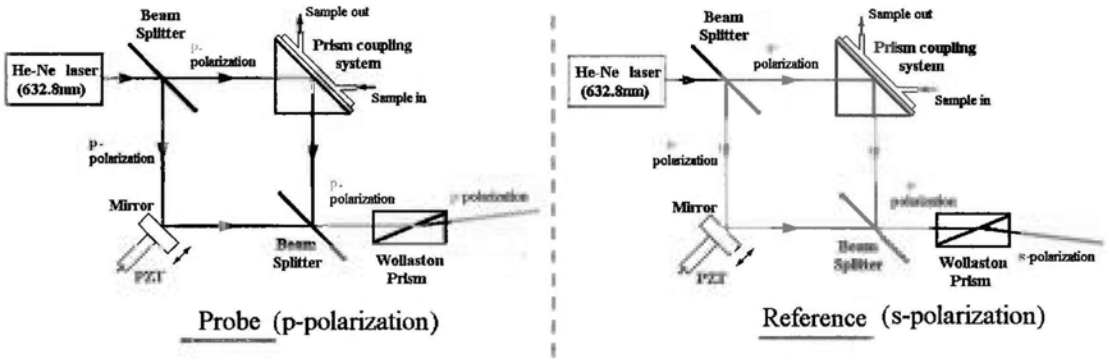

Fig. 5.3. *Two Mach-Zehnder interferometers work in parallel and phase shift due to SPR effect only on p-polarization*

Since both the probe and reference beams traverse identical optical paths in the system, unwanted disturbances are common to both beams and they may be cancelled through mutual phase subtraction. The phase analytical scheme will be discussed in detail in the coming section. Using this configuration, we have successfully measured small refractive index change associated with varying the constituent concentrations of glycerin/water mixture. A highly stable performance of our proposed scheme has demonstrated to achieve 10^{-2} degree level in its phase measurement fluctuation over 60 minutes.

5.1.3 Differential phase measurement

The fact that SPR only affects p-polarized light means that any small variations of ε_{sample}, which for example might be due to the adhesion of molecules to the gold surface, will cause a small change in the values of the Fresnel coefficient, r_{ij} ,of the two polarizations. Such a change is also accompanied by a phase shift, $\Delta\phi$.

For the detection of $\Delta\phi$, the Mach-Zehnder interferometer together with the Wollaston prism in the output arm causes the s- and p-polarizations to perform

interference within themselves. Effectively we have two independent interferometers working in parallel. The output signals are described by the standard interference equations as follows:

p-polarization (probe)

$$I_p = I_{p,ref} + I_{p,sig} + 2(I_{p,ref} I_{p,sig})^{1/2} \cos(\phi_{\mathrm{modulation}} + \phi_{noise} + \phi_p)$$

s-polarization (reference)

$$I_s = I_{s,ref} + I_{s,sig} + 2(I_{s,ref} I_{s,sig})^{1/2} \cos(\phi_{\mathrm{modulation}} + \phi_{noise} + \phi_s)$$

where I and ϕ denote intensity and phase angle, with the subscripts *s*, *p*, *ref*, *sig*, *modulation* and *noise* carry their respective definitions.

With periodic movement of the PZT, which produces a linear time variation of $\phi_{modulation}$ over a length of many wavelengths, the signal traces generated from the two photodetectors are truncated sine waves. A full range movement of PZT is captured and shown in Fig. 5.4.

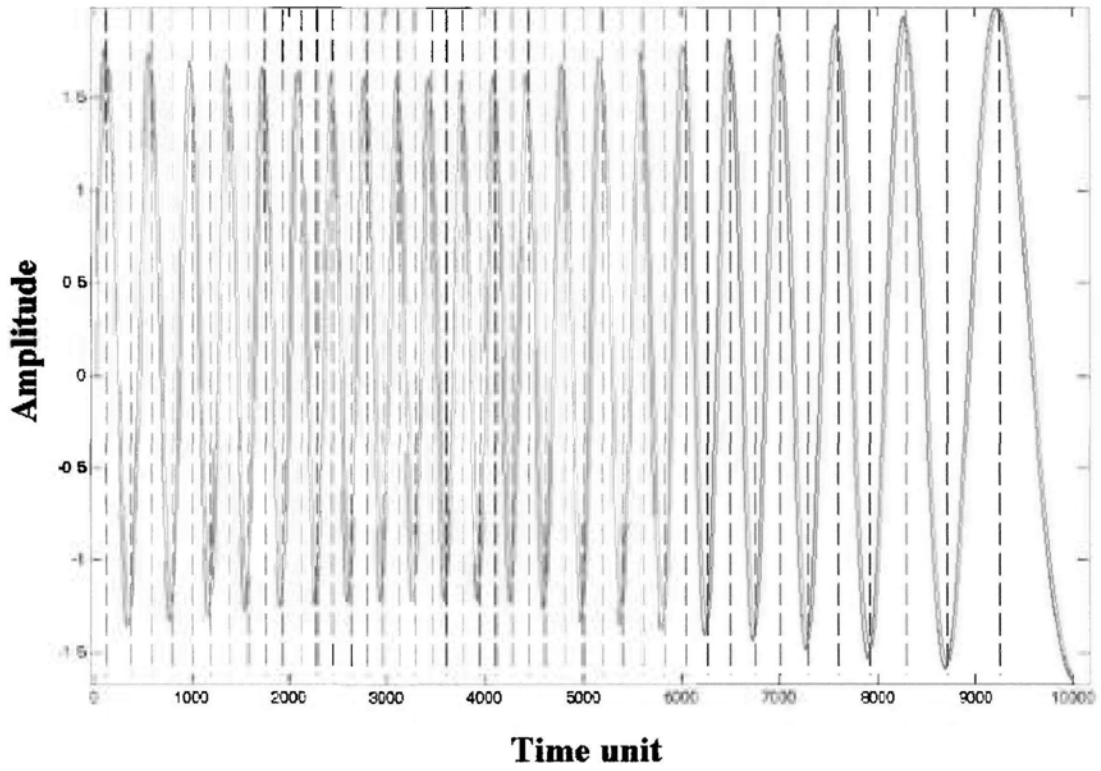

Fig. 5.4. *A fringe interference pattern is produced by a full range movement of PZT. The red colored one is probe signal and the blue one is reference signal.*

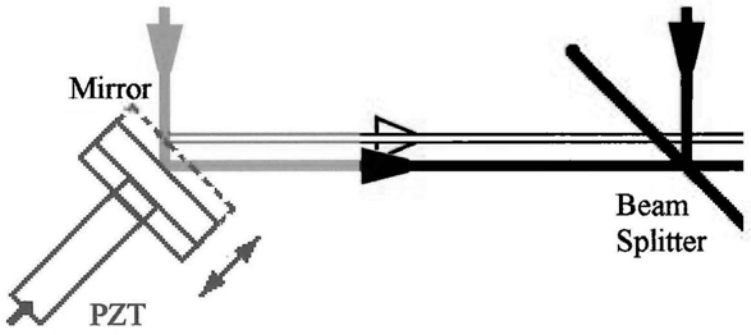

Fig. 5.5. *Beam displacement due to mirror movement during phase stepping*

The truncated sine waves are varying when the PZT travel in different position. It may be due to the displacement of the light pattern. Small misalignment of the light patterns can cause the sine waves to truncate. Therefore, only a relative linear respond region is used for analyzing the phase information. In appropriate signal processing steps, which involve first collecting the average of 200 traces to increase integration

time and removing unwanted frequency components using a digital low-pass filtering algorithm, smooth sinusoidal waveforms are obtained as shown in Fig. 5.6. The waveforms are normalized before they go through an arc-cosine algorithm to extract phase information of the two polarizations, i.e. $\phi_{modulation} + \phi_{noise} + \phi_{p\ (or\ s)}$. Point-wise subtraction between the two arrays of phase angles combined with calculating the arithmetic mean of the point-wise phase difference provides the value of $\Delta\phi = (\phi_p - \phi_s)$ between the two polarizations. Since both polarizations traverse identical paths within the interferometer except for the small region just after the Wollaston prism, unwanted phase fluctuations, which are being looked after by ϕ_{noise}, should be the same for both channels. The subtraction step is therefore effective in eliminating the disturbance of ϕ_{noise}.

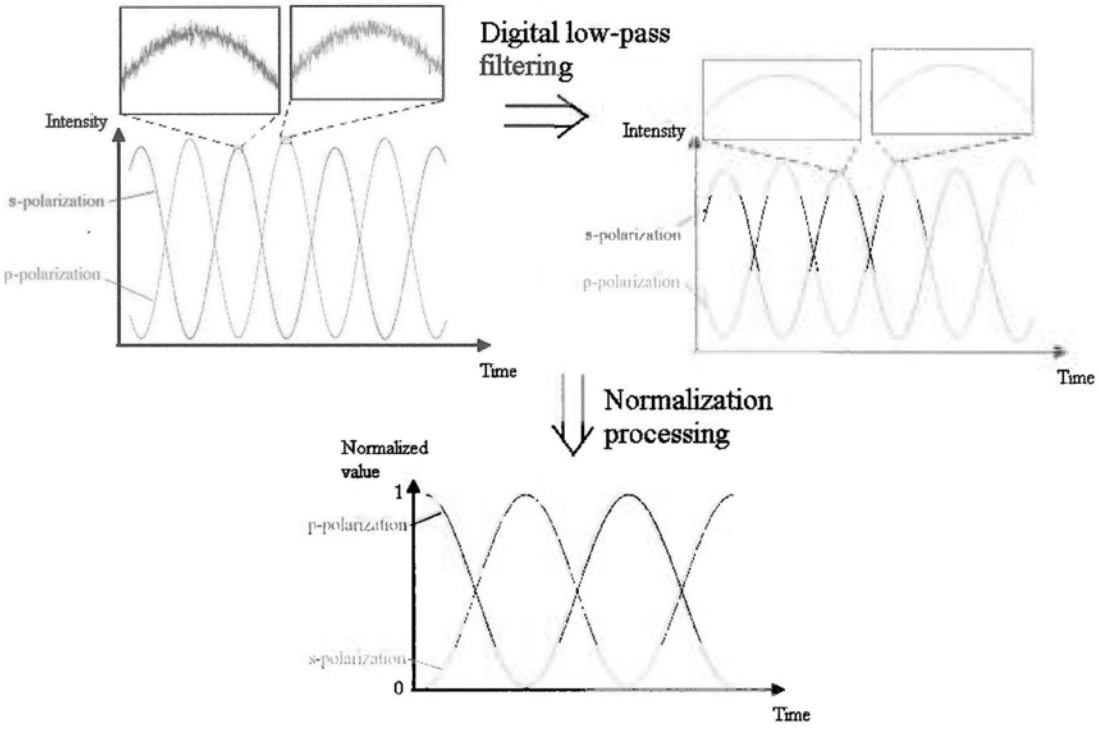

Fig. 5.6. *Raw data obtained from digital oscilloscope and smoothing by using digital low-pass filtering. Finally the waves are normalized.*

5.1.4 Sensing experiments on glycerin-water mixtures

In our first experiment, measurements were performed on glycerin-water mixtures from 0 to 8% in weight ratio. The corresponding refractive index ranges from 1.3330 to 1.3424 respectively [92]. Differential phase captured in real-time is shown in Fig. 5.7. The step-like differential phase response is caused by the increase in the concentration of glycerin. Fig. 5.8 shows the change of differential phase as a function of glycerin concentration.

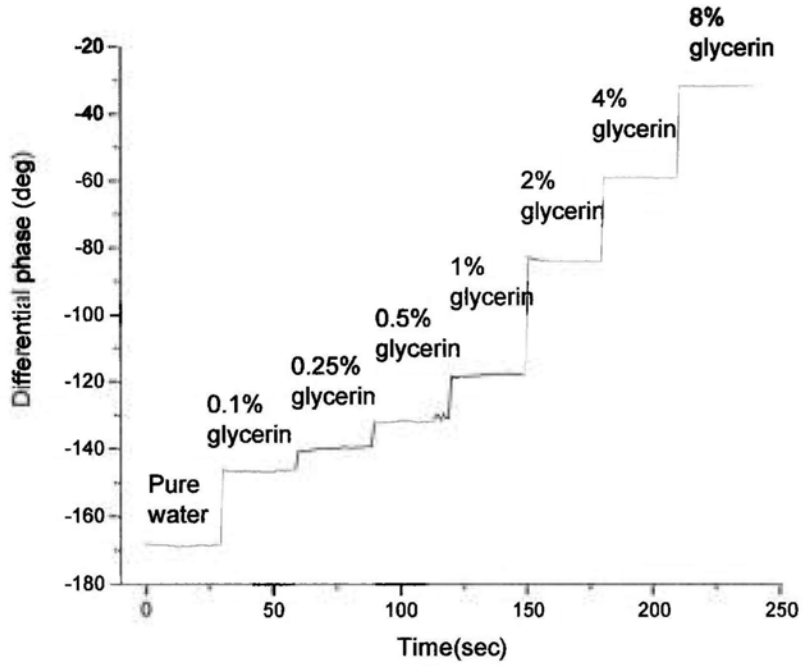

Fig. 5.7. *Real time differential phase measurement of glycerin/water mixtures with various weight ratios.*

In this plot, we highlight the most sensitive region, which occurs in the first two data points. We can see that after adding 0.1 % of glycerin to pure water, the refractive index has changed by 0.00012 RIU, and the corresponding phase change is 21.88 °. The experimental phase fluctuation of our setup is around 0.01° for a period of 60 minutes. Phase measurement fluctuation has been greatly reduced through temperature control, optimized digital low-pass filtering and phase locking. The measurement setup is located in an enclosed environment to ensure minimum

temperature fluctuation caused by air circulation. In order to minimize the possibility of error due to DC phase drift, a phase locking algorithm has been embedded in the computer control software so that the PZT-driven mirror always starts from a position corresponding to a fixed phase angle. Based on an experimental resolution of 0.01°, the calculated sensitivity threshold of our system is 5.48×10^{-8} RIU. This is significantly better than the best result of 3×10^{-7} RIU [11] we found in the literature. As seen from Figure 5.8, the steep region corresponds to a near resonance condition at which any slight change of refractive index in the sample medium will lead to a large phase change.

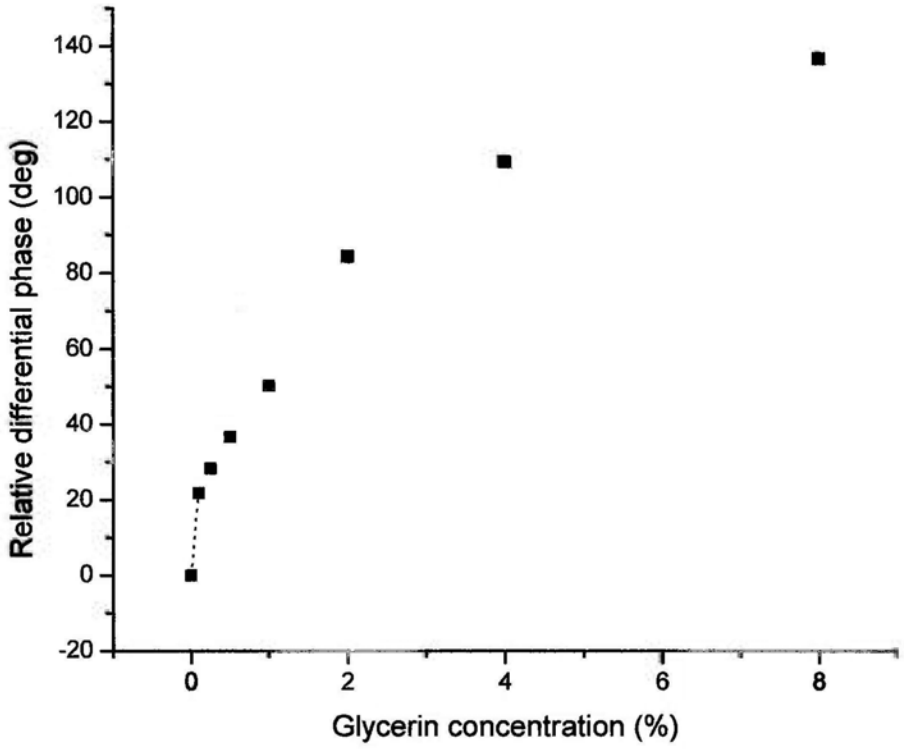

Fig. 5.8. *Variation of relative differential phase (reference to pure water) versus glycerin concentration*

However, the nonlinear property of the phase curve also indicates that special attention must be given to quantitative analysis of experimental data. In order to minimize systematic errors caused by such nonlinearity, one should first obtain a

calibration curve of the system using a range of sample media with well-defined refractive indices.

5.1.5 Sensing experiments on BSA-BSA antibody binding reaction

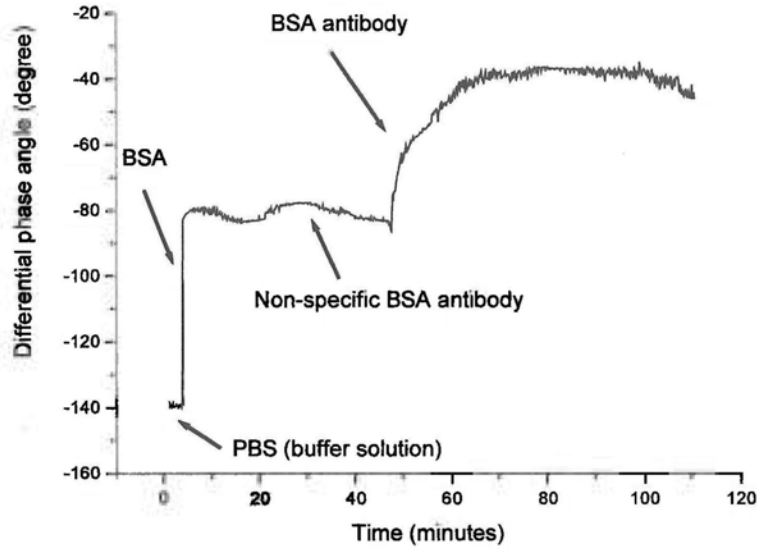

Fig. 5.9. *Response curve of differential phase after sequential addition of PBS, BSA, non-specific BSA antibody and BSA antibody into sensor head, indicating detection of specific BSA / anti-BSA binding.*

Figure 5.9 shows the result of the second experiment on measuring bio-molecules. The differential phase of Phosphate-Buffered Saline (PBS) was first measured as the baseline. PBS buffer containing BSA (1 mg/ml) was then introduced into the sensor head. As shown in figure 5.9, a sharp increase in phase angle occurred upon the addition of BSA-containing solution. The system was left to settle for 30 minutes, which would lead to a layer of BSA being assembled on the gold surface. PBS buffer was injected into the sensor head again and wash away the free BSA. Then a PBS buffer containing non-BSA antibodies (rat IgG, 37 μ g/ml) was loaded into the sensor

head to test whether there was any non-specific binding. The differential phase stayed constant afterwards, thus confirming that no non-specific binding had taken place. Finally, PBS buffering containing BSA antibodies (37 μ g/ml) was injected into the sensor head. A sharp increase of phase angle is observed, which signified the binding of BSA with BSA antibodies. An exponential curve characteristic to typical rate-dependent reactions is observed. Based on the fact that a concentration of 37 μg/ml BSA leads to an absolute phase change of 49.92 °, we estimate that the detection sensitivity of our setup is 7.4 ng/ml. (base on 0.01 ° resolution).

5.1.6 System stability

In order to give an assessment on the measurement drift of our setup, we monitored the variation of the phase measurement during a period of 60 minutes. The room temperature during this period was measured to be at a constant level of 24.8°C. The baseline drift was therefore assumed to be due to random fluctuation associated with the components in the system. In here the measured phase from pure water versus time is obtained and it is involved first collecting the average of 120 traces. The maximum phase difference variation is approximately 0.08°. In order to minimize the random fluctuation, the average number of traces was hugely increased to 2048. The trade off is a longer integration time. The result is shown in Fig. 5.10. The maximum phase difference fluctuation is minimized to approximately 0.01°. In fact this plot is not easy to obtain. Firstly we need to thermal seal everything. It means all optical components should be boxed up. Then we also wait for the room temperature to become stable. Any unwanted vibration and fluctuations will also increase the noise content on the result.

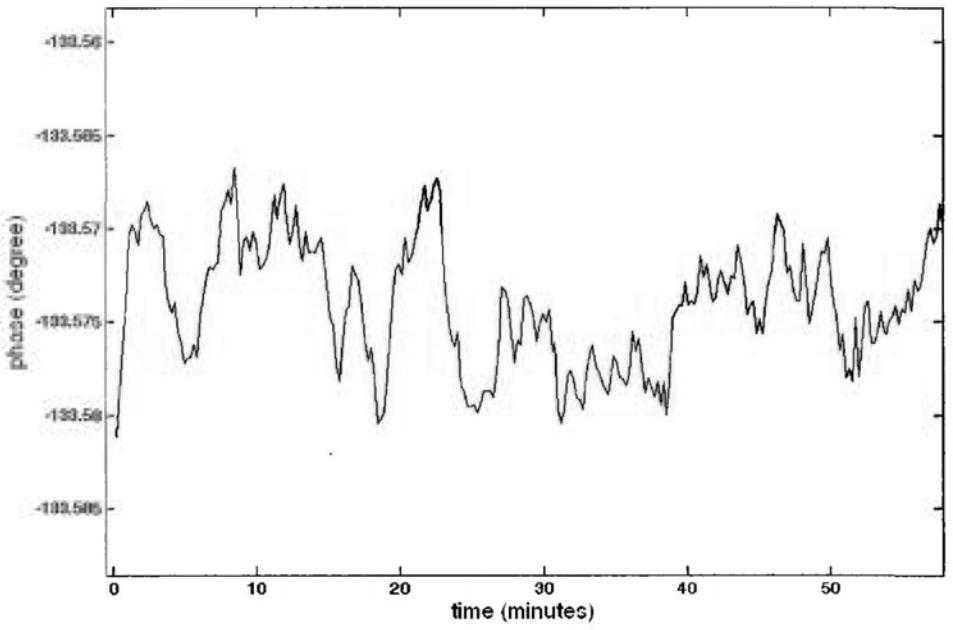

Fig. 5.10. *Systematic drift and noise observed over 60 minutes at constant temperature*

5.1.7 Summary

A new SPR biosensor design based on measuring the differential phase between the s- and p-polarizations has been demonstrated. Since both the reference (s-polarized) beam and the signal (p-polarized) beams traverse identical paths in the interferometer, the new technique offers better sensitivity because of its effectiveness in minimizing common-mode noise. Further improvement by compensating the variation of temperature and optimizing the thickness of gold on different applications is required. The sensitivity threshold of our system is 5.48×10^{-8} RIU, which is significantly better than the best result reported in the literature.

5.2 **Experiment II:** Single-beam self-referenced phase-sensitive surface plasmon

resonance sensor with high detection resolution

In this experiment, we show a versatile and low cost single-beam self-referenced phase-sensitive surface plasmon resonance (SPR) sensing system with ultra-high resolution performance. A liquid crystal cell is used as a phase retardation modulator. We successfully increase the phase retardation depth of more than 14π to make our system more practical. We construct an experimental setup (Fig. 4.10) and then it is used for measuring the concentrations of constituent components in a liquid mixture. Demonstrations of real-time monitoring DNA-DNA interaction for DNA detection (Herpes virus DNA) are also performed. A sensor chip with flow chamber design has also been developed during the experiment.

5.2.1 Simplified phase SPR system by using a single beam scheme

Compared our previous method, single beam self-referenced SPR sensing scheme is relatively simple and easy for practical use. Although a phase SPR system based on a Mach-Zehnder interferometer can provide a very good sensitivity, the optical alignment of the system is not user friendly in practical use for the optical requirement of the system to split the light beam into two to produce a probe arm and reference arm is required. Recombination of two beams is required to form an interference pattern to measure the SPR phase information. For measuring different samples, the different refractive indexes of sample medium have their own resonance angle. In order to optimize the system sensitivity, the incident angle of light for the sensor head may be required to match with resonance angle of sample medium. Therefore, alignment of the optical beam at the sensor head may be required to be adjusted for every measurement in different samples. The complicated optical alignment of the Mach-Zehnder interferometer is based on SPR measurement scheme. In this section,

we want to present a more practical, low cost and simple SPR phase measurement system.

5.2.2 Single beam phase SPR sensing

SPR phase detection is first demonstrated through heterodyne interferometry [33]. The phase signal is modulated by using an acousto-optic modulator (AOM). This sensor gives a resolution of 5×10^{-7} refractive index units (RIU), which is already quite a significant improvement at that time. Afterwards, some people try to simplify the situation of signal process to avoid using high frequency electronic hardware. An optical modulated lower beat frequency is obtained by using dual AOM with a bit shifted operation frequency between the two modulators [101]. The SPR phase information is carried out on optical beam modulated with the lower beat frequency caused by interference between the two orthogonal polarizations. To further simplify the hardware requirement, some researchers suggested using the Zeeman laser to reduce system complexity [49]. The beat frequency (typically in kilohertz to megahertz range) caused by interference between the two orthogonal polarizations within the Zeeman laser beam provides a direct measurement of the SPR phase through measuring the phase difference in the optical beam immediately before and after traversing the sensor head. The main drawback of these two approaches are their difficulty in operating at low frequencies required by imaging measurement - an important attribute for achieving two-dimensional (2D) SPR sensor arrays with high measurement throughput. To address this issue, it has been reported that a liquid crystal modulator (LCM), which may be used as a voltage-controlled optical retarder, can be incorporated to perform SPR phase measurement through a five-step phase-shifting method [102]. Indeed, this approach achieves a measurement resolution of

2×10^{-7}RIU. It should be mentioned that LCM has also been used by Hooper and Sambles [103] for performing SPR phase measurement through monitoring the amplitude of a 500Hz signal upon varying the retardation offset of the modulator.

In spite of its simplicity as a retardation modulator, the LCM has its own disadvantages namely, high temperature dependence, high non-linearity, low operation frequency and limited retardation modulation range. Small variations in temperature results in sizeable measurement drift. Indeed the situation is much more problematic for the phase-shifting approach reported by Yu et al. [49], as the accuracy of the final phase measurement relies entirely on the repeatability of the five data points obtained upon shifting of the retardation within a 2π circle. From the engineering point of view, the LCM offers a number of advantages such as low cost, long life time, small size, no mechanical moving parts, low power consumption, light weight and low operation voltage. The LCM is very suitable for portable SPR biosensor instruments if all of its shortcomings can be properly managed. With this as the objective, we build a single beam self-referenced phase-sensitive SPR sensing system that have extremely high stability through the incorporation of a temperature control to stabilized the retardation drift in the LCM, and also the use of differential phase measurement for further elimination of unwanted phase errors from the ambient. A novel beam-folding device to increase the retardation modulation depth to multiples of 2π has also been introduced to enhance accuracy in the phase extraction process.

5.2.3 Operation principle of our proposed single beam self referencing SPR sensor

For the operation principle of our system, we need to mention that SPR only affects the p-polarization of the incoming light. The s-polarization remains unperturbed and may be used as the reference. The resonance condition of SPR is primarily influenced by the refractive index of the medium near on the sensing surface. In our system, the phase difference between the s- and p-polarization (i.e. retardation) may come from three effects: 1) SPR, which is the quantity we aim to measure; 2) artificial retardation modulation introduced by the LCM; 3) unwanted phase polarization effects associated with the optical components. As seen from the experimental results presented later, errors due to item 3 are negligible due to the fact that our system is inherently a massively differential setup. The detected signal from the probe channel (V_{det}) with the retardation caused by SPR and the LCM may be described in the following equation:

$$V_{\det} \propto E_m{}^2 = (E_{os}\cos\theta_s)^2 + (|r|^2 E_{op}\cos\theta_p)^2 + 2(E_{os}\cos\theta_s)(|r|^2 E_{op}\cos\theta_p) \bullet (\cos(\Delta\psi_{LCM} + (\phi_p - \phi_s))$$

where E_m is the amplitude of the detected light; E_{op} and E_{os} are the amplitudes of the p- and s-polarization; r is the reflection coefficient of the SPR sensor head for the p-polarization; θ_p and θ_s are the off-axis angle of the polarizer between p- and s-polarization axis (45° for the present setup) respectively; (ϕ_p-ϕ_s) is the phase change associated with SPR; $\Delta\psi_{LCM}$ is the phase change introduced by the LCM.

$\Delta\psi_{LCM}$ can be found by analyzing the reference signal traces upon varying the drive voltage of the LCM. At the same time if we perform the same procedures in the probe signal traces, then we should expect to find [$\Delta\psi_{LCM}$ + (ϕ_p-ϕ_s)], as the beam would have then been further modified by the SPR sensor head. This means that if we

continuously analyze the signal traces from the reference channel as well as the probe channel, we should be able to find (ϕ_p-ϕ_s), the SPR phase change, through a phase subtraction step. Obviously the differential measurement approach helps us improve stability by minimizing the effects of unwanted changes in the characteristics of the LCM and also other disturbances from the surrounding environment.

5.2.4 Phase retardation modulator with enhanced modulation depth

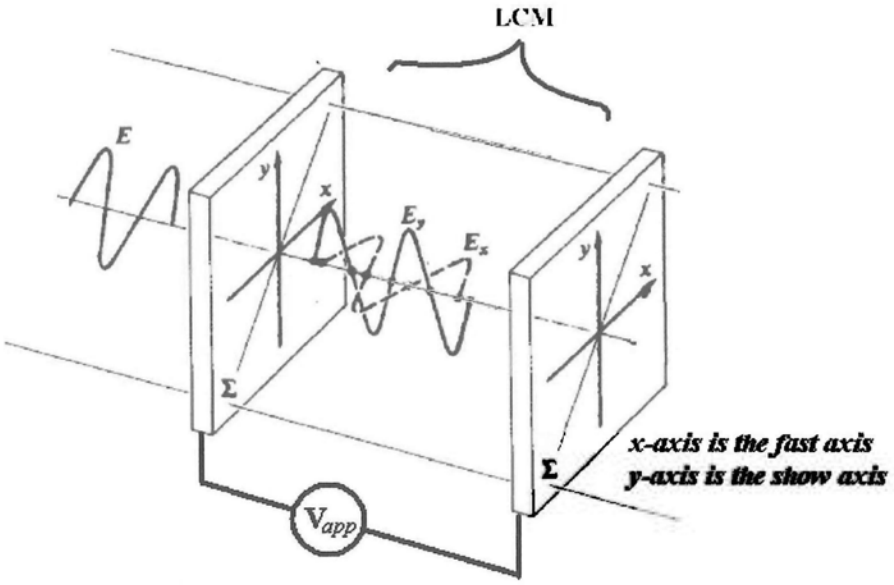

Fig. 5.11. *Variation of index of refraction on fast and show axis on LC device*

In our setup, one of the key optical components is the phase retardation modulator. A liquid crystal device is chosen as the phase retardation modulator. It has many advantages such as low cost, long life time, small size, low power consumption, light weight, low operation voltage and without mechanical moving parts. Moreover, the optical birefringence of the liquid crystal material can be changed by an applied electric field. Change of the birefringence effectively modifies the refractive index along the preferred axis commonly called fast or slow axis as seen by an incident light beam as shown in Fig. 5.11. It means the propagation speed of light varies in the

preferred axis. By controlling the voltage applied to the liquid crystal element, the polarization characteristics of a transmitted beam can be modified as shown in Fig. 5.12.

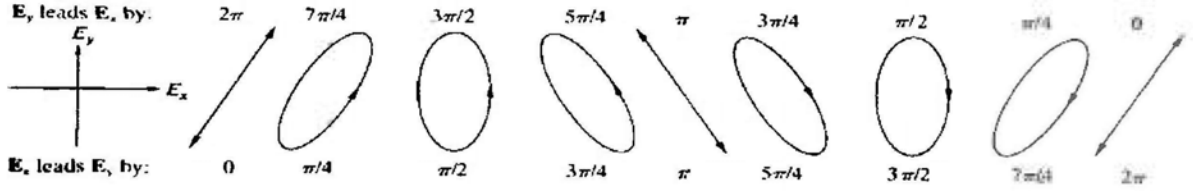

Fig. 5.12. *Variation of the polarization characteristics of a transmitted beam depends on retarded phase of light between the fast and show axis.*

In this figure, we can know the relationship between the phase retardation of light on the x- and y-axis from 0 to 2π and the polarization characteristics of the transmitted beam. In real situation, the fast axis or slow axis of LCM is set on the p- or s-polariation of the system. If we place two polarizers in front and end of the LCM with an off-axis angle of the polarizer ($\theta = 45°$) as shown in Fig. 5.13, the resultant intensity of the transmitted light beam vary due to the interference between the $Ex\ sin\theta$ and $Ey\ cos\theta$. Therefore, the $\Delta\psi_{LCM}$ can be observed from the resultant intensity modulation when a variation voltage is applied on the LCM. In Fig. 5.14, it is a real measurement for determining the characteristics for our employed LC device from the applied voltage from 0V to 13V. In fact, LC device is not a linear device so a truncated sine function response is obtained. Fortunately, the modulation depth is greater than 2π a bit. It just fulfills our minimum requirement.

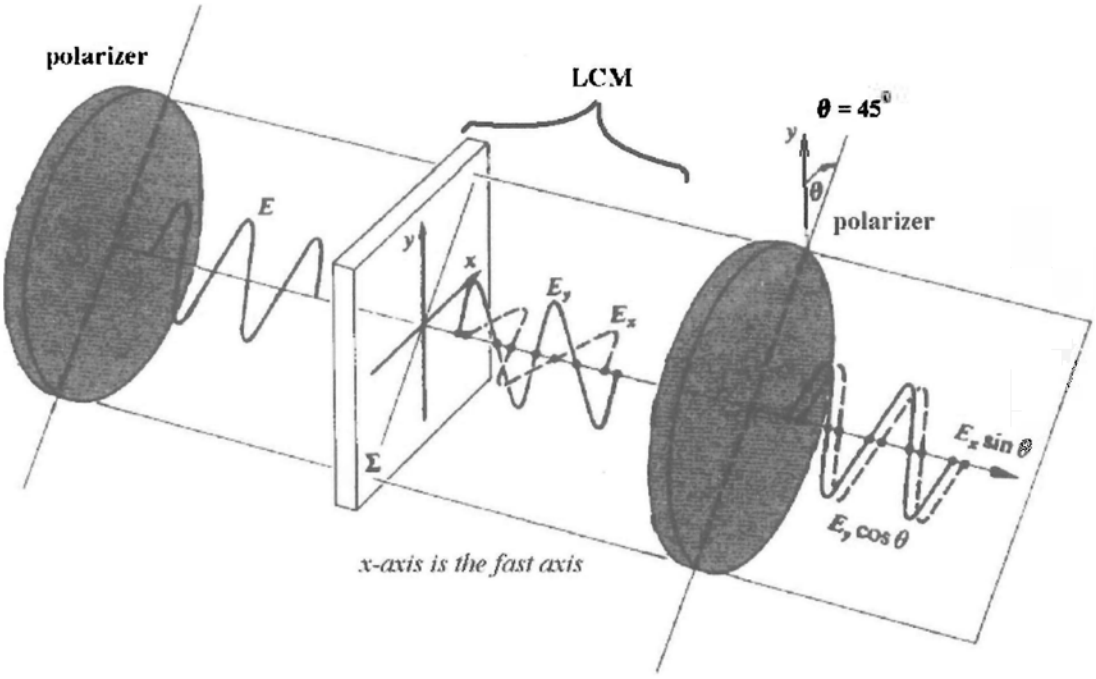

Fig. 5.13. *Operation of phase retardation modulator by using LC device*

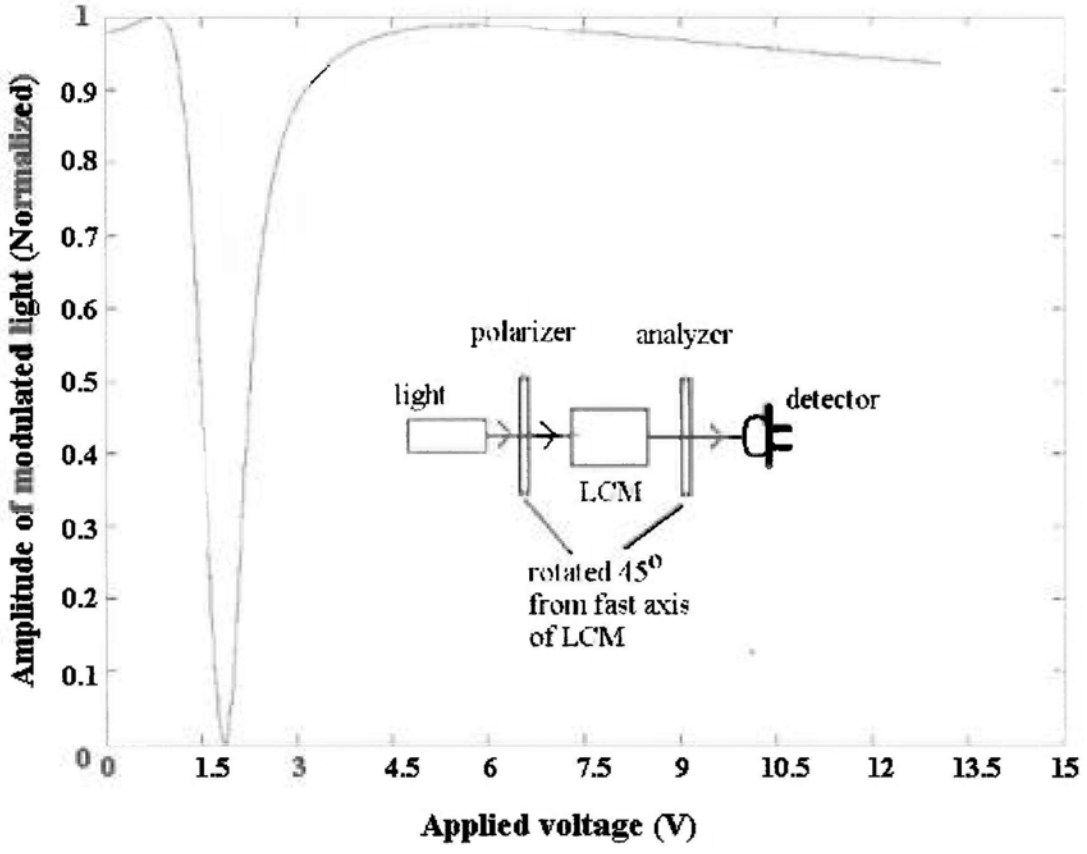

Fig. 5.14. *Intensity variation versus voltage applied to LCM from 0V to 13V*

To improve the performance for our phase retardation modulator, we propose two possible and simple methods to enhance the phase retardation capability for the LC device. 1.) We use several LC devices stacked together as shown in Fig. 5.15a. 2.) and two mirrors to reflect the incident light beam to transmit through the LC device many times as shown in Fig. 5.15b.

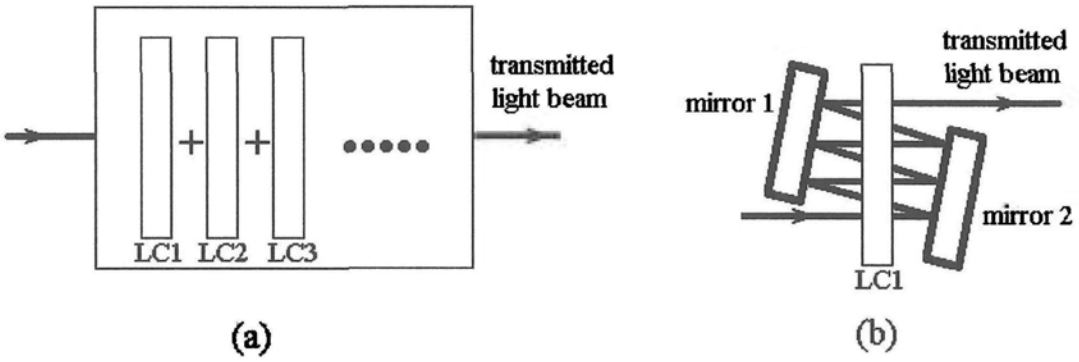

Fig. 5.15. *Phase retardation enhancement methods* (a) *by stacking up LC devices and* (b) *by using two mirrors to reflect the light beam multi-pass through the LC device.*

Due to resource limitation, we only tried the second enhance method, shown in Fig. 5.15b, in this experiment. We find that this is very important in achieving the expected performance in the sensor system. The LCM is placed between two mirrors so that the beam gets folded a number of times and experiences many times larger retardation modulation depth achievable by the LCM. In the case of the maximum phase retardation achievement, the total retardation depth is 18π (i.e. going through the LCM 9 times) as shown in Fig. 5.16. The significance of this technique is that we need to capture as many cycles of phase modulation as possible in every signal trace in order to increase the phase extraction accuracy as the subsequent data processing algorithm relies on comparing the phase locations of truncated sine waves.

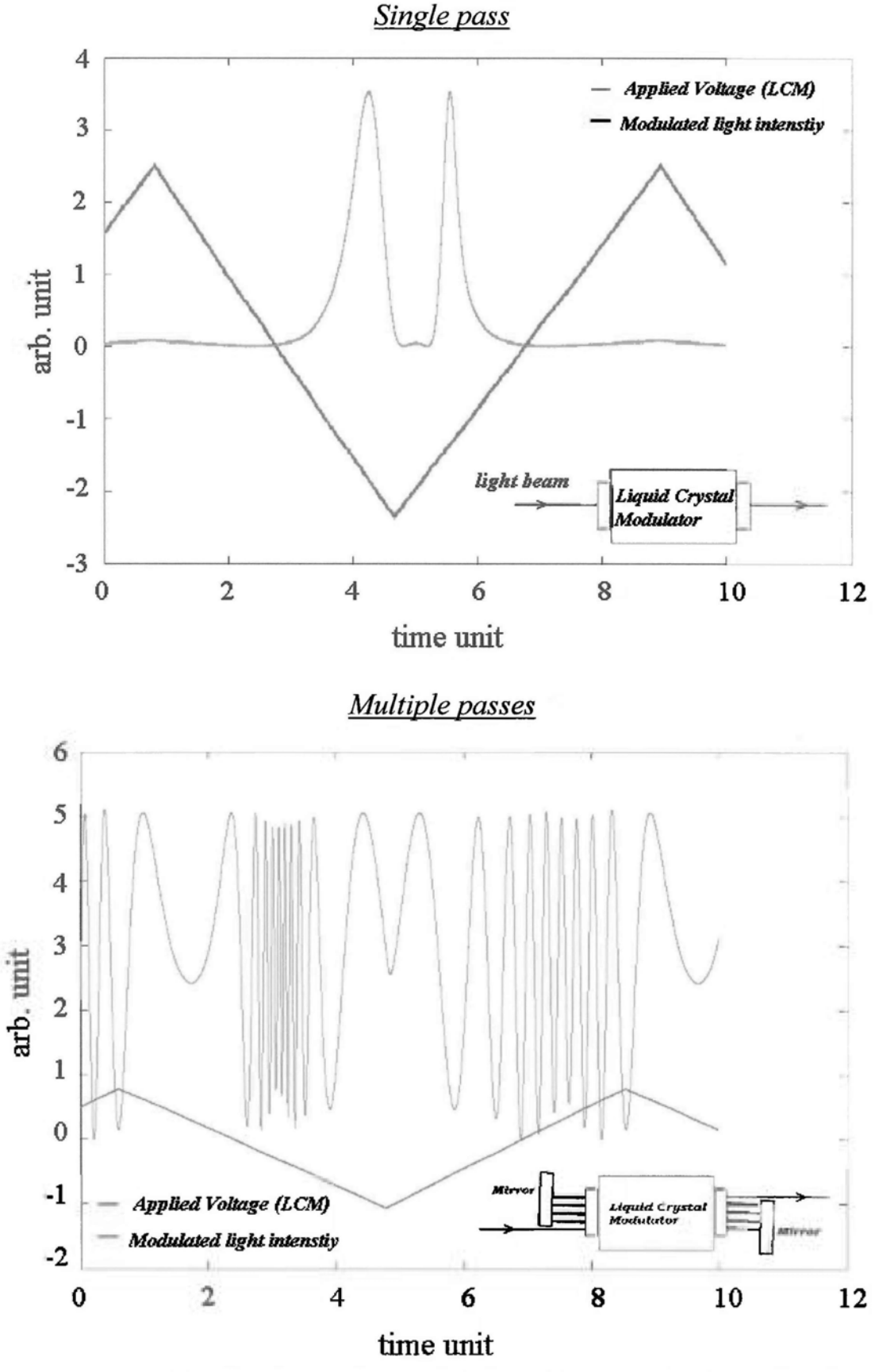

Fig. 5.16. *The response of phase retardation modulation by the setting of single pass and multiple passes method.*

5.2.5 Sensing experiments on glycerin-water mixtures

The samples are glycerin-water mixtures with 0% to 16% of glycerin in weight percentage, which correspond to a refractive index ranging from 1.3330 to 1.3521 refractive index unit (RIU) [92]. Fig. 5.17 shows the measured SPR phase versus concentration plot.

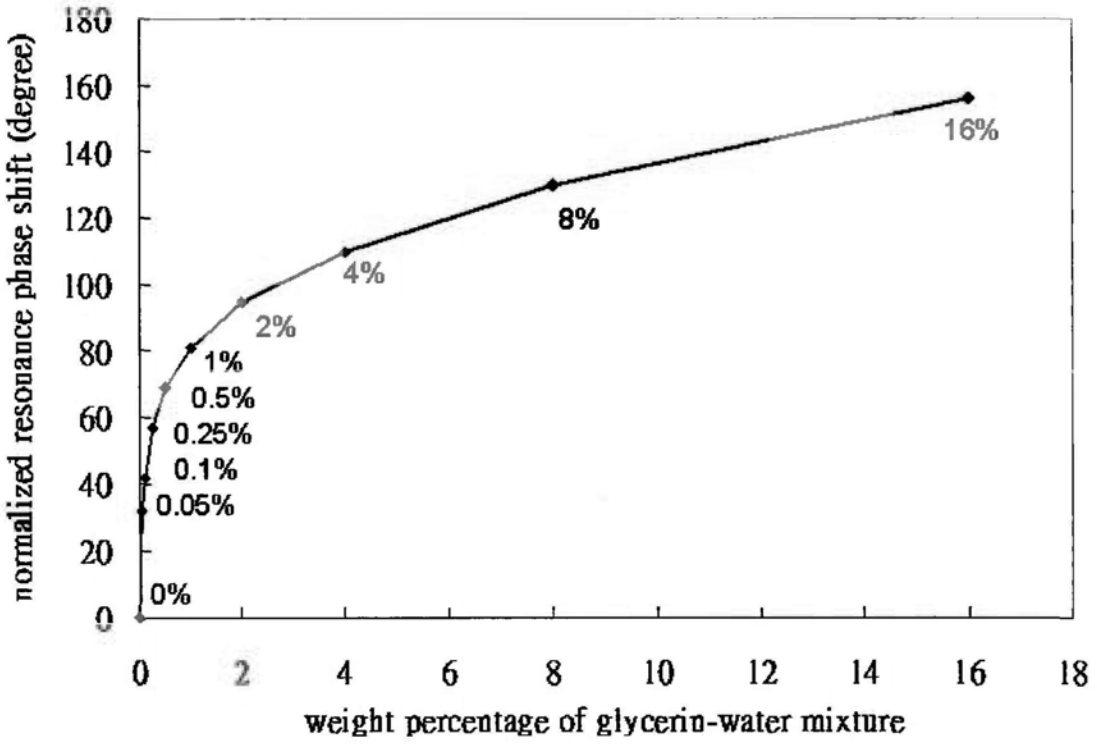

Fig. 5.17. *Variation of relative differential phase (reference to pure water) versus glycerin concentration*

As seen from this plot, we can only observe approximately 50% of the maximum SPR phase change across the SPR resonance dip. This is because experiments start at the minimum point of the SPR resonance dip, which was halfway through the phase jump across resonance. The system continuously shifted away from resonance as the refractive index of the sample increased from 1.3330 to 1.3521. To calculate the best resolution limit of our system, we use the first two data points from the plot, which

are obtained in the most sensitive region (near the resonance dip). They correspond to two sample mixtures, i.e. pure water and 0.05% glycerin in water, with a change of refractive index equivalent to 6×10^{-5} RIU and a SPR phase change of 32.12°. Moreover, as shown in Fig. 5.18, the short-term system stability is also monitored and we obtain a phase measurement fluctuation of ±0.0028° (root-mean-square) or 0.013° (peak-to-peak) within 45 minutes. It should be mentioned that the stability of the present system is significantly better than that reported in a similar LCM-based setup [102], which is around 0.1° (peak-to-peak). Using ±0.0028° as the baseline of our system stability, the calculated resolution limit is $\pm5.2\times10^{-9}$RIU. The long-term system stability is also monitored and we obtain a phase measurement fluctuation of 0.05° (peak-to-peak) over 8 hours as shown in Fig. 5.19.

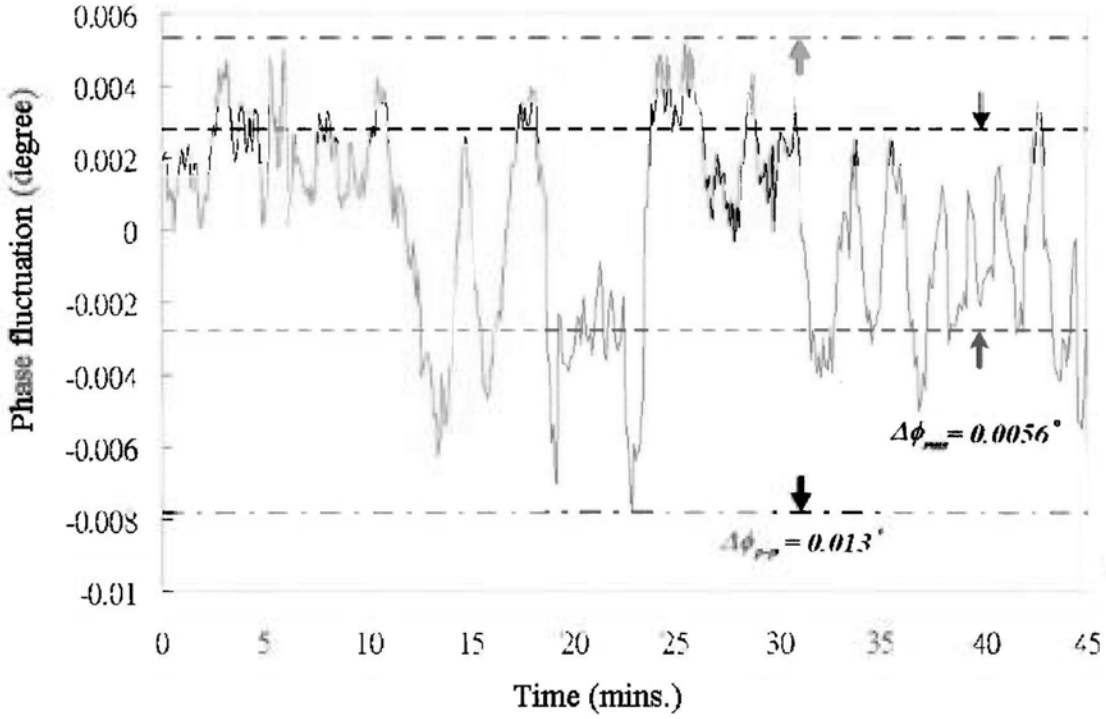

Fig. 5.18. *System stability measurement over 45 minutes*

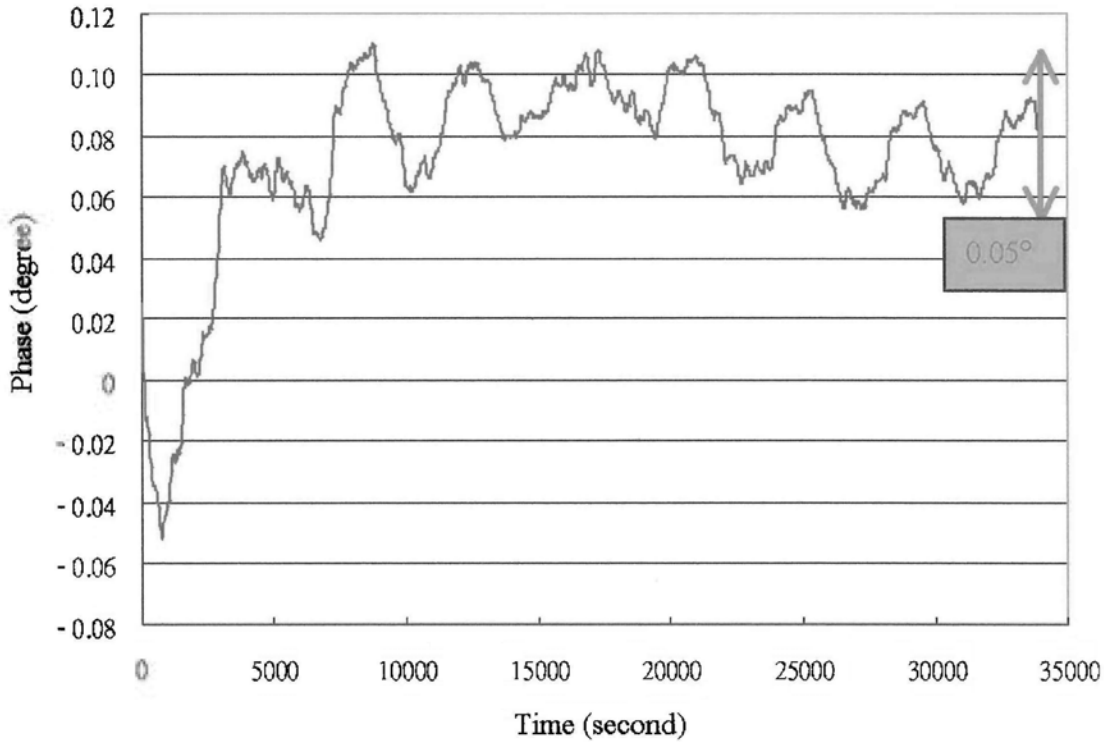

Fig. 5.19. *System stability measurement over 9 hours*

5.2.6 Monitoring DNA-DNA interaction for DNA detection (Herpes virus DNA)

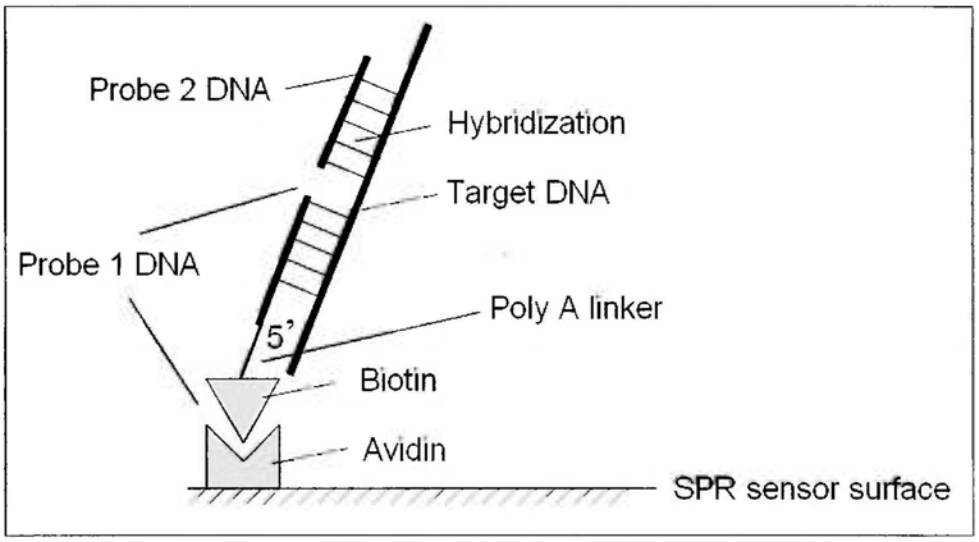

Fig. 5.20. *Schematic diagram of final DNA complex on sensor surface*

First of all the description of DNAs binding for detection of herpes virus DNA is depicted in Fig. 5.20. It describes the final DNA complex to bind the sensor surface. It starts from the treated gold surface by forming a monolayer of avidin, which is used as binding site of biotin moiety on the sensor surface. Avidin is a natural occurring protein and its properties is found to bind specifically and tightly to biotin moiety. The detection involved three different DNAs including probe 1, target and probe 2 DNA. Their details are listed below:

Probe 1 DNA:

Biotin-5'-AAAAAAAAAAACGAGTCCGTAGAAGGGTCCTC-3'

- A biotin group is labeled at one end for binding to the immobilized avidin and the ten 'A' (underlined) serve as linker.

Target DNA:

3'TGCTCAGGCATCTTCCCAGGAGCAGGTCGTTCTTCTCCTCCACCAT5'

- This DNA can bind Probe 1 to one end and Probe 2 to the other. It mimics the herpes viral DNA which can be found in patient samples.

Probe 2 DNA:

GTCCAGCAAGAAGAGGAGGTGGTA-3'-(Phase signal enhancement molecules)

- It binds to target DNA. Phase signal enhancement molecules can be linked at one end of DNA for amplifying the phase detecting SPR signal.

For the actual measurement, avidin and probe 1 DNA should be assembled on the sensor surface first. The measurement starts from the samples which come from patients. Finally the probe 2 DNA is applied to confirm the result. In this experiment, we aim to assess the capability of pSPR sensing system to monitoring the DNA-DNA interaction and we successfully demonstrated the use of pSPR for detecting herpes viral DNA. The result of the herpes viral DNA detection is shown in Fig. 5.20. 4μM of the herpes viral DNA resulted in a total of 12° phase change in the sandwich detection assay. The herpes viral DNA is first immobilizes on the sensing surface, which shifts the phase by 8°. Further molecular binding (probe 2 DNA), which was specific to the complex of the herpes viral DNA and its acceptor, gave an additional 4° phase change. This molecule has the potential of phase signal enhancement through providing a linkage for the other signal amplifying molecules.

Initially, an avidin monolayer coated on sensing surface is prepared. First step, 4μM Probe 1 DNA (with sequence complementary to Herpes virus DNA) is injected into the sensing surface and bind to avidin through its biotin moiety. Then 4μM Probe 2 DNA is injected as the control experiment as no target DNA (herpes virus DNA) exists. Target DNA (4μM, DNA fragment contains part of the sequence of Herpes

virus DNA) is then loaded. Probe 1 DNA bind to this target DNA through its complementary sequence. The captured target DNA is then detected by injecting 4μM Probe 2 DNA (where Probe 2 DNA also contains complementary sequence to target DNA). These immobilized DNA is detected by the change of the SPR signal as shown in Fig. 5.21. Taq buffer (20mM $(NH_4)_2SO_4$, 75mM Tris-HCl (pH 8.8), 1.5mM $MgCl_2$) is injected between each injection step of the DNA to rinse out the non-attached DNA.

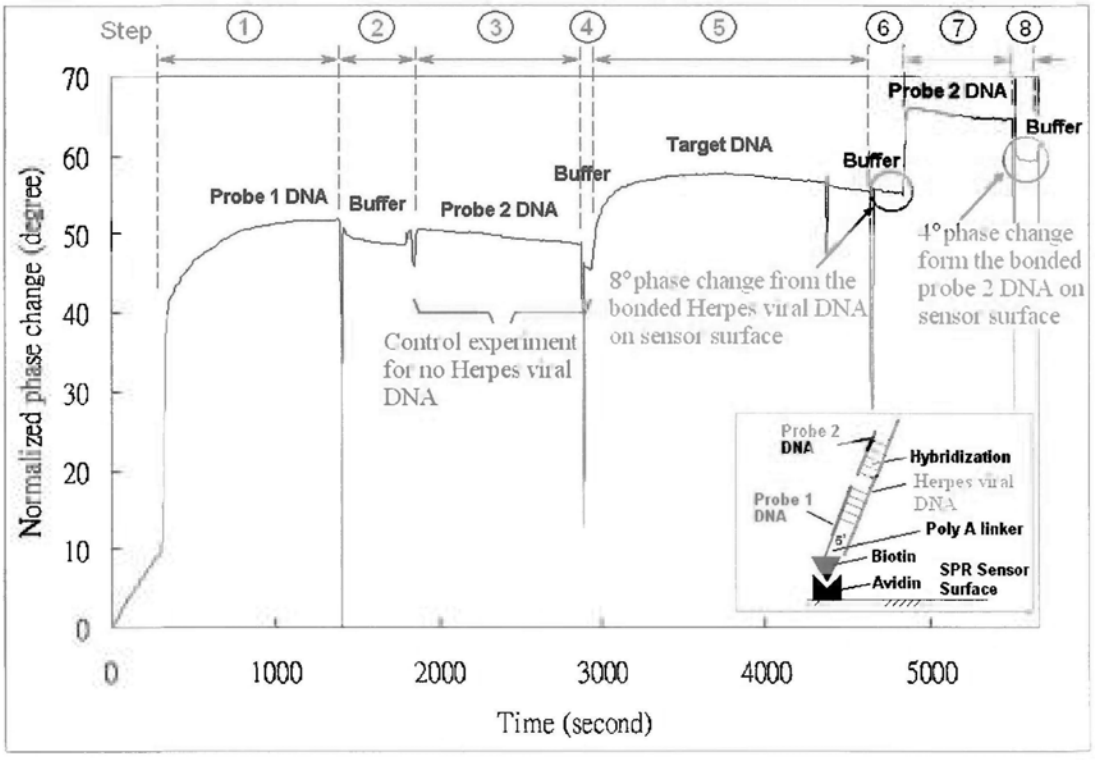

Fig. 5.21. *Herpes viral DNA detection by pSPR biosensor system*

5.2.7 Biosensor chip design

During this experiment, we also design a fabrication method for SPR biosensor chip. For different applications of SPR sensor, the requirement of the sensing chip design is different from typical flow-cell configurations in terms of size, number of channels and optical coupling surface quality. In order to fulfill the requirements of practical applications, we present several of our designs for both single and multi-channel bio-

chips in the following. These modules are only required to follow some sample steps to fabricate without any special tools. It is very important to fulfill our concept, simple and low cost, to develop a biochip integrated with a flow-chamber for a range of customized SPR sensing applications. While practically it is always better to use minimal quantity of sample fluid, the sample consumption of any flow-cell design is an important issue. Our design therefore aims to minimize the volume inside the flow-cell chamber. In order to achieve this target, we need to consider two items: (1) surface area and the shape of chamber; (2) thickness of the chamber. For item (1), we also need to consider the constraints of the optical system such as beam size and the physical dimensions of the optical detector to be used. As the number of chambers is increased, the surface area of each chamber decreases. This is illustrated in the sample chamber patterns shown in Fig. 5.22. As shown in Fig. 5.22(a), a single chamber flow-cell, which is for single-element or multi-element measurement, the flow-cell has one flow-in and one flow-out channel.

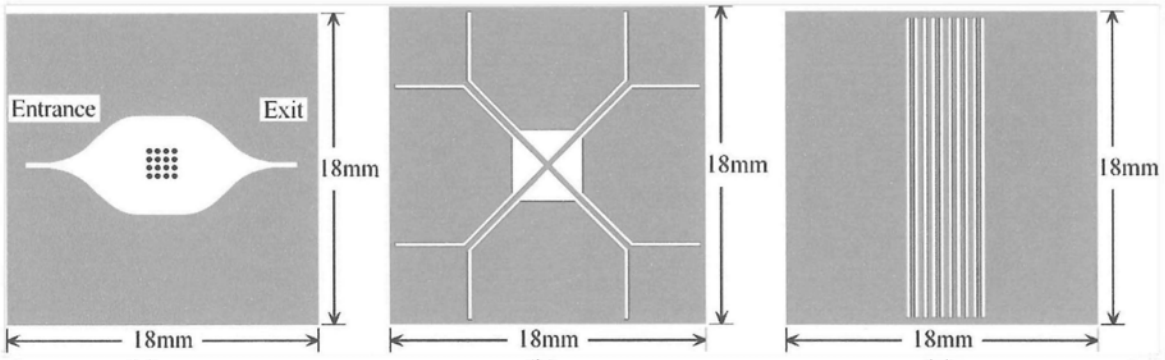

Fig. 5.22. *(a) A single chamber flow-cell with entrance and exit channels. (b) A four chamber flow-cell design. (c) A 10 chamber in-line flow-cell design.*

In fact, as shown in Fig. 5.23(a), this single-chamber design may be used with a charge coupled device (CCD) for capturing SPR phase images so that the sensing activities at each sensor site can be monitored. In this case, a 4×4 matrix of spots containing the conjugates of the target biomolecules have been pre-printed on the

center region of sensor surface. This design can provide a platform for the investigation of the specific binding interactions between various types of biomoleucles in parallel when the sample solution flows into to the chamber. Sensor dots containing biomolecules pre-printed on the sensor surface are shown in Fig 5.23(b). The shape of the chamber is also considered important as typical light beams from lasers are of a Gaussian profile. In SPR measurements, the beam is projected on the sensor surface at an angle. The circular beam therefore takes an elliptical shape. Correspondingly the shape of the flow chamber should be elliptical in order to achieve best power uniformity. In addition, an elliptical chamber also provides more uniform flow rate within the chamber and thereby minimizes any possibility of dead volume and reduces the chance of bubble formation. In a real SPR phase imaging system, the sensor chip is placed to a dove prism (sensor head) by using refractive index matching oil as shown in Fig 5.23(a). As shown in Fig 5.22(b) and (c), various designs for four chambers and 10 chambers with different shape may also be possible for different bio-sensing applications. For four-chamber version is in fact design for use with a four-quadrant detector, although CCD imager may be used, which matches with the shape of the photodetector elements. A practical implementation of this four-chamber flow-cell is shown in Fig 5.24(a). In Fig 5.22(c) and 5.24(b), we also present the design and a completed sample of a 10 chamber in-line flow-cell. In this case, one can use a CCD as usual, or a linear array of photodetectors. The incorporation of these flow-cells will certainly simplify system design for high-throughput SPR phase measurement. In practice, the in-line configuration has the advantage of being easier to manufacture and achieving lowest possible consumption of sample volume. The flow is also constant throughout the entire chamber.

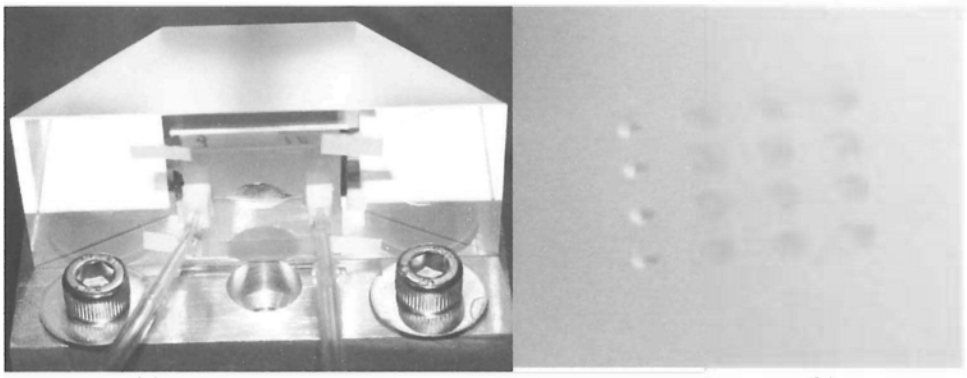

(a) (b)

Fig. 5.23. *(a) A single flow-cell with entrance and exit channels. This chip is attached to a dove prism by using refractive index matching oil. (b) For antibody-antigent measurement based on phase-sensitive imaging SPR biosensing, 4 different antigents (4×4 matrix form) have been pre-printed on the surface of the single chamber flow-cell biosensor chip.*

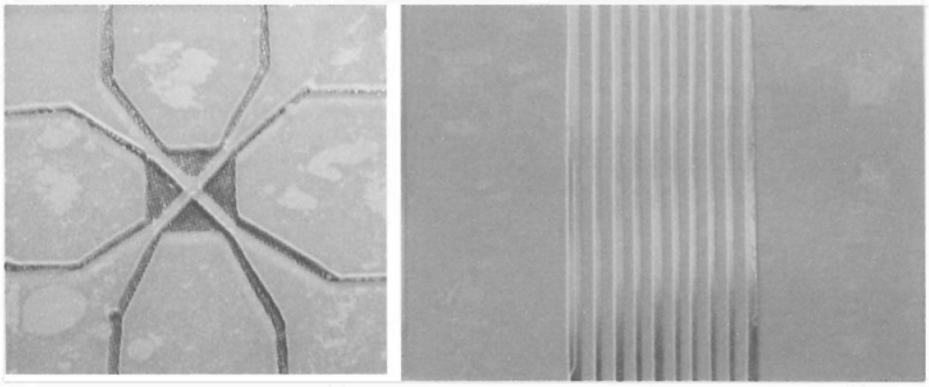

(a) (b)

Fig. 5.24. *(a) Practical four channel flow-cell sensor chip. (b) Practical 10 channel flow-cell design.*

5.2.8 Summary

A single-beam self-referenced phase-sensitive SPR sensor based on differential measurement between the probe and reference channel has been demonstrated. In order to address the limitations of LCM as a retardation modulator, we propose two simple techniques, to improve its modulation range and stability, i.e. the use of multi-pass and active temperature control. Since both s- and the p-polarization traverse an identical path in the system, the signal generated from direct interference between

them will eliminate unwanted common-mode errors not related to the shift in SPR condition. Errors due to temperature dependence and non-linearity of the LCM can also be removed by taking the differential change between the probe and reference signal obtained immediately before and after the sensor head. The experimental resolution limit of our system is estimated to be $\pm 5.1 \times 10^{-9}$ RIU. We also successfully demonstrate the real-time Monitoring DNA-DNA interaction for DNA detection (Herpes virus DNA).

5.3 **Experiment III:** Wide dynamic range phase-sensitive SPR sensor

In this experiment, we want to provide a possible solution to solve the problem of high sensitivity region only on a narrow dynamic range closed to resonance dip on pSPR sensing system. To demonstrate our idea and concept, the pervious setup, a single-beam self-referenced phase-sensitive SPR sensing system, has been modified. The principle of phase measurement scheme is the same as the previous experiment and discussed in Section 5.23. A liquid crystal cell is also used as a phase retardation modulator. Therefore, we would like to concentrate on discussion of the method of wide dynamic range achievement on pSPR system in this section. We have constructed an experimental setup (Fig. 4.15) and then it is used for measuring the concentrations of constituent components in a liquid mixture of glycerin and water in weight percentage. There are three different range of concentration range from 1.) 0% to 1% for investigating the response on high sensitivity range; 2.) 0% to 8% for observing the response of wide dynamic range measurement; 3.) 0% to 46% with 2% in weight percentage for one increment to investigate the maximum dynamic range of the system.

5.3.1 The dynamic range issue in phase-sensitive SPR

A typical SPR phase properties correspond to the absorption is shown in Fig. 5.25. There is a steep phase change to occur near on the absorption dip region. This is why pSPR can provide a better sensitivity compared with the conventional methods. When the refractive index of sample medium is increasing, the resonance dip shifts to a higher incident angle region. For our previous experiments, it is set at the center of absorption dip initially and fixed at that angle. Therefore high sensitivity region only can get from the initial of the measurement (Fig. 5.8 and Fig. 5.17). It is due to the

fact that the observation point is leaving from the dip region when the refractive index of the sample medium is increasing.

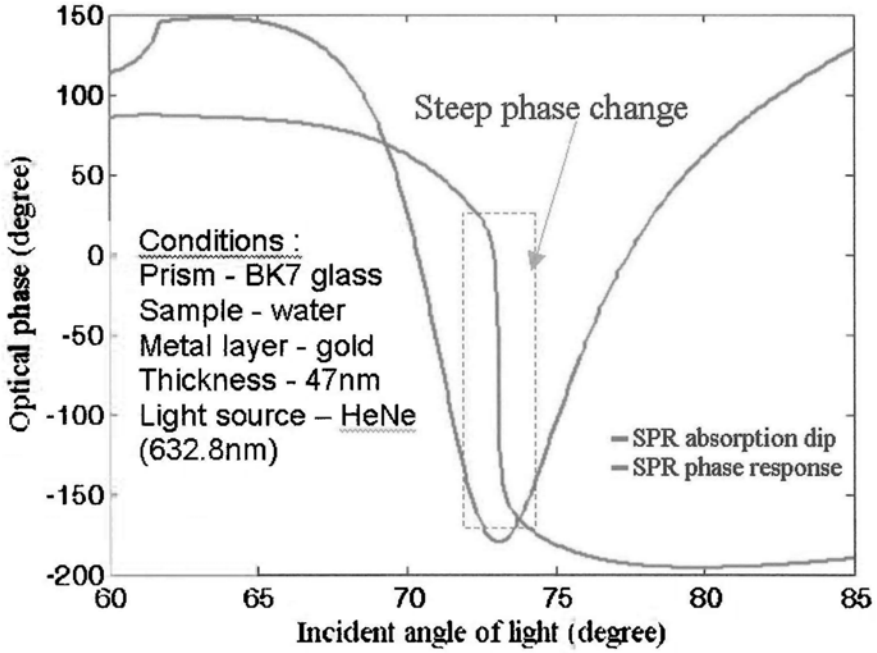

Fig. 5.25. *Typical optical properties of SPR for monochromatic light with different incident angle*

To achieve the wide dynamic range measurement with high sensitivity, we suggest using a linear detector array to capture the entire phase shift across the resonance dip. Any large change in refractive index simply leads to shifting the phase change transition by several pixels. Consequently, the high measurement resolution associated with pSPR is still preserved because of the fact that our detector elements are capable of capturing the sharp change across resonance. Fortunately, we have developed a single beam self-referenced phase-sensitive SPR sensor based on differential measurement by using a LCM as a retardation modulator. The concept of pSPR wide dynamic range measurement can be directly adopted onto it because the single beam system is given flexibility on the optical alignment and a LCM as a retardation modulator can provide a suitable operation frequency for CCD array signal

capturing. We have successfully demonstrated by using a 128-elements detector array association with a range of incident angle from around 63.5° to 78.5°. It is described in detail in the Section of 4.4.3.

5.3.2 Experiments on glycerin-water mixtures

Three sets of glycerin-water mixtures are prepared by mixing distilled water with glycerin to investigate the system performance from extremely small change, mid-range and extremely large change in refractive index of samples media.

5.3.2.1 Extremely small range

The samples are glycerin-water mixtures with 0% to 1% of glycerin in weight percentage, which correspond to a refractive index range from 1.3330 to 1.3342 RIU. Fig. 5.26 shows the measured SPR phase versus concentration plot. The data of this plot is collected from a single pixel of photodiode array. The pixel initially is located closely to the resonance dip region. As seen from this plot, we can only observe approximately a linear and high sensitivity region from the 0% to 0.01% at the plot. In this region, over 40% of the maximum SPR phase change across the SPR resonance dip occurs. The system continuously shifted away from resonance as the refractive index of the sample increased from 1.3330 to 1.3342 RIU. The table 1 is clearly to show the refractive index of each samples and its corresponding phase shift value. To estimate the resolution of our system, we use the first four data points from the plot, which are obtained in the most sensitive region (near the resonance dip). They correspond to fourth sample mixtures, i.e. pure water and 0.01% glycerin in water, with a change of refractive index equivalent to 1.2×10^{-5} RIU and a SPR phase change of 67.50°. Therefore, the estimated resolution is 1.78×10^{-7} RIU/degree.

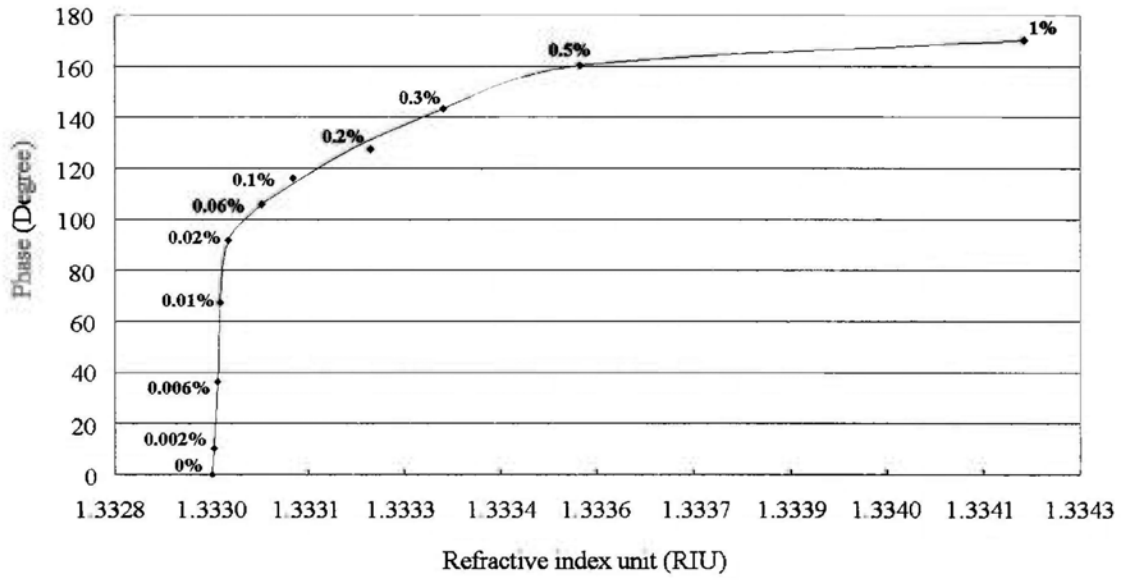

Fig. 5.26. *Phase response curve for different refractive index of glycerin and water mixture solution in single pixel measurement of CCD array detector*

Refractive index (RIU)	Phase (degree)
1.333000	0
1.333002	10.38
1.333007	36.35
1.333012	67.50
1.333024	91.73
1.333072	106.05
1.333120	116.29
1.333240	127.53
1.333360	143.20
1.333600	160.41
1.334200	170.17

Table 5.1. *Experimental data on refractive index of samples corresponding to its phase shift in degree*

5.3.2.2 Mid-range

The samples are glycerin-water mixtures with 0% to 8% of glycerin in weight percentage, which correspond to a refractive index range from 1.3330 to 1.3424 RIU. The increment of one step of refractive index of the samples is 1%. In this experiment,

we successfully demonstrate our proposed concept for pSPR wide dynamic range measurement by monitoring the phase changes across the dip. The CCD is used to capture the phase information across the resonance dip when the dip shifts are induced by increasing the refractive index of the sample media. The result is shown in Fig. 5.27.

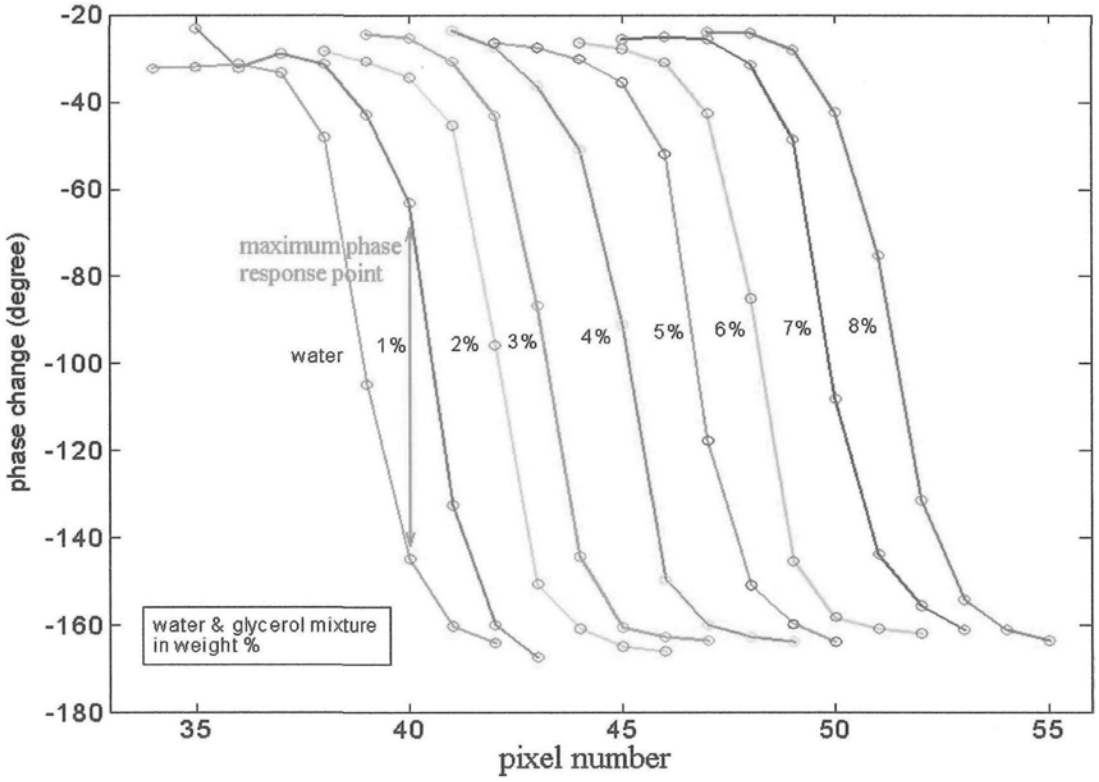

Fig. 5.27. *The phase changes across the resonance dip from 0% (water) to 8% glycerin and water mixture.*

Actually, we are observing the phase properties from the different incident angle across the dip as shown in Fig. 5.27. For the real application, the maximum phase response value on each refractive index increment arouses our interest and it can be obtained from the result. For example, the maximum phase response can be observed from the pixel number '40' occurring on the change of water to 1% glycerin-water mixture. The maximum phase response value of each refractive index increment on samples media are recorded and plotted in Fig. 5.28. As seen from this plot, we can

get an approximately linear respond on pSPR system and maintained its high sensitivity properties from the measurement range on 0% to 8% glycerin-water mixture. A very good calibration measurement should be conducted first as a basic reference for the real application. Otherwise, a huge refractive index change on sample medium will make the system lose the base line. It means the phase change cannot be quantified.

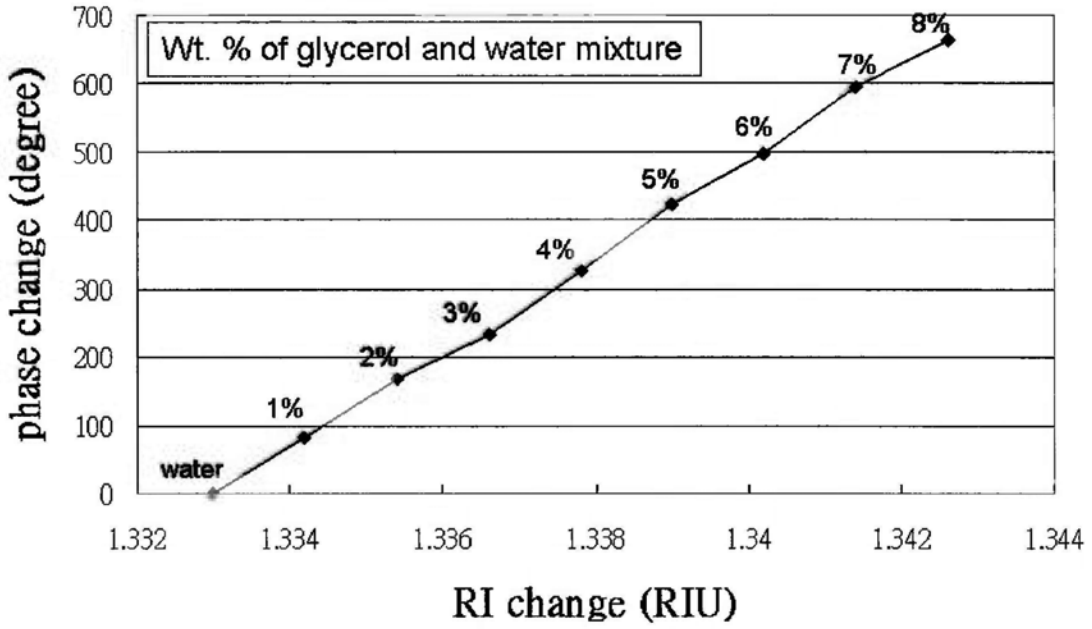

Fig. 5.28. *Accumulation of the phase changes record from maximum response on each refractive index increment*

5.3.2.3 Extremely large range

The samples are glycerin-water mixtures with 0% to 46% of glycerin in weight percentage, which correspond to a refractive index range from 1.3330 to 1.3887RIU. The increment of one step of refractive index of the samples is 2%. We have successfully demonstrated a wide dynamic range pSPR sensing system with an approximately linear respond from 1.3330 to around 1.39 RIU. The response of the system is not exactly linear as the resonance dip shift response itself is not. In most

cases, the measurement range of system from 1.3330 to over 1.38 RIU should be good enough for most real biosensing applications.

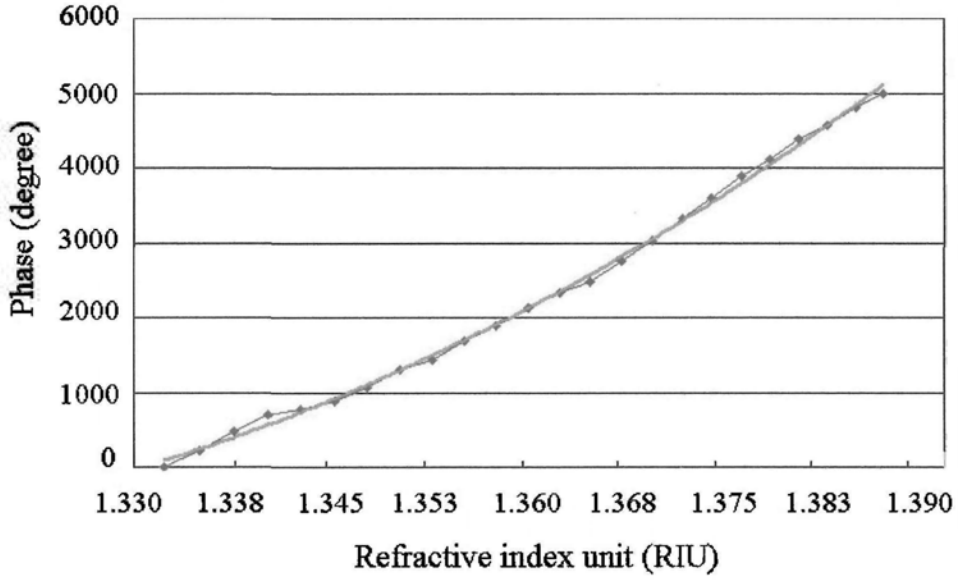

Fig. 5.29. *It is shown the system response from 0% (water) to 46% glycerin-water mixture. The red colored line is the fitted curve.*

5.2.3 Summary

A concept of wide dynamic range pSPR sensor has been proposed by monitoring the phase response across resonance dip region. It is successfully demonstrated through modifying the previous experimental setup, a single-beam self-referenced phase-sensitive SPR sensing system. A cylindrical lens is applied to focus the incident light beam onto sensor surface to produce a range of incident angle of light from around 63.5° to 78.5°. A 128-elements detector array is applied to capture the phase information from the reflected light beams. In order to verify the system performance, we have prepared three sets of glycerin-water mixtures samples on extremely small change, mid-range and extremely large change. The best sensitivity of the system can be verified through an extremely small change measurement. It can be found that the

best sensitivity is estimated to be 1.78×10^{-7} RIU/degree occurred in a narrow region near on the dip. In order to state clear for the concept of wide dynamic range pSPR system, a set of 0% to 8% glycerin-water mixture with 1% increment on each step has been used to demonstrate how the concept is formed. The CCD is used to capture the phase information across the resonance dip when the dip shifts are induced by increasing the refractive index of the sample media. The maximum phase response value can be obtained on each refractive index increment. It means we can get the maximum phase change information on each RI increment and the phase response is approximately close to linear in mid-range change. The maximum detection range of our system has also been investigated. The range is from 1.3330 (water) to around 1.39 RIU as shown in Fig. 5.29.

5.4 **Simulation Experiment I:** Phase response enhancement of using double-pass and multi-pass schemes

In this section we suggest a new idea to improve the sensitivity of phase SPR sensing system by enhancing the phase response. Generally, SPR effect can influence the p-polarized light for its intensity and phase properties. Our new phase enhancement method is based on the accumulation effect as the light beam hits the sensor surface by multiple numbers of times. Double pass arrangement is achieved conveniently by using a mirror to reflect the light beam back in the same path to strike the sensor surface again as shown in Fig. 4.17a. The multi-pass arrangement may be implemented as a Fabry-Perot configuration. Two semi-transparent mirrors are used to confine the light to hit the sensor surface many times as shown in Fig. 4.17b.

5.4.1 Operation principle and experimental results

For the double pass scheme, the SPR effect accumulated two times. By Fresnel equations, the reflection coefficient, *r*, of p- and s-polarized light after reflection off the sensor head can be expressed as $r_p = |r_p| \exp(i\phi_p)$. If the light hit the sensor surface two times, the effect will also accumulated and can be expressed as $r_{2p} = |r_p|^2 \exp(i2\phi_p)$. It is clear that the phase amplification immediately offers a factor of two.

For the multi-pass scheme, we can start from a Fabry-Perot interferometer configuration, as shown in Fig. 4.17b. The SPR sensor head is placed in between the two semi-transparent mirrors. An incoming light passing through the front semi-transparent mirror strikes the sensor surface and reflects off the sensor head. Then the reflected light will be returned to the sensor head by the end semi-transparent mirror. When the light hit to the sensor surface, the energy of the light will lose for SPR effect. As part of the light beam will be reflected back and forth between the two mirrors, any phase change caused by the SPR effect will also get amplified. The output signals, relative amplitude and net phase change of the p-polarized light, can be obtained from the two sides of mirrors, mode (1) and mode (2), to be expressed respectively by the following equations:

Mode (1) = pass(1) + pass(3) + …

$$|r_p| \cdot \Gamma \cdot \exp[i\phi_p] + |r_p|^3 \cdot \Gamma \cdot R^2 \cdot \exp[i3\phi_p] + \cdots$$

$$\overset{\Gamma = R}{=} \sum_{n=1}^{\infty} |r_p|^{(2n-1)} \cdot R^{(2n-1)} \cdot \exp[i(2n-1)\phi_p], \qquad \text{(Mode(1))}$$

Mode (2) = pass(2) + pass(4)+…

$$\left|r_p\right|^2 \cdot \Gamma \cdot R \cdot \exp\left[i2\phi_p\right] + \left|r_p\right|^4 \cdot \Gamma \cdot R^3 \exp\left[i4\phi_p\right] + \cdots$$

$$\overset{\Gamma=R}{=} \sum_{n=1}^{\infty} \left|r_p\right|^{(2n)} \cdot R^{(2n)} \cdot \exp\left[i(2n)\phi_p\right] \qquad \text{(Mode(2))}$$

where

$\left|r_p\right|^n R^n$ - the relative amplitude,

$n\phi_p$ - the net SPR phase change when the beam has undergone *n*th pass,

$|r_p|$ - the amplitude reflection coefficient of p- polarized light after reflection off the sensor head,

ϕ_p - the phase change induced by SPR effect on p-polarized light,

R - the amplitude reflectivity coefficient of semi-transparent mirror,

Γ- the amplitude transmission coefficient of semi-transparent mirror.

According to the description in Mode (1) and Mode (2), the accumulated phase change effect through beam folding is in fact a vector addition series. Due to the energy-absorption by SPR effect, the relative amplitude of output signals will also change exponentially, which lead to an insignificant effect of those vectors to whole phase amplification effect if the beam has traverse several times in this cavity. So basically we just take into account the first several items in the vector addition equations such as n = 2, and this leads to the conclusion that the multi-pass scheme offers a net phase change in the p-polarized light in excess of two times as shown in Fig. 5.30 when we extract the signal output from the Mode (2). However, when we extract the SPR phase from the Mode (1), phase amplification fact is relatively less pronounced. It only has closely to 1 on the amplification, so it can be ignored. We simulate a situation of single pass (conventional method) and phase enhancement on Mode (2). Light source is HeNe laser on 632.8nm and a BK7 glass prism as a sensor

head coated with 33nm gold film. The incident angle of light is fixed at 72.3°. For easier to present, a roughly linear phase response region is chosen for the refractive index of sample range on 1.3330 (water) to 1.3521. The result is shown in Fig.5.30

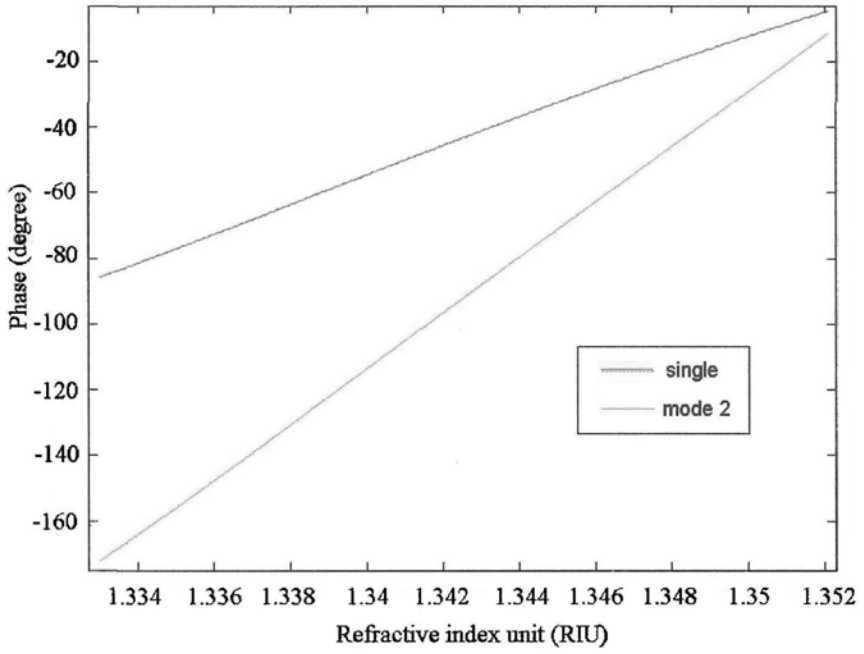

Fig. 5.30. *Simulation result of single pass and multi-pass on Mode (2)*

Our concept is further proofed by experimental result as shown in Fig. 5.31. It is a measurement on protein-DNA binding. The results clearly show that the phase change of single pass method is 7.8°, double pass method is 15.7° and multi-pass method is 17.6°. For further details of the experiment, please refer to our paper [93]

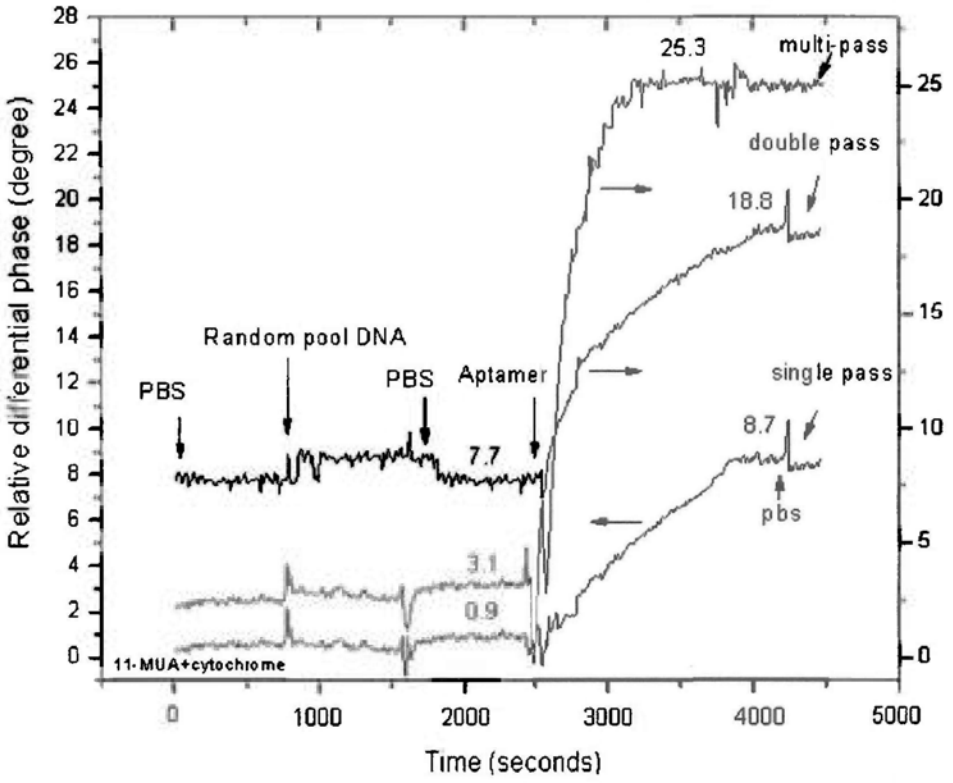

Fig. 5.31. *Real-time differential phase obtained from protein – DNA binding experiment. The random pool DNA works as nonspecific target and DNA aptamer as specific target.[93]*

5.4.2 Summary

Phase enhancement methods of double pass and multi-pass have been investigated both on simulation work and experiment work. For the results, it is agreed that the multi-pass scheme offers a net phase change in the p-polarized light in excess of two times enhancement.

5.5 **Simulation Experiment II:** Multi-layer structure for sensitivity improvement

In this section we suggest a novel idea to improve the sensitivity of phase SPR sensing system by optimizing the sensor surface. Generally, gold and silver are commonly used as the transducing layer for SPR sensors. Indeed, silver exhibits better optical properties for SPR sensing applications, but it has relatively poor chemical resistance and it deteriorates when exposed to ambient atmosphere or chemical solution [94,95]. Although gold layer is less sensitivity, it is still the most commonly used in SPR sensing surface. In order to further improve the performance, we propose to make a new sensor head structure for phase SPR sensing applications as shown in Fig. 4.18.

5.5.1 Long range SPR configuration and simulation results

To compare the performance of between the suggested system and the existing configuration, two different layer configuration of the transducing layer including classical single metal film and our proposed long range SPR configuration have been investigated. In order to have a fair comparison, same material of the transducing should be used. Since gold is commonly used, it is chosen in this simulation. The low refractive index glass prism, BK7, is also most commonly used for the optical coupler. The light source is HeNe laser on 632.8nm. The sample medium is started from water (1.3330 RIU). The dielectric constant of metals and glass can be referred to reference [104] and [105] respectively. We would like to compare their absorption dip profile first.

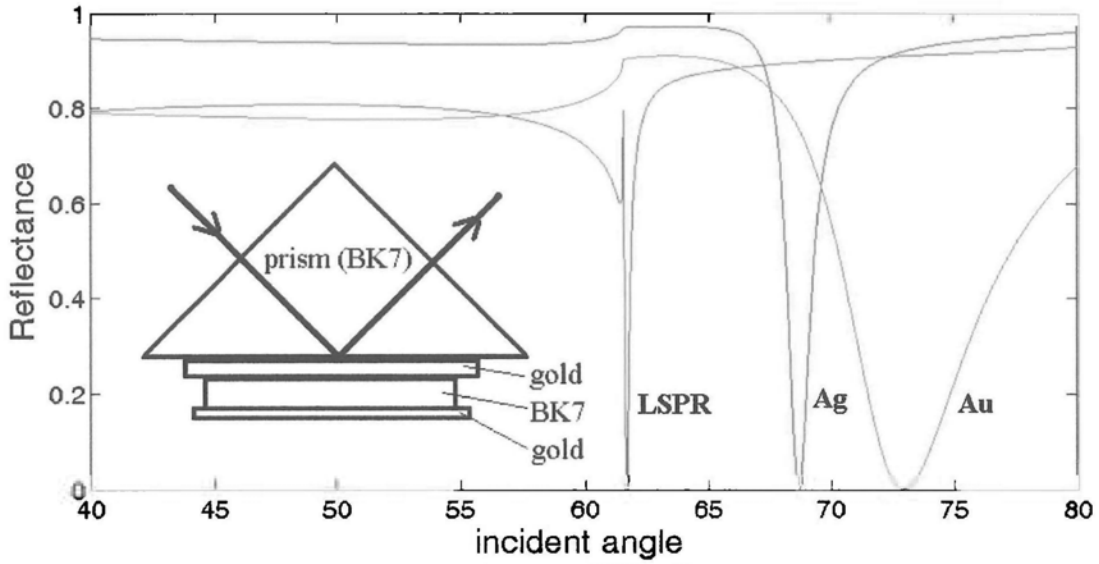

Fig. 5.32. *Comparison of absorption dip profile for existing single metal layer and LSPR structure*

The optimized thickness of the transducing layers for generating the strongest SPR absorption dip are 48nm-gold, 55nm-silver and 48nm-gold/335nm-BK7/2nm-gold for LSPR structure as shown in Fig. 5.32. The resonance angle is 73.03°, 68.72°and 61.76° for the gold layer, silver layer and LSPR configuration respectively. And then we can see from Fig. 5.32 that LSPR configuration can provide narrow absorption dip. It is highly related to the shape change of the phase near on resonance dip. Another aspect for governing the sensitivity of the phase measurement should be the resonance dip shift for varying the refractive index of sample medium. It is also investigated and the result is plotted in Fig. 5.33. The refractive index change of the sample medium is from 1.3330 (water) to 1.3530 RIU. The resonance dip shift is 3.33°, 2.59° and 1.51° for the gold layer, silver layer and LSPR configuration respectively. According to the result, gold can provide the best dip shift and the value is greater than LSPR one time more. Fortunately, LSPR can provide a narrow the resonance dip profile much more than gold layer. After mixing these two parameters, the LSPR may provide a better

phase response than the existing method. It is also studied and shown in Fig. 5.34.

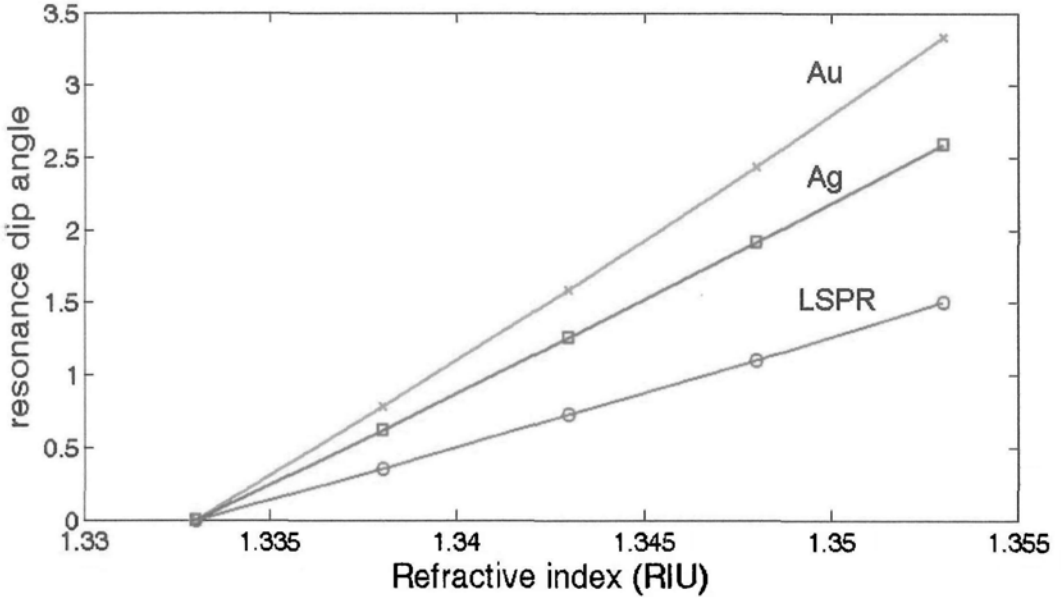

Fig. 5.33. *It shows the relation between the refractive change on sample medium and resonance dip angle shift.*

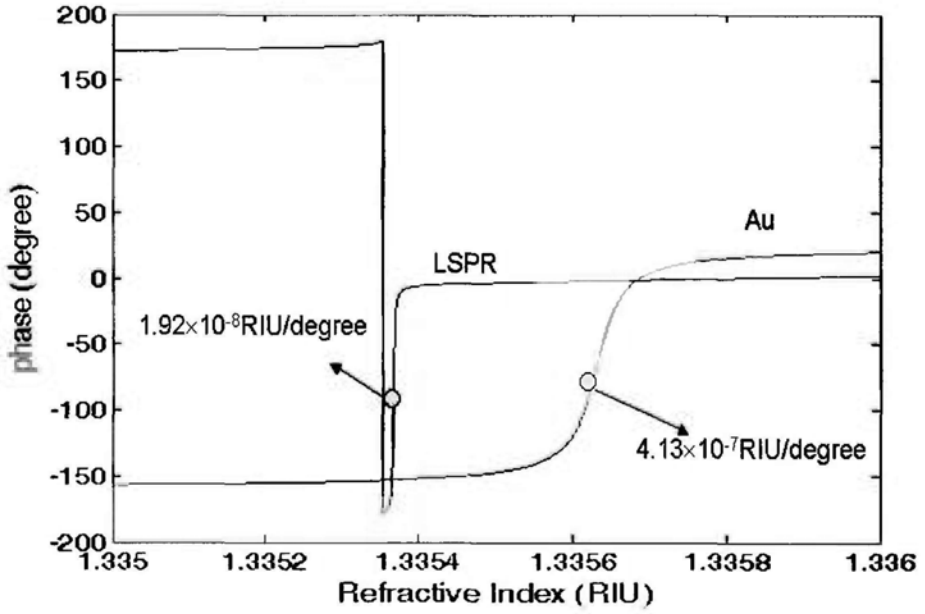

Fig. 5.34. *It shows the relation between the refractive change on sample medium and resonance phase response.*

We can see from Fig. 5.34 that LSPR configuration can provide the best sensitivity,

1.92×10^{-8}RIU/degree. It is ten times greater than the existing method.

5.5.2 Summary

A LSPR configuration has been proposed for sensitivity improvement and its performance has been simulated using Fresnel's formulas. Numerical results show that this configuration performs better than a gold film as a transducing layer more than ten times.

5.6 Simulation Experiment III: Eletro-optical tunable resonance for wide dynamic sensing

This section proposes to develop a novel tunable phase-sensitive SPR photonic biosensor system based on the use of electro-optic polymer within the SPR sensor layer stack as shown in Fig. 4.19. The primary objective is to make a model and simulate the proposed sensor system and demonstrate numerically that it can possibly perform with high sensitivity and wide dynamic range. The active window of refractive index detection can be shifted when applying a voltage to the sensor head. Consequently, the system is always kept at its maximum sensitivity regime throughout the biosensing process. We shall also fabricate tunable biosensor micro-arrays, and SPR phase measurements from individual biosensor sites are extracted using existing phase-imaging algorithms developed pervious in our team [96].

5.6.1 Electro-optic (EO) tuning in attenuated total reflection (ATR)

On the topic of electro-optic (EO) tuning in ATR, so far the technique has been demonstrated in optical modulators for optical telecommunication applications where the speed of response (up to GHz) and extinction ratio are the key considerations [97,98]. Typically, a voltage of ~10V was sufficient to shift the SPR dip by 0.02 angular degrees. The EO materials were made from dispersing non-linear chromophores in a polymer matrix (e.g. PMMA, polyurethane). Although the enabling technology platform is readily available, there is no reported work on using EO tuning in SPR biosensors.

5.6.2 Preparation of the EO layer

In practical processing of the EO layer, we shall adopt established procedures and material schemes. The non-linear EO polymer may be prepared by mixing a maleimide-containing non-linear optical chromophore, e.g. AJT100, with a precursor polymer, e.g. poly(methylmethacrylate-co-9-anthrylmethylmethacrylate)(PMMA-AMA), and spin-coated on the silver underlay. This will be followed by a corona poling method in which the polymer film is brought to above its glassy temperature while simultaneously a strong external electric field in the order of kV-MV/cm is applied to align the dipolar chromophores [99]. Finally, a gold film will be deposited on the EO layer. It should be noted that this structure is effectively a long range surface plasmon (LRSP) excitation scheme. The optical intensity in the analyte side tails off in a much deeper manner with a higher field enhancement factor [100]. Moreover, LRSP also offers a much sharper resonance dip. All these ultimately contribute to achieving higher RI resolution.

5.6.3 Simulation results on EO tuning SPR sensor

In order to highlight the significance of incorporating EO tuning in the SPR biosensor head for resolution improvement as well as its tuning range, we present simulation data for a practical 5-layer stack in which the EO layer is assumed to have RI, n = 1.42, which is common for most polymers, and n of – 2%. Fig.5.35 shows the corresponding SPR response curves for detecting RI variations of the analyte. The proposed EO scheme has a theoretical resolution of 7.8×10^{-8} RIU/degree to 9.3×10^{-8} RIU/ degree throughout the tunable RI range of 1.39 to 1.42.

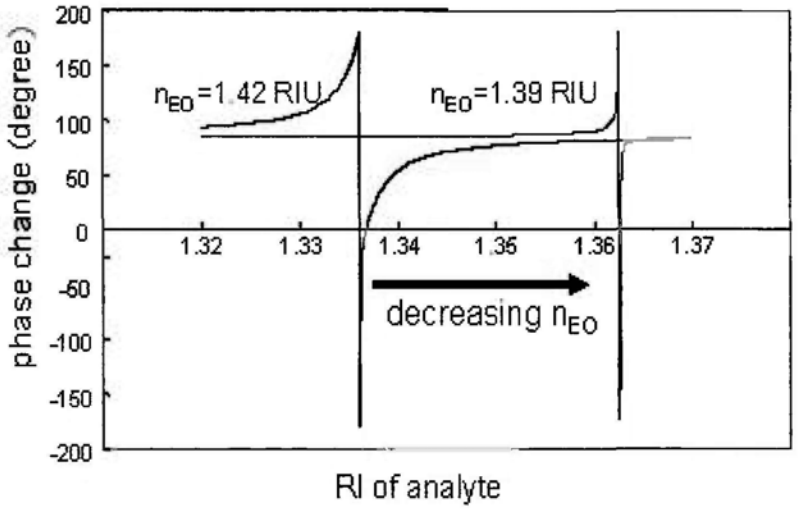

Fig.5.35. *SPR phase change of 5-layer scheme in response to EO turning [prism(BK7)/Ag(50.5nm)/EO(680nm)/Au(3nm)/water]*

As shown in Fig.5.36, because of the excitation of LRSP, the 5-layer scheme (resolution = 7.8×10^{-8} RIU/degree) offers an increase of slope by ~13 times as well as a larger phase swing in comparison to the common 3-layer (resolution = 1.0×10^{-6} RIU/degree) scheme. Clearly, any means that can independently shift the measurable range according to our needs will be extremely desirable. One then gets both high resolutions as well as wide dynamic range. The benefit is enormous.

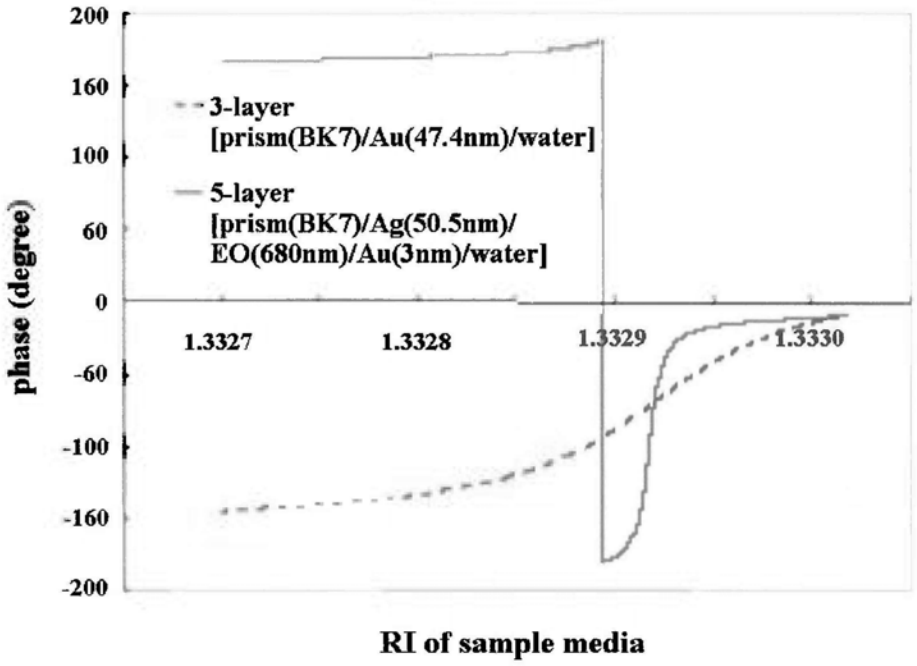

Fig.5.36. *SPR phase change comparison between 3-layer and 5-layer configuration*

5.6.4 Summary

We have demonstrated the possibility of a new concept on EO tunable SPR biosensor system with wide dynamic range by using numerical simulation method. According to the results, it not only can provide a wide dynamic range but also can improve the phase response greater than one order of magnitude by the LSPR effect to compare with conventional 3-layer structure configuration.

CHAPTER 6 Conclusions

6.1 Conclusions

In this thesis, possible solutions for improving the performance of phase SPR sensing system in terms of low-cost, simplicity, ease of assembly, robustness, long lift-time, small size, portability, low noise, wide dynamic range and signal enhancement have been inverstigated in detail. First it demonstrated that a high sensitivity SPR biosensor based on the Mach-Zehnder interferometer. The design primarily operates by taking advantage of the fact that SPR only affects the p-polarization while leave the s-polarization unchanged. This means that differential phase measurement between the p- and s- polarizations will results in SPR signals that are completely free from any disturbances that are common to both channels. Experimental results obtained from glycerin/water mixtures indicate that the sensitivity limit of our scheme is 5.48×10^{-8} refractive index unit based on 0.01° phase stability. To develop a more practical system for real application, we designed a versatile and low cost single-beam self-referenced phase-sensitive surface SPR sensing system. The enhanced performance has been achieved through the incorporation of three design elements: (i) a true single-beam configuration enabling complete self-referencing so that only the phase change associated with SPR gets detected; (ii) a differential measurement scheme to eliminate spurious signals not related to the sensor response; (iii) elimination of retardation drifts by incorporating temperature stabilization in the liquid crystal phase modulator. Based on these results, we have proposed and demonstrated a wide dynamic range phase SPR sensing system by using a multi-resonance angle measurement technique in conjunction with the single-beam self-referenced phase-sensitive SPR configuration. With the use of many incident angles, the system

provides sensing capability that covers a refractive index (RI) 1.33 to over 1.38. A 128-element linear detector array captures the entire phase shift across the resonance dip. Any large change in refractive index will simply lead to shifting the phase change transition by several pixels. Consequently, the high measurement resolution associated with pSPR is still preserved because of the fact that our detector elements are capable of capturing the sharp change across resonance.

This research work also investigated schemes that might enhance the phase change in the SPR sensor. The "double-pass" and "multi-pass" approaches through which the SPR phase can be amplified upon hitting the sensor surface more than once, have been experimentally studied and successfully demonstrated. A double-pass method can immediately offer twice phase change as compared to the single-pass one. Accordingly the multi-pass scheme offers even further phase enhancement. At the same time, a LSPR configuration has been proposed also for phase enhancement and its performance has been simulated using Fresnel's formulas. Numerical results show that this configuration performs better than a single gold film as a transducing layer more than ten times. Finally, we have demonstrated the possibility of a new idea on EO tunable SPR biosensor system with wide dynamic range by using numerical simulation method. According to the results, it not only can provide a wide dynamic range but also can improve the phase response greater than one order of magnitude by the LSPR effect comparing to conventional 3-layer structure configuration.

Reference

1. R.W. Wood, On a remarkable case of uneven distribution of light in a diffraction grating spectrum, Phil. Magm. 4 (1902) 396-402.
2. U. Fano, The theory of anomalous difrac5ion gratings and of Quasi-Stationary waves on metallic surfaces (Sommerfeld's Waves), J. Opt. Soc. Am. 31 (1941) 213-222.
3. R. H. Ritchie, Plasma losses by fast electrons in thin films, Phys. Rev. 106 (1957) 874-881.
4. A. Otto, Excitation of surface plasma waves in silver by the method of frustrated total reflection, Z. Physik 216 (1968) 395-410.
5. E. Kretschmann, H. Raether, Radiative decay of non-radiative surface plasmons excited by light, Z. Naturforsch. 23A (1968) 2135-2136.
6. C. Nylander, B. Liedberg and T. Lind, Gas detection by means of surface plasmons resonance, Sensors and Actuators 3 (1982) 79-88.
7. B. Liedberg, C. Nylander and I. Lundstrm, Surface plasmons resonance for gas detection and biosensing, Sensors and Actuators 4 (1983) 299-304.
8. S.E. Harding and B.Z. Chowdhry, Protein-ligand interactions: hydrodynamics and calorimetry, New York: Oxford University Press (2001).

9. T.P. Vikinge, Surface plasmon resonance for the detection of coagulation and protein interactions, Sweden: Linkopings Universitet (2000).

10. H.C. Hoch, L.W. Jelinski and H.G. Craighead, Nanofabrication and biosystems: integrating materials science, engineering, and biology, New York: Cambridge University Press (1996).

11. J. Homola, S.S. Yee and G. Gauglitz, Surface plasmon resonance sensors: review, Sensors and Actuators B 54 (1999) 3-15.

12. C.L. Baird and D.G.. Myszka, Current and emerging commercial optical biosensors, J. Mol. Recognit. 14 (2001) 261-268.

13. R.L. Rich and D.G. Myszka, Advances in surface plasmon resonance biosensor analysis, Current Opinion in Biotechnology 11 (2000) 54-61.

14. R.L. Rich and D.G. Myszka, Survey of the year 2000 commercial optical biosensor literature, J. Mol. Recognit. 14 (2000) 273-294.

15. J.S. Schildkraut, Long-range surface plasmon electrooptic modulator, Appl. Opt. 27 (1988) 4587-4590.

16. G.T. Sincerbox and J.C. Gordon, Small fast large-aperture light modulator using attenuated total reflection, Appl. Opt. 20 (1981) 1491-1494.

17. P.J. kajenski, Tunable optical filter using long-range surface plasmons, Opt. Eng. 36 (1997) 1537-1541.

18. Y. Wang, Voltage-induced color-selective absorption with surface plasmons, Appl. Phys. Lett. 67 (1995) 2759-2761.

19. G.J. Ashwell and M.P.S. Roberts, Highly selective surface plasmon resonance sensor for NO_2, Elect. Lett. 32 (1996) 2089-2091.

20. M. Niggemann, A. Katerkamp, M. Pellmann, P. Boismann, J. Reinbold and K. Cammann, Remote sensing of tetrachloroethene with a micro-fibre optical gas sensor based on surface plasmon resonance spectroscopy, Sensors and Actuators B 34 (1996) 328-333.

21. C.P. Cahill, K.S. Jahnston and S.S Yee, A surface plasmon resonance sensor probe based on retro-reflection, Sensors and Actuators B 45 (1997) 161-166.

22. Y.C. Cheng, W.K. Su and J.H. Liou, Application of a liquid sensor based on surface plasma wave excitation to distinguish methyl alcohol from ethyl alcohol, Opt. Eng. 39 (2000) 311-314.

23. I. Stemmler, A. Brecht and G. Gauglitz, Compact surface plasmon resonance-transducers with spectral readout for biosensing applications, Sensors and Actuators B 54 (1999) 98-105.

24. Charles E.H. Berger and J. Greve, Differential SPR immunosensing, Sensors and Actuators B 63 (2000) 103-108.

25. T. Akimoto, S. Sasaki, K. Ikebukuro and I. Karube, Refractive-index and thickness sensitivity in surface plasmon resonance spectroscopy, Appl. Opt. 38 (1999) 4058-4064.

26. K.S. Johnston, S.R. Karlsen, C.C. Jung and S.S. Yee, New analytical technique for characterization of thin films using surface plasmon resonance, Materials Chemistry and Physics, 42 (1995) 242-246.

27. C.L. Wong, H.P. Ho, K.S. Chan, P.L. Wong, S.Y. Wu and Chinlon Lin, Optical characterization of elastohydrodynamic lubricated (EHL) contacts using surface plasmon resonance (SPR) effect, Sensors and Actuators B 41 (2008) 356-366.

28. R. Rella, J. Spadavecchia, M.G. Manera, P. Siciliano, A. Santino and G. Mita, Liquid phase SPR imaging experiments for biosensors applications, Sensors and Actuators B 20 (2004) 1140-1148.

29. K. Matsubara, S. Kawata and S. Minami, "Optical chemical sensor based on surface plasmon measurement", *Appl. Opt.* 27 (1988) 1160-1163

30. B. Liedberg, I. Lundstrom, E. Stenberg, "Principles of biosensing with an extended coupling matrix and surface plasmon resonance", *Sensors and Actuators B*, 11 (1993) 63-72

31. H.P. Ho, S.Y. Wu, M. Yang and A.C. Cheung, "Application of white light-emitting-diode to surface plasmon resonance sensors", *Sensors and Actuators B*, 80 (2001) 89-94

32. R.C. Jorgenson and S.S. Yee, "A fiber-optic chemical sensor based on surface plasmon resonance", *Sensors and Actuators B*, 12 (1993) 213-220

33. S. G. Nelson, K. S. Johnston and S. S. Yee, High sensitivity surface plasmon plasmon resonance sensor based on phase detection, Sensors and Actuators B 35 (1996) 187-191.

34. A. V. Kabashin and P. I. Nikitin, nterferometer based on a surface-plasmon resonance for sensor applications,Quantum Electron. 27 *7* (1997) 653–654.

35. A. V. Kabashin and P. I. Nikitin, Surface plasmon resonance interferometer for bio- and chemical-sensors, Opt. Commun. 150 *1-6* (1998) 5–8.

36. A. N. Grigorenko, P. I. Nikitin and A. V. Kabashin, Phase Jumps and Interferometric Surface Plasmon Resonance Imaging, Appl. Phys. Lett. 75 *25* (1999) 3917–3919.

37. A. N. Grigorenko, A. A. Beloglazov, P. I. Nikitin, C. Kuhne, G. Steiner and R. Salzer, "Dark-field surface plasmon resonance microscopy," Opt. Commun. 174 *1-4* (2000) 151–155.

38. H. P. Ho, W. W. Lam and S. Y. Wu, Surface plasmon resonance sensor based on the measurement of differential phase, Rev. Sci. Instrum. 73 *10* (2002) 3534–3539.

39. Barnes, W.L., A. Dereux, and T.W. Ebbesen, Surface plasmon subwavelength optics, Nature 424 (2003) 824–830.

40. P. Yeh, Optical waves in layered media, New York: John Wiley & Sons. 1998.

41. P. Leonard, S. Hearty, J. Brennan, L. Dunne, J. Quinn, T. Chakraborty and R. O'Kennedy, Advances in biosensors for detection of pathogens in food and water, Enzyme. Microb. Tech. 32 (2003) 3–13.

42. B. Liedberg, C. Nylander, and I. Lundstrom, Biosensing with surface plasmon resonance—How it all started., Biosensor and Bioelectronic, 10 (1995)1–9.

43. J. Melendez, R. Carr, D.U. Bartholomew, H. Taneja, S. Yee, C. Jung and C. Furlong, Development of a surface plasmon resonance sensor for commercial applications, Sensors and Actuator B, 38–39 (1997) 375–379.

44. J. Homola, On the sensitivity of surface plasmon resonance sensor with spectral interrogation, Sensors and Actuator B, 41 (1997) 207–211.

45. K. Kurihara, H. Ohkawa, Y. Iwasaki, O. Niwa, T. Tobita and K. Suzuki, Fiber-optic conical microsensors for surface plasmon resonance using chemically etched single-mode fiber, Anal. Chem. Acta, 523 (2004) 165–170.

46. J. Dosta´lek, J. C ˇ tyroky´, J. Homola, E. Brynda, M. Skalsky´, P. Nekvindova´, J. S ˇ pirkova´, J. S ˇ kvor and J. Schro¨fel, Surface plasmon resonance biosensor based on integrated optical waveguide, Sensors and Actuator B, 76 (2001) 8–12.

47. M. Piliarik, , J. Homola, Z. Manı´kova´ and J. C ˇ tyroky´, Surface plasmon resonance sensor based on a single-mode polarization-maintaining optical fiber, Sensors and Actuator B, 90 (2003) 236–242.

48. S.R. Karlsen, K.S. Johnston, S.S. Yee and C.C. Jung, First-order surface plasmon resonance sensor system based on a planar light pipe. Sensors and Actuator B, 32 (1996) 137–141.

49. X. Yu, L. Zhao, H. Jiang, H. Wang, C. Yin and S. Zhu, Immunosensor based on optical heterodyne phase detection, Sensors and Actuator B, 76 (2001) 199–202.

50. X. Yu, D. Wang and Z. Yan, Simulation and analysis of surface plasmon resonance biosensor based on phase detection, Sensor and Actuator B, 91 (2003) 285–290.

51. J. Guo, Z. Zhu, W. Deng and S. Shen, Angle measurement using surface-plasmon-resonance heterodyne interferometry: A new method, Optical Engineering, 37 (1998) 2998–3001.

52. S.F. Wang and R.S. Chang, D-type fiber biosensor based on surface-plasmon resonance technology and heterodyne interferometry, Optics Letter, 30(2005) 233–235.

53. H.P. Ho and W.W. Lam, Application of differential phase measurement technique to surface plasmon resonance imaging sensors, Sensors and Actuator B, 96 (2003) 554–559.

54. S.Y. Wu, H.P. Ho, W.C. Law, C. Lin and S.K. Kong. Highly sensitive differential phasesensitive surface plasmon resonance biosensor based on the Mach–Zehnder configuration, Optics Letter, 29 (2004) 2378–2380.

55. H.P. Ho, W.C. Law, S.Y. Wu, C. Lin and S.K. Kong, Real-time optical based differential phase measurement of surface plasmon resonance. Biosensors and Bioelectronic, 20 (2005) 2177–2180.

56. A.K. Sheridan, R.D. Harris, P.N. Bartlett, and J.S. Wilkinson, Phase interrogation of an integrated optical SPR sensor, Sensors and Actuator B, 97 (2004) 114–121.

57. I. Lundstro¨m, Real-time dispecific interaction analysis, Biosensors and Bioelectronic, 9 (1994) 725–736.

58. R. Karlsson, M. Kullman-Magnusson, M.D. Ha¨ma¨la¨inen, A. Remaeus, K. Andersson, P. Borg, E. Gyzander and J. Deinum, Biosensor analysis of drug-target interactions: Direct and competitive binding assays for investigation of

interactions between thrombin and thrombin inhibitors, Anal. Biochem., 278 (2000) 1–13.

59. P.O. Markgren, M. Ha¨ma¨la¨inen, and U.H. Danielson, Kinetic analysis of the interaction between HIV-1 protease and inhibitors using optical biosensor technology, Anal. Biochem., 279(2000) 71–78.

60. A. Frostell-Karlsson, A. Remaeus, H. Roos, K. Andersson, P. Borg, M. Ha¨ma¨la¨inen and R. Karlsson, Biosensor analysis of the interaction between immobilized human serum albumin and drug compounds for prediction of human serum albumin binding levels, J. Med. Chem., 43 1986–1992.

61. E. Danelian, A. Karle´n, R. Karlsson, S. Winiwarter, A. Hansson, S. Lo¨fa°s, H. Lennerna¨s and M.D. Ha¨ma¨la¨inen, SPR biosensor studies of the direct interaction between 27 drugs and a liposome surface: Correlation with fraction absorbed in humans, J. Med. Chem. 43 2083–2086.

62. P. Bjurling, G.A. Baxter, M. Caselunghe, C. Jonson, M. O'Connor, B. Persson and C.T. Elliott, Biosensor assay of sulfadiazine and sulfamethazine residues in pork, Analyst., 125 1771–1774.

63. M. Bostro¨m-Caselunghe and J. Lindeberg, Biosensor based determination of folic acid in fortified food, Food Chem., 70 (2000) 523–532.

64. J.D. Wright, J.V. Oliver, R.J.M. Nolte, S.J. Holder, N.A. J.M. Sommerdijk and P.I. Nikitin, The detection of phenols in water using a surface plasmon resonance system with specific receptors, Sensors and Actuator B, 51 (1998) 305–310.

65. V. Koubova´, E. Brynda, L. Karasova´, J. S ˇ kvor, J. Homola, J. Dosta´lek, P. Tobisˇka and J Rosˇicky´., Detection of foodborne pathogens using surface plasmon resonance biosensors, Sensors and Actuator B, 74: 2001.100–105.

66. D. Aivazian and L.J. Stern, Phosphorylation of T cell receptor is regulated by a lipid dependent folding transition, Nat. Struct. Biol., 7 (2000) 1023–1026.

67. B. Bader, K. Kuhn, D.J. Owen, H. Waldmann, A. Wittinghofer and J. Kuhlmann, Bioorganic synthesis of lipid-modified proteins for the study of signal transduction, Nature, 403 (2000) 223–226.

68. E. Bitto, M. Li, A.M. Tikhonov, M.L. Schlossman and W. Cho, Mechanism of annexin I-mediated membrane aggregation, Biochemistry, 39 (2000) 13469–13477.

69. R.G.Chapman, E. Ostuni, L. Yan and G.M. Whitesides, Preparation of mixed self-assembled monolayers (SAMs) that resist adsorption of proteins using the reaction of amines with a SAM that presents interchain carboxylic anhydride groups, Langmuir, 16 (2000) 6927–6936.

70. H.M. Chen, W. Wang and D.K. Smith, Liposome disruption detected by surface plasmon resonance at lower concentrations of a peptide antibiotic, Langmuir, 16 (2000) 9959–9962.

71. C.L. Baird and D.G. Myszka, Current and emerging commercial optical biosensors, J. Mol. Recognit., 14 (2001) 261–268.

72. R.L. Rich and D.G. Myszka, Advances in surface plasmon resonance biosensor analysis, Curr. Opin. Biotechnol., 11 (2000) 54–61.

73. R.L. Rich and D.G. Myszka, Survey of the year 2000 commercial optical biosensor literature, J. Mol. Recognit., 14 (2000) 273–294.

74. P. Gomes and D. Andreu, Direct kinetic assay of interactions between small peptides and immobilized antibodies using a surface plasmon resonance biosensor, J. Immunol. Methods, 259 (2002) 217–230.

75. M. Alterman, H. Sjo¨bom, P. Sa¨fsten, P.O., Markgren, U.H. Danielson, M. Ha¨ma¨la¨inen, S. Lo¨fa°s, J. Hulte´n, B. Classon, B. Samuelsson and A. Hallberg, P1/P1` modified HIV protease inhibitors as tools in two new sensitive surface plasmon resonance biosensor screening assays, Eur. J. Pharm. Sci., 13 (2001) 203–212.

76. J.R. Krone, R.W. Nelson, D. Dogruel, P. Williams, and R. Granzow, BIA/MS: Interfacing biomolecular interaction analysis with mass spectrometry, Anal. Biochem., 244 124–132

77. H. Raether, Surface plasmons on smooth and rough surfaces and on gratings, Springer tracts in modern physics, Heidelberg: Springer-Verlag. (1988).

78. J. Davies, Surface analytical techniques for probing biomaterial processes, Boca Raton, Florida: CRC Press. (1996).

79. J. Homola, I. Koudela, and S.S. Yee, Surface plasmon resonance sensors based on diffraction gratings and prism couplers: sensitivity comparison, Sensors and Actuator B, 54 (1999) 16–24.

80. P.I. Nikitin, P.M. Anokhin, and A.A. Beloglazov, Chemical sensors based on surface plasmon resonance in Si grating structures, Transducers 97 International Conference on Solid-State, Sensors and Actuators, Chicago, June 16–19, (1997) 1359–1362.

81. E. Charles H. Berger, and J. Greve. Differential SPR immunosensing, Sensors and Actuator B, 63 (2000) 103–108.

82. M.A. Fardad, H. Luo, Y. Beregovski, and M. Fallahi, Solgel grating waveguides for distributed Bragg reflector lasers, Optics Letter, 24 460–462.

83. N.L. Dmitruk, O.I. Mayeva, S.V. Mamykin, and O.B. Yastrubchak, On a control of photonsurface plasmon resonance at a multiplayer diffraction grating, The Third International EuroConference on Advanced Semiconductor Devices and Microsystems, (2000) AQ6.

84. M.J. Jory, P.S. Vukusic, and J.R. Sambles, Development of a prototype gas sensor using surface plasmon resonance on gratings, Sensors and Actuator B, 17 (1994) 1203–1209.

85. D.C. Cullen, R.G. Brown, and C.R. Lowe, Detection of immuno-complex formation via surface plasmon resonance on gold-coated diffraction gratings, Biosensors 3 (1987) 211–225.

86. M. Weisser, B. Menges, and S.M. Neher, Refractive index and thickness determination of monlayers by multi mode waveguide couple surface plasmons, Sensors and Actuator B, 56 (1999) 189–197.

87. R. Slavk, J. Homola, J. C ˇ tyroky´, and E. Brynda, Novel spectral fiber optic sensor based on surface plasmon resonance, Sensors and Actuator B, 74 (2001) 106–111.

88. E. Fontana, Chemical sensing with gold coated optical fibers, SBMO/IEEE MTT-S IMOC 99 Proceedings.

89. E. Fontana, H.D. Dulman, D.E. Doggett, and R.H. Pantell, Surface plasmon resonance on a single mode optical fiber, IEEE Trans. Instrum. Meas., 47 (1998) 168–173.

90. S.Y. Wu and H.P. Ho, Proc. SPIE 6099, 60990R (2006).

91. P.K. Madhavan Unni, M.K. Gunasekaran and A. Kumar, ±30μK temperature controller from 25 to 103°C: Study and analysis, Review of Scientific Instruments, 74 (2003) 231-242.

92. R.C. Weast (Ed.), CRC handbook of chemistry and physics, 68th ed., CRC Press, Boca Raton, FL (1987) D232

93. H.P. Ho, W. Yuan, C.L. Wong, S.Y. Wu, Y.K. Suen, S.K. Kong and Chinlon Lin, Sensitivity enhancement based on application of multi-pass interferometry in phase-sensitive surface plasmon resonance biosensor, Optics Communications, 275 (2007) 491 - 496.

94. R.P.H. Kooyman, H. Kolkman, J.Van Gent, J. Greve, Surface plasmon resonance immunosensors: sensitivity considerations, Anal. Chim. Acta, 213 (1988) 35-45.

95. T. Akimoto, S. Sasaki, K. Ikebukuro, I. Karube, Refractv-index and thickness sensitivity in surface plasmon resonance spectroscopy, Applied Optics, 38 (1999) 4058-4064.

96. C. L. Wong, H. P. Ho, T. T. Yu, Y. K. Suen, W. W. Chow, S. Y. Wu, W. C. Law, W. Yuan, W. J. Li, S. K. Kong, and C. Lin, Two-dimensional biosensor arrays based on surface plasmon resonance phase imaging, Applied Optics, 46 (2007) 2325–2332.

97. Y. Yang, Z. Cao, Q. Shen,, J. Hao, L. Qiu, Y. Shen, W. Yuan and P. Xiao, Multi-channel light modulation based on the attenuation total reflection, *Opt. and Laser Technol.*, 37 (2005) 225-228.

98. Y. Jiang, Z. Cao, G. Chen, X. Dou, Y. Chen, Low voltage electro-optic polymer light modulator using attenuated total internal reflection, Opt. and Laser Technol., 33 (2001) 417-420.

99. J.-W. Kang, T.-D. Kim, J. Luo, M. Haller and A.K.-Y. Jen, Very large electro-optic coefficients from in situ generated side-chain nonlinear optical polymers, Appl. Phys. Lett.,.87 (2005) 071109-071111,

100. A. Kasry and W. Knoll, Long range surface plasmon fluorescence spectroscopy, Appl. Phys. Lett., 89 (2006) 10116-10119.

101. C.M. Wu and M.C. Pao, Sensitivity-tunable optical sensors based on surface plasmon resonance and phase detection, Optics Express, 12 (2004) 3509-3514.

102. Y.D. Su, S.J. Chen and T.L. Yeh, Common-path phase-shit interferometry surface plasmon resonance imaging system, Optics Letter 30, (2005) 1488-1490.

103. I.R. Hooper and J.R. Sambles, Differential ellipsometric surface plasmon resonance sensors with liquid crystal polarization modulators, Applied Physics Letter, 85 (2004) 3017-3019.

104. M.A. Ordal, L.L. Long, R.J. Bell, S.E. Bell, R.R. Bell, R.W. Alexander, Jr., and C.A. Ward, Optical properties of the metals Al, Co, Cu, Au, Fe, Pb, Ni, Pd, Pt, Ag, Ti, and W in the infrared and far infrared, Appl. Opt. 22 (1983) 1099-1119.

105. Schott Glass Technologies Inc., Durea, PA.

Appendix A

List of publications related to this project

Journal paper

[1] H.P. Ho, W.W. Lam and **S.Y. Wu**, Surface plasmon resonance sensor based on the measurement of differential phase, Review of Scientific Instruments, 73(2002), 7534-7539.

[2] **S.Y. Wu**, H.P. Ho, W.C. Law, Chinlon Lin and S.K. Kong, Highly sensitive differential phase-sensitive surface plasmon resonance (SPR) biosensor based on Mach-Zehnder configuration, Optics Letters, 29(2004), 2378-2381.

[4] H.P. Ho, W. Yuan, C.L. Wong, **S.Y. Wu**, Y.K. Suen, S.K. Kong and Chinlon Lin, Sensitivity enhancement based on application of multi-pass interferometry in phase-sensitive surface plasmon resonance biosensor, Optics Communications, 275 (2007) 491 - 496.

[5] C.L. Wong, H.P. Ho, T.T. Yu, Y.K. Suen, W.W. Chow, **S.Y. Wu**, W. C. Law, W. Yuan, W. J. Li, S.K. Kong, and C. Lin, Two-dimensional biosensor arrays based on surface plasmon resonance phase imaging, Applied Optics, 46 (2007) 2325–2332.

[6] **S.Y. Wu** and H.P. Ho, Single-beam self-referenced phase-sensitive surface plasmon resonance sensor with high detection resolution, Chinese Optics Letters, 6(2008), 176-178.

Book Contribution

[1] H.P. Ho and **S.Y. Wu** , Bio-molecule Sensing using surface plasmon resonance (SPR), in: Tuan Vo-Dinh (ed), Nanotechnology in Biology and Medicine: Methods, Devices and Applications, CRC Press, LLC (in press).

Patent

[1] H.P. Ho, C.L. Wong, **S.Y. Wu**, W.C. Law, Chinlon Lin and S.K. Kong, Optical Sensing Devices with SPR Sensors Based on Differential Phase Interrogation and Measuring Method Using the Same, U.S. Patent (08/2005).

[2] H.P. Ho, **S.Y. Wu**, C. Lin, S.K. Kong, A simple differential phase imaging surface plasmon resonance sensor using liquid crystal modulator, U.S. Patent (01/2006).

[3] **S.Y. Wu**, H.P. Ho, Y.K. Suen, S.K. Kong, W.W. Wong, K.C. Lo, Method and Apparatus for Phase Sensitive Surface Plasmon Resonance, U.S. Provisional Patent (03/2008).

Conference Paper

[1] **S. Wu** and H. Ho, A bio-imaging biosensor chip design based on phase-stepping interferometry of surface plasmon resonance, BIOS 2006, in SPIE Photonics West, San Jose, USA, 21-26 January 2006.

[2] **S.Y. Wu**, C.L. Wong, H.P. Ho, S.K. Kong and Chinlon Lin, Application of Fabry-Perot interferometer for signal amplification in phase-sensitive surface plasmon resonance biosensors, Biosensors 2006, The 9th World Congress on Biosensors, Toronto, Canada, 10 -12 May 2006.

[3] H.P. Ho and **S.Y. Wu**, Simulation of a novel high sensitivity and wide dynamic range phase-sensitive surface plasmon resonance sensor, IEEE Conference on Electron Devices and Solid-State Circuits, Hong Kong, 20 -22 December 2007.

[4] **S.Y. Wu** and H.P. Ho, Highly sensitive single-beam phase-sensitive surface plasmon resonance biosensor with a wide dynamic range, BIOS 2008, in SPIE Photonics West, San Jose, USA, 19-24 January 2008.

[5] **S.Y. Wu** and H.P. Ho, Wide dynamic range phase-sensitive surface plasmon resonance sensors by incorporating tunable materials in the sensor layer, in 10th World Congress on Biosensors, Shanghai, China, 14-16 May 2008.

Appendix B

Relationship Between Concentration and Refractive Index of Glycerin-Water Mixture

The table gives the refractive indexes of glycerin-water mixtures as a function of concentrations. All data refer to a temperature of 20°C and at a wavelength of 589.26nm. The refractive index n of aqueous solution of glycerin with increasing glycerin concentration was assumed to be identical over the whole wavelength region under investigation [92].

Sodium Chloride, $CH_2OHCHOHCH_2OH$

Molecular weight = 92.09,

Relative Specific Refractivity = 1.109,

Table A Concentration versus Refractive index for glycerint-water mixture

% by Weight	Refractive Index (n)
0.00	1.3330
0.5	1.3336
1.00	1.3342
2.00	1.3353
3.00	1.3365
4.00	1.3376
5.00	1.3388
6.00	1.3400
7.00	1.3412
8.00	1.3424
9.00	1.3436
10.00	1.3448
12.00	1.3472
14.00	1.3496
16.00	1.3521
18.00	1.3547
20.00	1.3572

% by Weight	Refractive Index (n)
22.00	1.3596
24.00	1.3620
26.00	1.3645
28.00	1.3669
30.00	1.3693
32.00	1.3717
34.00	1.3741
36.00	1.3766
38.00	1.3790
40.00	1.3814
42.00	1.3838
44.00	1.3862
46.00	1.3887